The role of Cadherin-13 in serotonergic neurons during different murine developmental stages

Die Rolle von Cadherin-13 in serotonergen Neuronen während verschiedener Entwicklungsstadien in der Maus

Doctoral thesis for a doctoral degree
at the Graduate School of Life Sciences,
Julius-Maximilians-Universität Würzburg,

Section Neuroscience/ Human Medicine

Submitted by

Laura Sophie Pennington

from
Eggenfelden, Germany

Würzburg, 2017

Submitted on: **18th August 2017**

Members of the *Promotionskomitee*:

Chairperson:	**Prof. Dr. rer. nat. Martin Eilers**
Primary Supervisor:	**Prof. Dr. med. Klaus-Peter Lesch**
Supervisor (Second):	**Prof. Dr. med. Esther Asan**
Supervisor (Third):	**Prof. Dr. rer. nat. Erhard Wischmeyer**
Advisor:	**Dr. rer. nat. Jonas Waider**

Date of Public Defence: **18th May 2018**

Table of Contents

Abstract

Background: Attention-deficit/ hyperactivity disorder (ADHD) ranges among the most common neurodevelopmental disorders worldwide with a prevalence of 3-12% in childhood and 1-5% for adults. Over the last decade extensive genetic research has been conducted in order to determine its causative genetic factors. None of the so far identified susceptibility genes, however, could explain the estimated ADHD heritability of 76%. In this thesis one of the most promising candidates -Cadherin 13 (Cdh13) - was examined in terms of its influence on the central serotonergic (5-HT) system. In addition to that, the Cdh13 protein distribution pattern was analysed over time.

Methods: The developing serotonergic system was compared over three embryonic and postnatal stages (E13.5, E17.5 and P7) in different Cdh13 genotypes (WT, HZ and KO) using immunohistochemistry and various double staining protocols.

Results: The raphe nuclei of the 5-HT system develop in spite of Cdh13 absence and show a comparable mature constellation. The cells in the KO, however, are slightly more scattered than in the WT. Furthermore the dynamics of their formation is altered, with a transient delay in migration at E13.5. In early developmental stages the total amount of serotonergic cells is reduced in KO and HZ, though their proportional distribution to the raphe nuclei stays constant. Strikingly, at P7 the absolute numbers are comparable again.

Concerning the Cdh13 protein, it shows high concentrations on fibres running through hindbrain and midbrain areas at E13.5. This, however, changes over time, and it becomes more evenly spread until P7. Furthermore, its presence in serotonergic cells could be visualised using confocal microscopy. Since the described pattern is only in parts congruent to the localisation of serotonergic neurons, it is most likely that Cdh13 is present in other developing neurotransmitter systems, such as the dopaminergic one, as well.

Conclusion: It could be proven that Cdh13 is expressed in serotonergic cells and that its knockout does affect the developing serotonergic system to some degree. Its absence, however, only slightly and transiently affects the measured parameters of serotonergic system development, indicating a possible

compensation of CDH13 function by other molecules in the case of Cdh13 deficiency. In addition further indicators could be found for an influence of Cdh13 on outgrowth and path finding of neuronal processes.

Zusammenfassung

Hintergrund: Das Aufmerksamkeits-Defizit/ Hyperaktivitäts-Syndrom (ADHS) gehört zu den häufigsten psychiatrischen Erkrankungen weltweit und betrifft 3-12% aller Kinder und 1-5% der Erwachsenen. In den letzten Jahren wurde eine große Anzahl verschiedener genetischer Studien durchgeführt, um die zugrunde liegenden genetischen Ursachen genauer zu bestimmen. Von den vielen hundert bis dato gefundenen Kandidatengenen erreichte jedoch keines eine ausreichende statistische Signifikanz. Diese Arbeit befasst sich mit Cadherin 13, einem der vielversprechendsten Kandidatengene, und untersucht einen möglichen Zusammenhang mit der Entwicklung des serotonergen Systems. Zusätzlich wird das Cdh13 Verteilungsmuster im ZNS über die Zeit analysiert.

Methoden: Es wurden embryonale und postnatale Entwicklungsstadien des serotonergen Systems (E13.5, E17.5 und P7) in drei Cdh13 Genotypen mit (WT, HZ, KO) verglichen. Dabei kamen Methoden der Immunhistochemie und diverse Doppelfärbungsprotokolle zum Einsatz.

Ergebnisse: Die Raphe Kerne des serotonergen Systems entwickeln sich trotz fehlendem Cdh13 und zeigen im ausgereiften Zustand eine ähnliche Morphologie in allen Genotypen. Allerdings liegen die Neurone der Raphe Kerne im KO etwas weiter verstreut. Zudem hat es den Anschein als wäre die Dynamik ihrer Entwicklung beeinträchtigt. So liegt beispielsweise um E13.5 der KO im Vergleich zum WT vorübergehend etwas zurück. Außerdem weisen die frühen Entwicklungsstadien im KO und HZ deutlich reduzierte Zellzahlen auf, wobei deren anteilmäßige Verteilung zu den einzelnen Raphe Kernen zwischen den Genotypen unverändert ist. Überraschenderweise finden sich in P7 wieder vergleichbare Zellzahlen.

Was die Verteilung von Cdh13 betrifft, so liegt es ab E13.5 vor allem auf Fasern von Hirnstamm und Mittelhirn in hohen Konzentrationen vor. Im Laufe der

Entwicklung verliert Cdh13 diese begrenzte Lokalisation und zeigt sich homogen in weiten Teilen des ZNS verteilt. Da sein Verteilungsmuster nur teilweise Ähnlichkeiten mit dem 5-HT System aufweist, muss davon ausgegangen werden, dass es noch in anderen Neurotransmittersystemen wie etwa dem dopaminergen System eine Rolle spielt.

Schlussfolgerung: Es ist gezeigt worden, dass Cdh13 in serotonergen Zellen exprimiert wird und seine Abwesenheit Einfluss auf die Entwicklung des serotonergen Systems nimmt. Angesichts seiner geringen Auswirkungen lässt sich allerdings vermuten, dass sein Fehlen teilweise von anderen Molekülen kompensiert wird. Darüber hinaus sind weitere Hinweise darauf gefunden worden, dass Cdh13 eine Rolle bei der Lenkung auswachsender neuronaler Fortsätze spielt.

1. Introduction

1.1 Cadherin 13 as a candidate molecule in ADHD

Since its first mentioning in the Diagnostic and Statistical Manual of Mental Disorders (DSM) 3rd edition in 1980, the attention deficit/ hyperactivity disorder (ADHD) has attained its position as one of the most widely noticed neurodevelopmental psychiatric disorders of our times. The tremendously increasing frequency of the diagnosis very soon caused controversial discussions, with some people denying its existence whatsoever, whereas others categorise it less as an illness, than as a side product of our performance- and success-oriented society, which leaves no space for inadequately effective individual characters. In medical circles it is clear, however, that there are in fact people suffering from this disorder. Therefore extensive research has been conducted in these last decades in order to understand its origins in more detail. This work is focused upon its genetics and possible connections to disturbances of the molecule cadherin 13 (Cdh13).

1.1.1 Clinical picture of attention deficit/ hyperactivity disorder

ADHD ranges among the most common psychiatric behavioural disorders in childhood and adolescence worldwide (Lesch et al., 2011), with an estimated prevalence of 3-12% for children (Zhang et al., 2012; Franke et al., 2009; Williams et al., 2012; Neale et al., 2010a/b) and 1-5% for adults (Franke et al., 2009; Neale et al., 2010a/b). It belongs to the group of neurodevelopmental disorders, which also comprises schizophrenia and autism (Rivero et al., 2013). The clinical picture of ADHD is defined by “developmentally inappropriate levels of hyperactive, impulsive and inattentive behaviours” (Neale et al., 2008), as well as by the disability to successfully adapt to psychosocially demanding contexts (Lesch et al., 2011; Zhang et al., 2012; Neale et al., 2010b; Hackenberg and Aichhorn, 2012; Hamshere et al., 2013). It is frequently associated with various comorbidities (up to 80%), like anxiety, mood (e.g. depression) or substance use disorders. The typical onset of ADHD lies in early childhood before the age of six, with 30-50% persistence into adulthood

(Schneider and Weber-Papen, 2010; Hackenberg and Aichhorn, 2012; Williams et al., 2010), resulting in “deleterious effects on education and social outcomes” (Kebir et al., 2009). ADHD has a clear androtropic tendency, with boys being four times more often affected in childhood and twice as often in adulthood (Schneider and Weber-Papen, 2010; Hackenberg and Aichhorn, 2012). According to the DSM 5th edition (DSM-V), the syndrome can be diagnosed when the core symptoms mentioned above appear before the age of twelve (with inattentiveness and hyperactivity being obligatory), in at least two different situations, e.g. school and family, and persist for a minimum of six months (Bakker et al., 2003; Hackenberg and Aichhorn, 2012). Deficits in emotional self-regulation, a common trigger for comorbidities, were left out in the new manual (Schuch et al., 2015). The diagnosis is, however, only reason for pharmacological treatment if the disorder constitutes a severe burden to patient and/ or family (Hackenberg and Aichhorn, 2012). Diagnosis in adulthood (defined as age over 17 years; DSM-V) is only possible when ADHD has already been present during childhood. Then the diagnosis criteria are the same as for children, only supplemented with the Wender-Utah Criteria, which comprise conditions like affect instability, impulsiveness and disorganised behaviour (Schneider and Weber-Papen, 2010). The clinical picture of ADHD changes in adolescence and adulthood with hyperactivity, impulsiveness and inattentiveness transforming into inner restlessness, disorganisation, extreme impatience and irritability (Hackenberg and Aichhorn, 2012). ADHD thus constitutes an extremely complex and heterogeneous clinical syndrome (Kebir et al., 2009; Baroni and Castellanos, 2015). Given that common therapeutics, impacting the dopamine (DA), the norepinephrine (NE) and the serotonin (5-HT) systems, like the psychostimulant methylphenidate (MPH), the NE reuptake inhibitor atomoxetine (ATX), as well as 5-HT-reuptake inhibitors, successfully stabilise symptoms of ADHD, an involvement of these monoaminergic systems in its pathophysiology seems likely (Rivero et al., 2013).

The susceptibility for this multifactorial disease is dependent on environmental and genetic factors, as well as their interactions (GxE; Williams et al., 2012). In the last years intense research has been conducted, in order to define GxE

parameters more closely and to further illuminate the so far incompletely understood aetiology of ADHD (Zhang et al., 2012). Exposure to maternal alcohol and nicotine during pregnancy, accumulating toxins like lead or polychlorinated biphenyls (PCBs), as well as high psychosocial adversity have been discussed as environmental factors, increasing the risk for ADHD (Faraone and Mick, 2011; Kebir et al., 2008: Banerjee et al., 2007). It is well known that genetic factors also contribute a great deal to the manifestation of complex psychiatric diseases (Smoller et al., 2013). Using twin studies, researchers therefore tried to determine to what extent gene variability influences the development of ADHD, resulting in a mean heritability of about 76% (Faraone et al., 2009; Kebir et al., 2008). In consequence, a significant contribution of genetic factors to development and progress of ADHD was expected (Banaschewski et al., 2010), “making this condition a promising target for molecular genetic studies” (Neale et al., 2008).

1.1.2 Genetics of ADHD

In order to figure out the genetic foundation of ADHD, different approaches were pursued: hypothesis-driven candidate gene association studies, hypothesis-free genome-wide linkage studies and genome-wide association studies (GWAS), the latter combining the advantages of the before-mentioned techniques, which are the abilities to find genetic variants of little effect size and to analyse the whole genome without hypothesis (Franke et al., 2009; Banaschewski et al., 2010), with the potential to find unknown risk genes (Yang et al., 2013).

1.1.2.1 Candidate gene association studies

With the aid of candidate gene association studies, specific genes, suspected to play a role in the pathophysiology of ADHD, were examined (Hudziak and Faraone, 2010). Given that efficient stimulating psychotropic drugs like MPH and ATX act via direct (i.e. blocking of DA or NE transporters, Banaschewski et al., 2010) or indirect dopaminergic activation in prefrontal cortex (PFC) and striatum (Hackenberg and Aichhorn, 2012), it seemed self-evident to focus on

proteins involved in DA signalling pathways (Hudziak and Faraone, 2010). In addition to that, the serotonergic system, which “has been related to impulsive disorder in children” (Banaschewski et al., 2010) and the noradrenergic system, being plausibly involved in executive control and attentional processes, have also been examined. Unfortunately, in all these association studies only very little evidence for possible candidate genes could be found, some of the few exceptions being the D4 DA receptor gene (*DRD4*), the human DA transporter gene (*DAT1*), the DA decarboxylase gene (*DDC*), the adrenergic receptor alpha 2A (*ADRA2A*) and tryptophan hydroxylase 2 genes (*TPH2*; Kebir et al., 2008; Banaschewski et al., 2010; Faraone and Khan, 2006; Roman et al., 2009). These findings can only account for a very small part (about 5%) of the calculated 76% genetic influence in ADHD (Hudziak and Faraone, 2010; Cortese et al., 2011). This phenomenon is called *missing heritability* and has been observed for many psychiatric diseases (Hebebrand, 2011; Lesch, 2014). Therefore Hudziak and Faraone (2010) proposed to abandon the concept of disease polygenes and postulated the existence of many susceptibility genes of small effect, increasing the risk for ADHD without being mandatory for its appearance.

1.1.2.2 Genome-wide linkage analyses

In genome-wide linkage analyses another strategy is pursued. “This approach examines many DNA markers across the genome to determine, if any chromosomal regions are shared more often than expected among ADHD family members” (Faraone and Mick, 2010). Linkage analysis is based on the observation that the chances of recombination are indirectly correlated with the distance between two loci. The frequency of recombination is described using the unit centimorgan (cM) with 1cM being equivalent to 1% probability per meiosis and approximately one million base pairs (bp) distance between two optional loci, respectively. So, in contrast to association studies, which are interested in significantly correlated *alleles*, linkage studies investigate the relationship of genome *loci* (Pulst, 1999). Until 2015 twelve genome-wide linkage studies (Fisher et al., 2002; Bakker et al., 2003; Arcos-Burgos et al.,

2004; Hebebrand et al., 2006; Ogdie et al., 2006; Faraone et al., 2007; Asherson et al., 2008; Romanos et al., 2008; Rommelse et al., 2008; Amin et al., 2009; Vegt et al., 2010; Saviouk et al., 2011) had been conducted and compared in one meta-analysis (Zhou et al., 2008a) without revealing large overlaps (Banaschewski et al., 2010). The most significant finding was that a region situated on chromosome 16 between 64Mb and 83Mb: 16q23.1-16q24.3 (Zhou et al., 2008a; Faraone et al., 2010) could be linked to ADHD, an area also containing *CDH13*. However, when strict criteria are applied no significant replications of these findings could be created up till now. Since linkage studies mainly detect strong genetic effects of >10% variance, this could point to only small to moderate additive or interactive effects of ADHD-linked traits (Neale et al., 2008).

1.1.2.3 Genome-wide association studies

Contrary to expectations, the above-mentioned approaches failed to reliably provide sufficient ADHD-associated genes or markers (Lesch et al., 2011), so that only the results of the various GWAS remain to be discussed. With the aid of single-nucleotide polymorphisms (SNP) (Hudziak and Faraone, 2010), which are the most frequent of DNA-polymorphisms (Pulst, 1999), and copy-number variants (CNV) (Rivero et al., 2013), which are rare chromosomal deletions and duplications (Langley et al., 2011), GWAS screen the whole genome for gene-disease associations. Until 2015 eleven GWAS for SNP (Lasky-Su et al., 2008; Lesch et al., 2008; Neale et al., 2008; Mick et al., 2010; Neale et al., 2010a; Hinney et al., 2011; Stergiakouli et al., 2012; Yang et al., 2013; Ebejer et al., 2013; Alemany et al., 2015; Zayats et al., 2015), eight GWAS for CNV (Elia et al., 2010; Williams et al., 2010; Elia et al., 2011; Lesch et al., 2011; Lionel et al., 2011; Williams et al., 2012; Yang et al., 2013; Jarick et al., 2014) and several meta-analyses (e.g. Zhou et al., 2008b; Neale et al., 2010b) have been conducted (Hawi et al., 2015; ADHDgene). For these studies huge sample sizes are necessary, in order to reach sufficient statistical power. For ADHD it has been calculated that 10,000-20,000 data sets would be needed in order to significantly identify reliable susceptibility genes. Even the meta-analysis (Neale

et al., 2010b), where seven preceding GWAS had been pooled, fell far short of this standard (Cortese et al., 2011). This might be one explanation why none of the revealed associated SNP or CNV so far bore up against correction with multiple testing for genome-wide significance, a threshold Neale et al. (2008, 2010a) defined as $5x10^{-8}$ (Franke et al., 2009; Yang et al., 2013; Hudziak and Faraone et al., 2010; Stergiakouli et al., 2012). However, GWAS add some interesting new aspects to the so far centric collective of candidate genes, at the same time providing only very little supportive evidence for the suspected genes (Franke et al., 2009; Neale et al., 2008; Banaschewski et al., 2010; Roman et al., 2009). Under the top-hit genes several are expressed in the central nervous system (CNS) (Franke et al., 2009) and seem to be involved in neurodevelopmental processes like synaptic plasticity, neurite outgrowth, neuronal morphogenesis, as well as cell adhesion, cell migration and transcriptional regulation (Yang et al., 2013; Lesch et al., 2008; Sowell et al., 2003). This data is consistent with “the hypothesis that mis-wiring of the brain during neurodevelopment might cause ADHD” (Yang et al., 2013), as well as with delayed maturation of neural networks in the cortex (Franke et al., 2009; Lesch et al., 2008). Especially fronto-striatal, fronto-temporal, fronto-parietal, and/ or fronto-striato-parieto-cerebellar circuits are suspected to be malfunctioning in ADHD (Schuch et a., 2015). Two of the more significant findings of GWAS concern the gene for the glucose-fructose oxidoreductase domain containing protein 1 (*GFOD1)*, which is said to correlate with inattentiveness (Banaschewski et al., 2010), as well as the gene for cadherin 13 (*CDH13)*.

1.1.2.4 Indicators towards Cdh13

Cadherin 13 appears to be of major interest, since *CDH13* lies on chromosome 16q24 and thus within the most significant ADHD-linked area reported in genome-wide linkage scans (cf. 1.1.2.2; Banaschewski et al., 2010). Furthermore, rs6565113, one of its intronic SNPs (Arias-Vásquez et al., 2011), was associated with ADHD in four of the so far conducted GWAS (Lasky-Su et al., 2008; Lesch et al., 2008; Neale et al., 2010a; Zhou et al., 2008) and in one

meta-analysis (Neale et al., 2010b; cf. 1.1.2.3). In addition to that, Uhl et al. (2008) found *CDH13* to be highly expressed in addiction-linked brain regions like hippocampus, frontal cortex, amygdala, thalamus and substantia nigra (see also Lesch et al., 2008). This could explain why disturbances of Cdh13 show strong correlation with phenotypes related to drug dependence and abuse, common comorbidities in ADHD (Neale et al., 2010a). Finally, the volume of brain regions expressing *CDH13* is significantly reduced in ADHD patients (Franke et al., 2009), suggesting that Cdh13-linked structural aberrations might be contributing. These combined evidences point to a possibly important role of Cdh13 in the pathophysiology of ADHD and make it a valuable candidate for extensive further investigation, as it was performed in the course of this thesis.

1.2 Cadherin 13 in comparison to classical cadherins

Cdh13 is the human homologue of T-cad in chicken and equivalent to the former H-cad (Philippova et al., 2009), which has been named after the organ it was first found in: the heart (Huntley, 2002). Ranscht and Dours-Zimmermann were the first to describe Cdh13 in 1991, when they isolated an unknown 95kDa glycoprotein out of embryonic chicken brain. They named it T-cad because of its truncated structure (cf. 1.2.1) and classified it as a member of the large superfamily of cadherins. This group of multifunctional calcium-dependent adhesion proteins contains more than 100 different molecules, categorised for example in classical cadherins, protocadherins, desmosomal cadherins or seven transmembrane cadherins (Angst et al., 2001), with organ-specific expression patterns (Redies et al., 2012). Cdh13 shows strong expression in the cardiovascular, as well as in the nervous system (Mavroconstanti et al., 2013). It has been detected in many regions of the human CNS: in neurons of cerebral cortex, medulla oblongata, nucleus olivaris, spinal cord and hypothalamus (Rivero et al., 2013; Philippova et al., 2009), as well as in astroglia of cerebral cortex and medulla oblongata (Takeuchi et al. 2000). In the following its specific role in the CNS, as well as its differences to classical cadherins, like N-, E- and P-cadherin, will be illustrated.

1.2.1 Structure of Cdh13

Classical cadherins consist of a cytoplasmic domain, one transmembrane-spanning region and an ectodomain (cf. Figure 1.1). The highly conserved C-terminal cytoplasmic segment provides a binding site for (α-, β- and γ-) catenins, which directly connect cadherins to the actin cytoskeleton. This is a crucial prerequisite for adhesion processes. Furthermore catenins provide a link to various downstream cell-signalling pathways and like that exert specific influence on cadherin activity (Huntley, 2002; Ranscht, 1994). The ectodomain at the N-terminus is composed of five, "tandem repeats of a unique, [about; L.P.] 100 amino acid motif (EC1-EC5)" (Huntley, 2002), containing four calcium-binding sites in between (Angst et al., 2001; Ranscht, 1994). The intercalation of calcium (Ca^{2+}) is required to enable stable and efficient adhesion (Ranscht and Dours-Zimmermann, 1991) via rigidification of the ectodomain (Huntley, 2002) and prevents proteolysis (Redies, 1995). The EC1 repeat contains the highly conserved HAV motif, which is suspected to play a role in specific recognition and adhesive interaction of cadherins. Immature precursor cadherins possess a pre-region at the N-terminus that needs to be cleaved off before maturation (Ranscht, 1994).

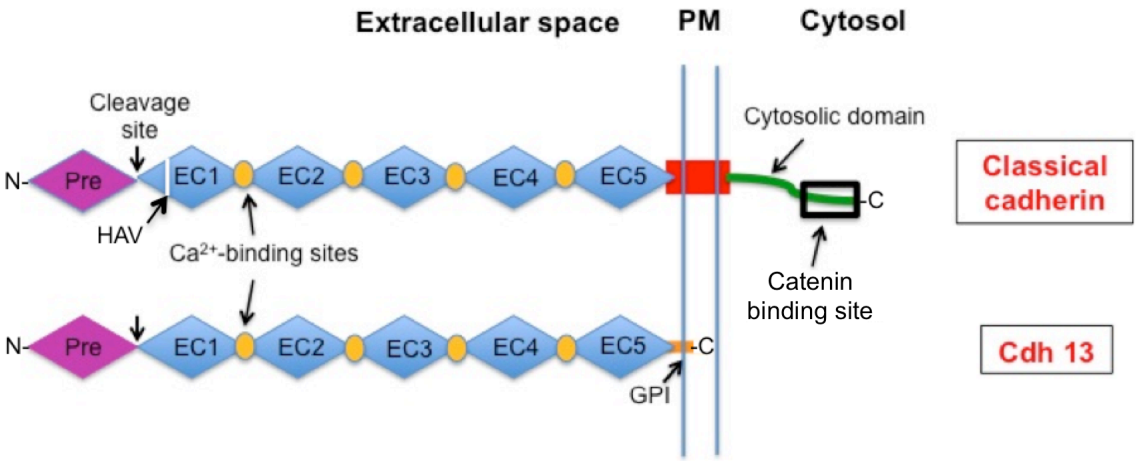

Figure 1.1 Structure of Cdh13 in comparison to classical cadherins (adapted from Ranscht (1994) and Philippova et al. (2009)). While classical cadherins possess a transmembrane-spanning region and a cytosolic domain (C-terminus), the latter allowing the binding of catenins, Cdh13 lacks any link to the cytosol and is instead fixated in the plasma membrane (PM) via a glycosylphosphatidylinositol (GPI)-anchor. In both structures, the ectodomain at the N-terminus consists of five tandem-repeats (EC1-5) with interposed Ca^{2+}-binding sites, only that in Cdh13 the HAV motif in EC1 is missing.

The structure of Cdh13 clearly deviates from the one of classical cadherins in several aspects (cf. Figure 1.1). Despite general similarity of the extracellular domain (Joshi et al., 2007), the HAV motif in the EC1 subunit is missing (Ranscht and Dours-Zimmermann, 1991). It plays an important role in homotypic interactions of classical cadherins (Rivero et al., 2013). Furthermore, Cdh13 is lacking the transmembrane, as well as the intracellular domain and is instead fixated in the plasma membrane via a glycosylphosphatidylinositol (GPI) anchor (Joshi et al., 2007; Akins et al., 2007). Unlike classical cadherins, it is thus devoid of the ability to directly interact with catenins at its C-terminus (Akins et al., 2007; Philippova et al., 2008), an interaction, which is crucial for their adhesive function (Ranscht and Dours-Zimmermann, 1991). The Cdh13 gene is highly conserved among vertebrate species (Rivero et al., 2013), displaying for example about 80% homology with the murine T-cad (Philippova et al., 2009; Takeuchi et al., 2000). Nevertheless, the protein appears in various isoforms of different size, generated by pre-protein processing (like protease cleavage of the pre-peptide; Ranscht and Dours-Zimmermann, 1991), alternative splicing mechanisms, as well as posttranslational modifications, like glycosylation (Philippova et al., 2009).

1.2.2 Signalling mechanisms of Cadherin 13

Classical cadherins, possessing an extracellular, as well as an intracellular domain, can transmit signals directly from the intercellular room to the cytoplasm. There they interact with a multitude of signalling molecules like β-catenin or plakoglobin, linking cadherins to the cytoskeletal actin filament system via alpha-catenin, as well as to the Wnt signalling pathway (Angst et al., 2001). For Cdh13 with its above-mentioned structural aberrations (cf. 1.2.1) alternative signalling mechanisms must exist (Rivero et al., 2013), which involve adapter molecules at the outer surface of the plasma membrane (PM; Mavroconstanti et al., 2013; Philippova et al., 2008). These extracellular transmitter-receptors co-localize with Cdh13 in membrane lipid rafts (Lesch et al., 2008; Joshi et al., 2007), which serve as “signal transduction platforms” (Philippova et al., 2008), facilitating the interaction between various lipid-

anchored molecules. In 2005, Philippova et al. identified two small GTPases, Rac1 and RhoA/ROCK, that convey Cdh13-triggered cell detachment and polarization. Furthermore integrin-linked kinase was found to couple Cdh13-signalling to the intracellular PI3K/Akt/GSK3β pathway, thus indirectly exerting influence on β-catenin-activity (Joshi et al., 2007; Philippova et al., 2008).

1.2.3 Function of Cadherin 13

Since Cdh13 plays a special role concerning structure and signalling mechanisms, it seems likely that its function is also different from the one of classical cadherins. In order to gain an adequate perspective on this aspect, it is important to first understand the function of classical cadherins.

Many cadherins can be found in developing as well as in adult CNS (Takeuchi et al., 2000), where they show “characteristic spatiotemporal expression profiles” (Redies et al., 2012). Classical cadherins are mainly localised at neuronal cell surfaces, with a particular concentration at points of intercellular adhesion, like synapses, a fact that underlines their role in building cellular junctions (Bekirov et al., 2002). At given points in development, in most tissues only one type of cadherin is expressed (Jessell, 1988). It is a well-known fact that different cadherin expression patterns influence the organisation and segregation of embryonic tissues in development (Ranscht, 1994). Classical cadherins normally show preferential adherence to cells expressing the same subtype of cadherins (=*homophilic* or *homotypic interaction*; Akins et al., 2007; Rivero et al., 2013; Jessell, 1988). Furthermore, they dissociate from cells with divergent cadherin expression (Redies et al., 2012). Heterotypic bonds can also occur under special circumstances, but show lower affinity (Jessell, 1988). The principle of homotypic adhesion could possibly support the segregation of different neuronal structures or layers (Akins et al., 2007), as well as the generation of specific synapses (Bekirov et al., 2002) and influence the migratory paths of early neurons (Redies et al., 2012). Accordingly, cadherins might not only work as *synaptic glue*, joining pre- and postsynaptic sites via tight adhesive connections, but also as *synaptic specifiers*, playing an important role in development of the nervous system (Bekirov et al., 2002; Huntley, 2002).

It is consistent with this idea that cadherins have been shown to participate in “neural tube regionalization, neuronal migration, grey matter differentiation, neural circuit formation, spine morphology, synapse formation and synaptic remodelling” (Redies et al., 2012). Consequently, disturbances in the cadherin system might severely impact brain function, synaptic connectivity and plasticity (Huntley, 2002; Redies et al., 2012).

In contrast to the function of classical cadherins**,** it can be supposed that the primary task of Cdh13 is not to establish intercellular junctions (Philippova et al., 2008). This theory is underlined by the observation that Cdh13 is not mainly located at cell-cell contacts or synapses (Rivero et al., 2013; Ranscht, 1994), but shows a punctate distribution all over the cell body, with preference to membrane lipid rafts (Philippova et al., 2005). Apart of the plasma membrane, though, the occurrence of Cdh13 has also been reported in other cellular compartments such as cytoplasm, nucleus or centrosomes (Mavroconstanti et al., 2013). In case of brain tissue damage, however, Cdh13 abandons its global superficial distribution and accumulates at the leading ends of migrating axons, possibly influencing their paths (Philippova et al., 2009). Indeed, atypical Cdh13 was found to act as a negative regulator of (motor) neuron outgrowth and axon guidance in embryonic development (Ranscht and Dours-Zimmermann, 1991; Redies, 1995; Philippova et al., 2008; Franke et al., 2009; Mavroconstanti et al., 2013). Its inhibitory effect on migrating neurons is achieved via homophilic interaction of membrane-bound or soluble Cdh13 molecules. This suggests that Cdh13 takes part in the cadherin-driven mediation of outgrowth and maintenance of distinct neuronal circuits in embryonic development (Rivero et al., 2013). Its expression in the developing nervous system (Takeuchi et al. 2000), however, showed much weaker concentrations than in adult CNS (Philippova et al., 2009). This fact supports the assumption that Cdh13 not only plays a role in establishing neuronal circuits, but also in maintaining them (Rivero et al., 2013).

1.2.4 Conclusion

Cadherin 13 is highly expressed in the CNS. Although it is counted as a member of the cadherin superfamily, it stands out in several aspects. The above-mentioned structural aberrations (cf. 1.2.1), explain why its signalling has to be facilitated by membrane lipid rafts and cannot result from intracellular interactions (cf. 1.2.2). Furthermore, they point to other than adhesive functions of Cdh13 in the CNS. Its highly conserved genetic sequence, however, suggests an important functional contribution. Cdh13 shows a punctate distribution all over the cell, which is abandoned only under specific circumstances (cf. 1.2.3). It then accumulates at the leading ends of migrating processes and negatively regulates their outgrowth and guidance. As for classical cadherins, one of the main mechanisms of this phenomenon is *homophilic interaction*. Thus it seems very likely that Cdh13 actively participates in the formation and maintenance of distinct neuronal circuits.

Given the regulatory involvement of Cdh13 in the guidance of migrating axons and the maintenance of synaptic circuits, it would not be surprising, if genetic alterations caused severe structural problems. This thesis examines possible Cdh13 functions, as well as consequences of its absence with regard to the serotonergic system. Therefore an understanding of this system is essential and will be provided in the following.

1.3 The mammalian serotonergic system

1.3.1 Serotonin – Discovery and function

Serotonin first appeared in literature as a molecule called *enteramine* in 1937, which had been extracted from enterochromaffin gut cells and showed the ability to cause smooth muscle cell contractions (Erspamer and Vialli, 1937). Independently, in 1948, a substance, which was able to increase vascular tonus, was found in mammalian serum and in consequence was given the name *serotonin* (Rapport et al.). It was only some years later that the identical nature of *enteramine* and *serotonin* could be chemically proven and was given the neutral name 5-hydroxytryptamine (5-HT, Erspamer and Asero, 1952). Its chemical structure is shown in Figure 1.2 and can be precisely described in chemical terms as 3-(β-aminoethyl)-5-hydroxyindole (Kim and Camilleri, 2000). The primary amine, which is connected to the aromatic indole ring by a two-carbon-chain (CH_2-CH_2), is typical for monoamines, a group that not only comprises serotonin, but also DA, NE and adrenalin (Benninghoff and Drenckhahn, 2008). The single hydroxyl group at the 5 position of the indole nucleus, as well as the primary amine group characterise it as a hydrophilic molecule. In consequence, 5-HT is incapable of passing the lipophilic blood-brain barrier, so that all central serotonin has to be synthesised in the CNS.

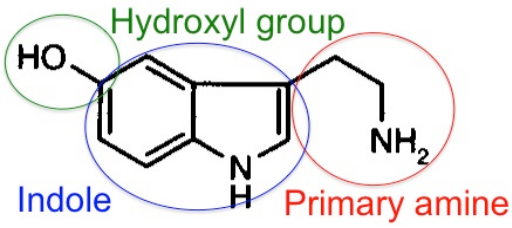

Figure 1.2 Chemical structure of 5-hydroxytryptamine (5HT; adapted from Frazer and Hensler, 1999). The amino group, which is connected to the aromatic indole ring by a two-carbon-chain (CH_2-CH_2), is typical for monoamines.

Today, 5-HT is known as one of the phylogenetically most ancient signalling molecules (Lesch and Waider, 2012), appearing in vertebrates, invertebrates (e.g. molluscs, arthropods or coelenterates), as well as in edible fruits or nuts, like the walnut (Kim and Camilleri, 2000). Thinking of its wide distribution in human brain (Lesch and Waider, 2012), it is quite astonishing, that 95% of all body 5-HT is actually found in enterochromaffin cells and neurons of the gut, and only 5% in the brain (Kim and Camilleri, 2000).

Outside the brain, Serotonin plays a role in a wide range of metabolic processes, like in vaso- and bronchoconstriction, in various gastrointestinal functions (e.g. peristalsis, intestinal secretion), in the liberation of histamine or adrenalin, as well as in the regulation of capillary permeability and platelet aggregation (Kim and Camilleri, 2000; Lang and Verrey, 2010).

In the adult CNS, it is involved in the endogenous analgesic system (Benninghoff and Drenckhahn, 2008), in the regulation of emotions, autonomic responses, e.g. food intake and arousal, as well as in motor activity and in sensory and cognitive processes, e.g. decision making (Sparta and Stuber, 2014; Lesch and Waider, 2012; Dorocic et al., 2014). In addition to that, 5-HT was among the first neurotransmitters, for which a role in neurodevelopment has been hypothesised (Gaspar et al., 2003). This idea is supported by the early presence of 5-HT in the CNS during embryogenesis (Deng et al., 2007) and its release by growing axons before synaptogenesis (Gaspar et al., 2003), observations, which suggest a regulatory impact on differentiation, cell migration and synaptogenesis in other neuronal systems (Deng et al., 2007). In addition to that, 5-HT was found to participate in proliferation and migration of early neurons, as well as in neurite outgrowth and axonal guidance (Gaspar et al., 2003; Riccio et al., 2009; Lesch and Waider, 2012). Given this overarching involvement in brain functioning, it is not surprising, that deficits in the serotonergic system increase the risk for diverse neurodevelopmental disorders, like depression, schizophrenia or ADHD (Lesch and Waider, 2012; Kim and Camilleri, 2000).

1.3.2 Synthesis and metabolism of serotonin

Contrary to expectations, not all cells that contain 5-HT are also able to synthesise it. This is true for platelets, which possess an active transporter, collecting 5-HT from the plasma (Frazer and Hensler, 1999), as well as for divers neurons in brain development (Gaspar et al., 2003). The biosynthesis of serotonin takes place in two consecutive enzymatic reactions, hydroxylation and decarboxylation, starting with the amino acid tryptophan (cf. Figure 1.3)

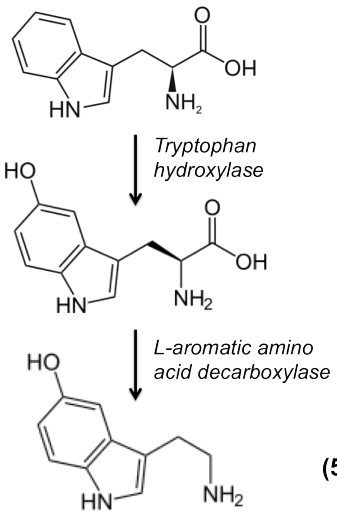

Figure 1.3 Biosynthesis of serotonin in the brain (adapted from Frazer and Hensler (1999) and Kim and Camilleri (2000)).
First, tryptophan is hydroxylated to 5-hydroxytryptophan (5-HTP) by the enzyme tryptophan hydroxylase. This reaction constitutes the rate-limiting step of the synthesis. Then 5-HTP is converted into 5-HT via decarboxylation, which is accomplished by the enzyme L-aromatic amino acid decarboxylase.

First, tryptophan is needed to cross the blood-brain barrier, which is facilitated by an unspecific carrier, also used by phenylalanine, leucine and methionine. This implicates that 5-HT synthesis in the CNS is not only influenced by the tryptophan concentration in the blood, but also by dietary habits, since tryptophan is *essential* and cannot be synthesized in our body, as well as by the concentration of the competing amino acids (Frazer and Hensler, 1999).

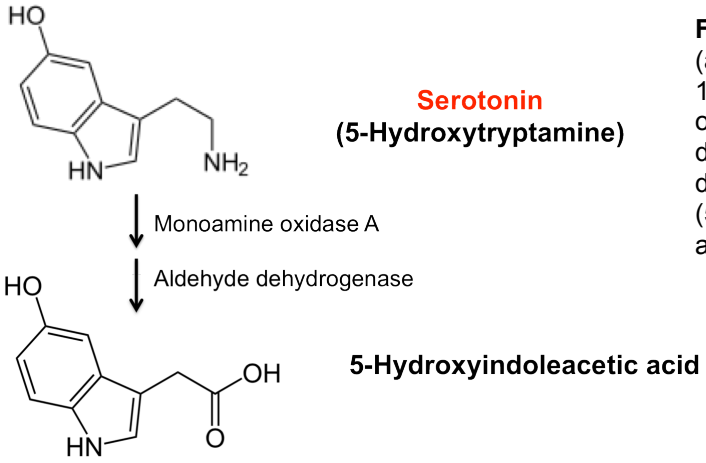

Figure 1.4 Degradation of serotonin (adapted from Frazer and Hensler, 1999). Two enzymes (monoamine oxidase A (MAO-A) and aldehyde dehydrogenase) are involved in the degradation of 5-HT. The product (5-HIAA= 5-hydroxyindoleacetic acid) is excreted with the urine.

In the following, a hydroxyl group is added to the indole ring of tryptophan by the enzyme tryptophan hydroxylase (Tph), thus converting it into 5-hydroxytryptophan (5-HTP). This hydroxylation constitutes the rate-limiting step of the 5-HT synthesis (Kim and Camilleri, 2000; Frazer and Hensler, 1999). Tph exists in two isoforms, one being specific for central (Tph2) the other for peripheral 5-HT synthesis (Tph1; Gutknecht et al., 2008). Since Tph2 is only

expressed in serotonergic neurons of the brainstem, this reaction can only take place there (Frazer and Hensler, 1999). Finally, 5-HTP is decarboxylated by the L-aromatic amino acid decarboxylase, leading to serotonin (Kim and Camilleri, 2000). Contrary to Tph2, this enzyme also exists in catecholaminergic neurons, where it catalyses the transformation of 3,4-dihydroxyphenylalanine (DOPA) to DA. Consequently, these neurons hold the potential, dependent on pH or substrate concentrations, to also synthesize 5-HT (Frazer and Hensler, 1999).

After synthesis the 5-HT molecules are actively transported into presynaptic vesicles and stored until the next action potential causes depolarisation and thus exocytosis into the synaptic cleft (Frazer and Hensler, 1999). In the dorsal raphe the release is limited by serotonin-triggered activation of the 5-HT_{1A} autoreceptor at the presynaptic membrane. This G-protein coupled receptor measures 5-HT release and launches a negative feedback mechanism to decrease the firing rate of serotonergic neurons (Lesch and Waider, 2012). On the postsynaptic membrane of other target neurons 5-HT binds to heteroreceptors. So far fourteen of these mostly metabotropic receptors (only 5-HT_3 is ionotropic) have been found and classified into seven families: 5-$HT_{1A/B/D/E/F}$, 5-$HT_{2A/B/C}$, 5-HT_3, 5-HT_4, 5-$HT_{5A/B}$, 5-HT_6 and 5-HT_7 (Waider, 2008; Kim and Camilleri, 2000). RNA editing and alternative splicing mechanisms further increase the diversity of these receptors, thus creating varying affinities (Paul and Lowry, 2013). Serotonin's high-affinity reuptake from the synaptic cleft is regulated by the plasmalemmal 5-HT transporter (5-HTT or SERT; Lesch and Waider, 2012), which is in possession of twelve transmembrane domains. This mechanism represents the primary way of 5-HT inactivation in the central, as well as in the peripheral nervous system (PNS), and constitutes the point of action of the antidepressant selective serotonin reuptake inhibitors (SSRI), like fluoxetine (Kim and Camilleri, 2000). Back in the pre-synapse 5-HT can be either repacked into vesicles by vesicular membrane transporters 1 and 2 (VMAT 1/2) or it can be rapidly degraded by the enzymes monoamine oxidase A (MAO-A) and aldehyde dehydrogenase, which is illustrated in Figure 1.4.

Like Tph2, MAO exists in two isoforms: A and B. Though 5-HT is preferentially metabolized by MAO-A, serotonergic cells contain more MAO-B than MAO-A –

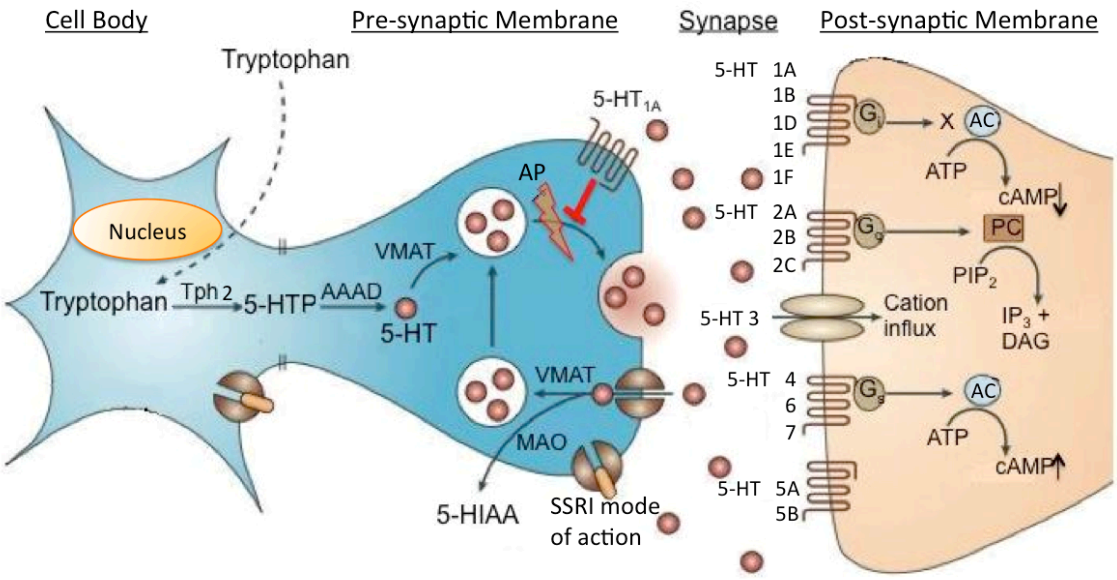

Figure 1.5 Metabolic processes in serotonergic neurons and synapses (adapted from Jonas Waider, Doktorarbeit, 2012)**.** After having been synthesised out of tryptophan, 5-HT is packed into pre-synaptic vesicles. Incoming action potentials (AP) trigger its release into the synaptic cleft, a reaction that is negatively regulated by 5-HT_{1A} autoreceptor stimulation. In the following, binding to post-synaptic heteroreceptors activates various signal cascades. High-affinity reuptake is controlled by SERT. Selective serotonin reuptake inhibitors (SSRI), which act as antidepressants, can inhibit SERT and thus prolong synaptic 5-HT effects. Back in the pre-synapse, VMAT store the transmitter in vesicles or MAO degrades it to 5-HIAA. AAAD= L-aromatic amino acid decarboxylase, AC= adenylate cyclase, ATP= adenosine triphosphate, cAMP= cyclic adenosine monophosphate, PIP_2= phosphatidylinositol 4,5-biphosphate, IP_3= inositol triphosphate, DAG= diacylglycerol, PC= phospholipase C

The above-mentioned meanings of AP and PC are only valid for this figure. For all other contexts the list of abbreviations at the end of this thesis is to be consulted.

an observation that can be extended to the enzymes' distribution in human CNS. In case of absence of MAO-A, the degradation of 5-HT can also be catalysed by MAO-B (Frazer and Hensler, 1999). 5-Hydroxyindoleacetic acid (5-HIAA), which is the primary product of this reaction in the brain, is eliminated with the urine (Kim and Camilleri, 2000). Figure 1.5 presents an overview of the above-described processes in the serotonergic system.

1.3.3 Development and structure of the serotonergic system

Due to the extensive research of Alonso et al. (2013), many previously well-acknowledged facts concerning structure and compartmentation of the murine hindbrain, had to be revised. For the following structural explanations, this work and the Allen Brain Atlas (ABA) constitute the central references.

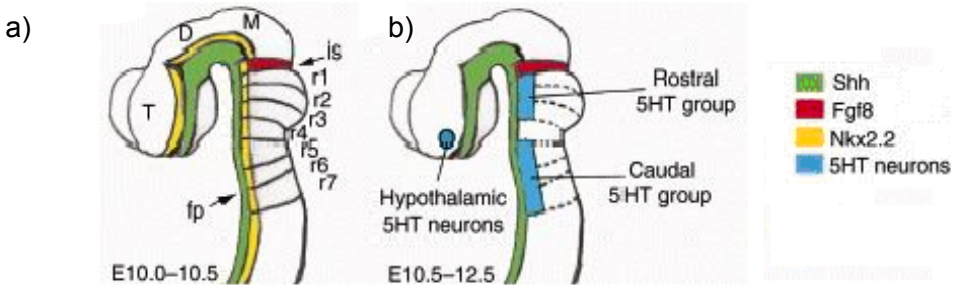

Figure 1.6 Mid-sagittal views on the embryonic anlage of the mouse brain. The 5-HT system develops in two waves (adapted from Cordes, 2005). At E 10-10.5 (a) the first neurons form near the floorplate (fp) and later (b) migrate to form rostral and caudal cell clusters. Differentiation and movement are regulated by a Shh signalling pathway. At that stage of embryogenesis the hindbrain is subdivided into 12 compartments – 11 rhombomeres (r) and the isthmus (Is), separating them from the midbrain (M). According to the findings from Alonso et al. (2013), r7-11 should not be encompassed in one big rhombomere, but treated as molecularly distinguishable hindbrain subunits. D= diencephalon, T= telencephalon

In early embryogenesis, the hindbrain consists of 12 “transverse neuromeric units” (Alonso et al., 2013), referred to as rhombomeres (r1-11) and isthmus (Is/r0), which subdivide it along its rostro-caudal axis. Some papers encompass Is and r1 or r8-r11, respectively, as singular big rhombomeres, although they can be distinguished precisely by their characteristic genetic profiles. It can be differentiated between prepontine (Is, r1), pontine (r3, r4), pontomedullary or retropontine (r5, r6), as well as medullary (r7-r11) hindbrain subregions (Alonso et al., 2013; ABA).

The formation of serotonergic precursor cells starts very early in development in the ventral hindbrain area of the mammalian brainstem (Gaspar et al., 2003; Donovan et al., 2002; Deng et al., 2007). 5-HT neurons are generated in two waves: the first one takes place around E9.5-E10.5, the second one between E10.5-E12.5 (cf. Figure 1.6). They develop bilaterally in proximity of the floorplate (fp), which constitutes the midline of the neural tube (Jensen et al., 2008; Cordes, 2005), and later migrate by somal translocation (Hawthorne et al., 2010) to form two distinct cell clusters. The rostral one (Is-r4), however, forms about 1-2 days (d) before the caudal one (r5-r11; Lowry et al., 2008; Alonso et al., 2013). Their differentiation and migration is steered by a complex cascade of signalling molecules induced by sonic hedgehog (Shh). Cells of notochord and fp produce this regulator of vertebrate organogenesis (Cordes, 2005). It acts in concert with the fibroblast growth factors Fgf2, Fgf4 and Fgf8.

Since the latter is emitted from the Is, it only influences rostral 5-HT neurons (Gaspar et al., 2003). These mediators act on the zinc-finger transcription factors Gli2 and Gli3 and induce differentiation and serotonergic cell fate dose-dependently. Further downstream of this cascade, factors like Nkx2.2 and Ascl1/Mash1 are activated and act on the transcription factors GATA 2/3, thus regulating 5-HT neurogenesis. GATA 2 is required for 5-HT neuron development all over the hindbrain, while GATA 3 only influences the more caudal cells (Cordes, 2005). These regulating factors trigger the consecutive expression of the homeobox gene *Lmx1b* and the ETS domain transcription factor *Pet1* (Gaspar et al., 2003; Hawthorne et al., 2010). Both play an important role in migration, initial differentiation, as well as in maturation and determination of the neurochemical phenotype of 5-HT neurons (Cordes, 2005; Lesch and Waider, 2012; Liu et al., 2010). In absence of Pet1, which is at all developmental stages "strictly limited to the raphe nuclei" (Hendricks et al., 1999; Gaspar et al., 2003) and can normally be detected 6-12h before 5-HT production, about 70-80% of serotonergic cells fail to develop (Cordes, 2005; Andrade and Haj-Dahmane, 2013). The same applies to *Lmx1b*$^{-/-}$ mice, where nearly 100% are affected (Cordes, 2005). Figure 1.7 summarises the explained signalling cascades.

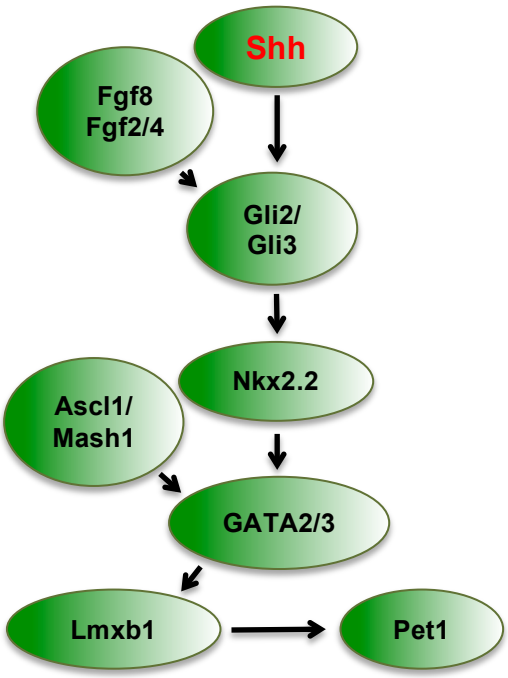

Figure 1.7 Sonic hedgehog signalling pathway in the development of 5-HT neurons (adapted from Cordes (2005) and Gaspar et al., 2003).

Altogether, serotonergic cells account for a very small fraction of all central neurons: in rats they only provide about 20.000 5-HT neurons out of a total amount of 10^{10} (Gaspar et al., 2003). The majority of 5-HT cells are organised in two clusters between the mesencephalic and the pontine flexure (Cordes, 2005; Wallace and Lauder, 1983) and thus mostly limited to the hindbrain. Only

small fractions can be found in adjacent caudalmost midbrain (mesomere 2) and rostral spinal cord (Alonso et al., 2013).

Table 1.1 New nomenclatures of the raphe nuclei in adult mice (adapted from Alonso et al., 2013). They form a rostral cluster, comprising B9-B5 (underlined), and a caudal one with B3-B1 (italic). Whilst the first is located in the area of Is-r4, the latter can be found in r5-r11.

Terminology according to Alonso et al. (2013)	**Subunits**	**Alpha-numeric terminology**	**Traditional terminology**
Dorsal raphe nn. (DR)	mDR isDR r1DR	B7 B6	Dorsal raphe n. DRD/ DRV/ DRVL/ DRL/ DRI/ DRC
Caudal linear n. (CLi)	IsCLi IsCLiW	B8	Caudal linear n.
Median raphe nn. (MnR)	r1MnRr r1MnRc		Central superior raphe n.
Prepontine raphe nn. (PPnR)	r2PPnR		
Supralemniscal raphe nn. (SuLR) Lateral extension from MnR	r1SuLR r2SuLR r3SuLR	B9	Supralemniscal n.
Pontine raphe nn. (PnR) Caudal extension from MnR	r3PnR (r4PnR)	B5	Raphe pontis n.
Supragenual raphe nn. (GeR)	r5SGeR r6SGeR	B4	Extraraphe cells
Raphe magnus nn. (RMg)	r5RMgD r6RMgD r5RMgV r6RMgV	*B3*	Raphe magnus n.
Parapyramidal raphe nn. (RPPy)	r5RPPy r6RPPy		
Raphe obscurus nn. (ROb)	r7-r11ROb	*B2*	Raphe obscurus n.
Raphe pallidus nn. (RPa)	r7-r11RPa	*B1*	Raphe pallidus n.
Parapyramidal raphe nn. (Medullary parts; RPPy)	r7-r11RPPy		

The main part of the rostral cluster lies below the mesencephalic flexure in (pre-) pontine hindbrain (Hendricks et al., 1999). It precedes the caudal one in 5-HT cell presence by 1-2 days (Wallace and Lauder, 1983). During development, migrating 5-HT neurons gradually form nine distinct groups (Lesch and Waider, 2012), developing as “bilateral nuclei” (Levitt and Moore, 1978). Between E 18 and postnatal day (P) 6, six of them fuse in the midline,

following a rostrocaudal gradient, while the later B9, B6 and B3 remain paired (Levitt and Moore, 1978). The nuclei are later referred to as *raphe nuclei* (raphe (Gr.)= fold/ seam) or as B1-B9, respectively (Cordes, 2005).

The rostral cluster (B9-B4; Jensen et al., 2008) is formed by the dorsal raphe nucleus (DR), together with the median raphe nucleus (MnR) and the caudal linear nucleus (CLi), which lies in the paramedian intermediate isthmic tegmentum (Tg). Also contributing are the supralemniscal raphe nucleus (SuLR) and the (pre-) pontine raphe nuclei ((P)PnR), building lateral and caudal extensions, respectively, to the MnR. The DR, which corresponds to B6 and B7, is the most extensive one of the raphe nuclei, also showing the highest cell density. Lying mostly in the paramedian periventricular stratum of the prepontine hindbrain, it reaches from caudalmost midbrain (mDR) over the isthmus (IsDR), where most of its cells are located, into r1 (r1DR; Alonso et al., 2013; Cordes et al, 2005). This disagrees with former convictions, where most of it was assigned to the midbrain (Alonso et al., 2013). Apart from this anatomically oriented tripartition, the DR can also be differentiated into dorsal (DRD), ventral (DRV), ventrolateral (DRVL), lateral (DRL), caudal (DRC) and interfascicular (DRI) subregions (Lowry et al, 2008; Brooks et al., 2014). The DR and its ascending projections constitute the main source of brain 5-HT (Soiza-Reilly & Commons, 2014). The MnR, corresponding to B8, lies in the paramedian intermediate stratum of r1. The SuLR (=B9) extends to r3, constitutes its lateral extension, whereas the (P)PnR (or B5) ranges from r2-r3 and thus constitutes the caudal extension. R4 marks the border between the two clusters (Andrade and Haj-Dahmane, 2013) and is devoid of 5-HT neurons (Wylie et al., 2010). Alonso et al. (2013) discovered some Pet1-immunoreactive (ir) cells in r4, however, without the ability to produce 5-HT (Tph2-negative). This is why they are not considered mature serotonergic neurons in this thesis.

The caudal cluster (B1-B3) lies below the pontine flexure in (ponto-) medullary hindbrain (Hendricks et al., 1999) and consists of the raphe pallidus nucleus (RPa), the raphe obscurus nucleus (ROb) and the raphe magnus nucleus (RMg) (Cordes, 2005; Alonso et al., 2013). The RMg is the most rostral one of these nuclei and lies in the superficial and intermediate paramedian strata of r5

and r6. The ROb and RPa, however, are located caudal to the RMg in the medulla. They extend from r7 to r11, lying paramedian in the intermediate (ROb) and superficial stratum (RPa), respectively. The parapyramidal raphe nuclei (RPPy, which also contribute to the caudal cluster, lie laterally in the superficial stratum and reach from r5-r11 (Alonso et al., 2013).

It is to be noted, that not all cells within the raphe nuclei are serotonergic. For instance the DR contains only 40-50% of 5-HT neurons, the MnR only 20-30% (Dorocic et al., 2014; Frazer and Hensler, 1999). Table 1.1 and Figure 1.8 give an overview of the above-described anatomic distinctions.

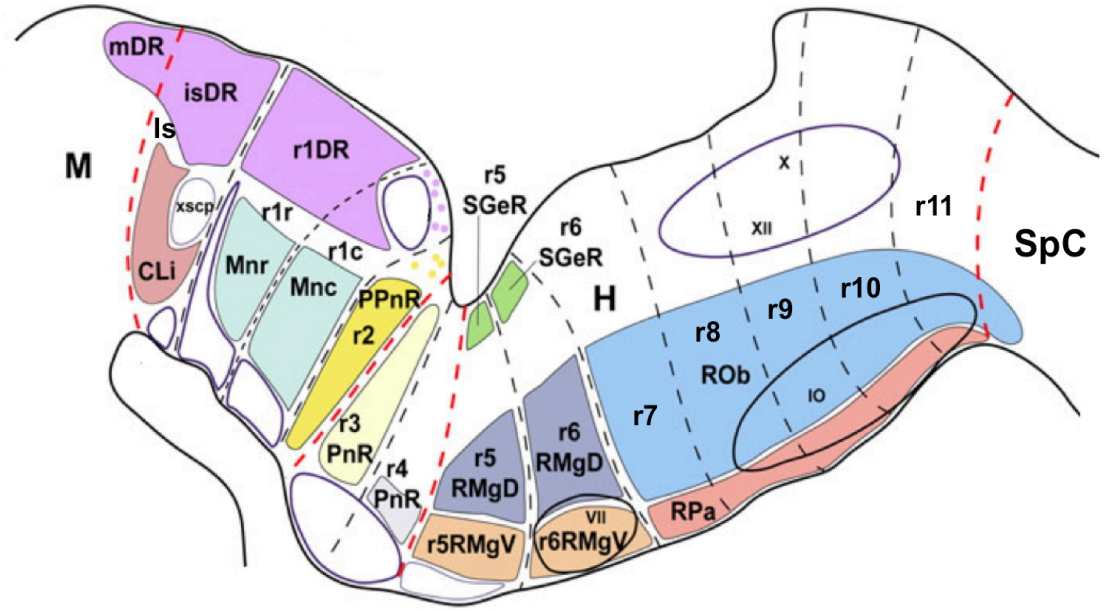

Figure 1.8 The raphe nuclei in relation to their corresponding neuromeric units. The image shows a paramedian sagittal section of adult murine hindbrain (adapted from Alonso et al., 2013; with kind permission of Mr. Luis Puelles). The rostral cluster consists of the DR with its mesencephalic, isthmic and r1 part, the CLi, the rostral (r1r) and caudal (r1c) MnR, as well as the r3PnR as its caudal extension. The caudal cluster consists of the RMg, RPa and ROb, extending from r5-r11. The lateral parts (CLiW, SuLR, RPPy) are not displayed. Due to its Tph2-negativity, the r4PnR is not counted as a collective of mature 5-HT neurons in this thesis. M= midbrain, H= hindbrain, SpC= spinal cord, xscp= decussation of the superior cerebellar peduncle, VII/X/XII= corresponding cranial nerve nuclei, IO= inferior olivary nucleus,

1.3.4 Serotonergic projections

During development the rostral and caudal cell clusters send out a multitude of projections with different destinations (cf. Figure 1.9). Even though only a relatively small number of central 5-HT neurons exist, they grow out to establish a complex network, which interlinks almost the entire neuroaxis, by extensive

collateralisation (Gaspar et al., 2003; Brüning et al., 1997; Andrade and Haj-Dahmane, 2013). The caudal part provides descending projections mainly to the spinal cord, taking part in the regulation of nociception, movement and autonomic functions, like thermoregulation (Wylie et al., 2010; Lesch and Waider, 2012). Afferent 5-HT projections of the rostral cluster, however, ascend via at least six distinct pathways (Azmitia and Segal, 1978). Destinations are cerebellar sites, as well as virtually all forebrain regions (e.g. cerebral cortex, amygdala, hippocampus, hypothalamus, and basal forebrain; Levitt and Moore, 1978; Cordes, 2005), where they take part in the regulation of emotional response and circadian rhythms (Wylie et al., 2010).

Two out of six ascending pathways – the dorsal raphe forebrain tract (DRFT) and the median raphe forebrain tract (MRFT) – travel within the medial forebrain bundle (MFB, Lowry et al., 2008), which comprises a multitude of ascending and descending projections, connecting forebrain and midbrain regions (Azmitia and Segal, 1978). The dorsal raphe cortical tract (DRCT) runs ventrolateral to the medial longitudinal fascicle towards putamen and parieto-temporal cortex. The dorsal raphe periventricular tract (DRPT) lies beneath the midbrain aqueduct and ascends to (hypo-)thalamic regions. Furthermore, the dorsal raphe arcuate tract (DRAT) runs at the ventrolateral edge of the midbrain and reaches geniculate body nuclei, as well as suprachiasmatic nuclei. Finally, the raphe medial tract (RMT) originates in both, the DR and the MnR, and travels between the fasciculi retroflexus, heading towards the interpeduncular and mammillary nuclei (Lowry et al., 2008). The tracts follow a topographic pattern, with the MnR fibres predominantly projecting to hippocampus, septum and hypothalamus and the DR ones to basal ganglia and amygdala. The nuclei not only differ in their destinations, but also in their fibre morphologies with the DR having finer axon terminals and varicosities than the MnR (Wilson and Molliver, 1991). Both raphe nuclei innervate the neocortex in an overlapping manner (Frazer and Hensler, 1999). Serotonergic fibres range among the first ones to innervate selected forebrain areas (Donovan et al., 2002): They travel through basal diencephalon at E13, reach the septal complex at E15 (Brüning et al., 1997) and finally arrive at the rodent cortex by E16.5, which corresponds to

gestational week ten in humans (Riccio et al., 2009; Deng et al., 2007; Janusonis et al., 2004). Full maturation of this complex network with the formation of 5-HT synapses, however, is only achieved after birth (Brüning et al., 1997; Gaspar et al., 2003).

Given the above-mentioned (cf. 1.3.3/4) differences between the rostral and caudal 5-HT cluster, it is not surprising, that whole genome profiling recently indicated that they arise from implementation of two different genetic programs (Andrade and Haj-Dahmane, 2013). There is growing evidence that they enrich different gene sets and thus follow diverging molecular and biological pathways in their differentiation and specification (Wylie et al., 2010; Cordes, 2005). Consequently, they are to be treated as “distinct classes of serotonergic neurons” (Andrade and Haj-Dahmane, 2013).

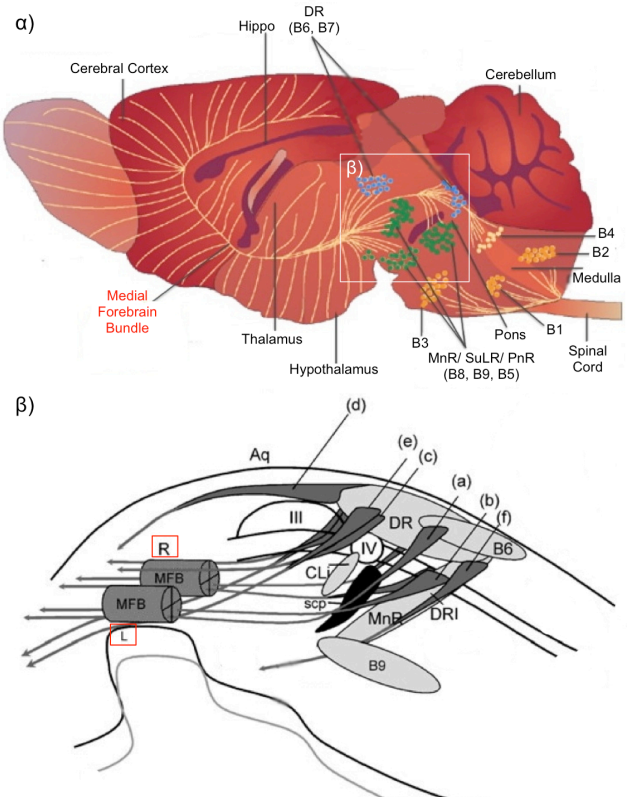

Figure 1.9 Schematic presentations of the raphe nuclei and their forebrain projections (adapted from Murphy and Lesch, 2008 (α) and from Lowry et al., 2008 (β)). The nuclei build a rostral (B9-B4) and a caudal cluster (B3-B1). The first comprises the DR, (blue), the CLi, as well as the MnR (green) and its extensions (SuLR/ PnR). At least six fibre tracts ascend from these nuclei. The DRFT (a) and MRFT (b) are the only ones travelling within the right (R) and left (L) medial forebrain bundle (MFB). The DRCT (c) runs ventrolateral to the medial longitudinal fascicle, the DRAT (e) through the ventrolateral edge of the midbrain. The DRPT (d) is located below the midbrain Aq and the RMT (f), originating from both, DR and MnR, lies between the fasciculi retroflexus. The caudal cluster (orange) sends projections to medulla and spinal cord. Aq= aqueduct, III/ IV= 3rd/4th cranial nerve nuclei, scp= superior cerebellar peduncle

1.3.5 Conclusion

The serotonergic system is one of the most extensive central neurotransmitter systems, already developing very early in embryogenesis. With Tph2 being exclusively present in the raphe nuclei, 5-HT-synthesis is limited mostly to this

area (cf. 1.3.2). Taking their origin in the rostral and caudal raphe clusters, ascending and descending projections grow out into various brain regions (cf. 1.3.3), and contribute – at least in parts – to the MFB. Thus an extensive network is formed with Pet1 being one of the major motors. Like that the 5-HT system is able to impact differentiation, cell migration and proliferation, as well as synaptogenesis in other neuronal systems at an early stage (cf. 1.3.1). Given its huge influence on forming central neuronal structures, it seems self-evident that disturbances might result in neurodevelopmental disorders (cf. 1.1.1).
Since 5-HT is generally assumed to play a major role in ADHD and Cdh13 might be a possible susceptibility gene (cf. 1.1.2.4), the idea has been raised, that disturbances in these systems might be related and together provoke errors in CNS development. One way to explore this possibility is the generation of Cdh13 knock out mice, which was also performed in the course of this thesis and is explained in 2.2.2.

1.4 Aim of the thesis

Cdh13 is suspected to play a role in ADHD genetics. With the serotonergic system being of major importance for this condition, as well as for related psychiatric diseases, this thesis focuses upon Cdh13 expression in 5-HT neurons of the raphe nuclei. Given the suggested influence of Cdh13 on neuron outgrowth and path finding during development, the main question will be, whether the absence of Cdh13 has an impact on the developing circuitry of the central serotonergic system and its axon outgrowth from the rostral raphe nuclei towards cortical targets.
In order to answer this question, the first step will be to establish a specific staining method for Cdh13, using immunohistochemistry. With the help of Cdh13 WT, HZ and KO mouse models, the above-stated hypothesis will be investigated in three different developmental stages (E13.5, E17.5, P7). Therefore mouse brains will be double-stained for Cdh13 and 5-HT. In a different approach, Cdh13 will be co-visualised with Pet1-promoter driven eGFP-expression. Examination under the confocal microscope might provide interesting information concerning the exact localisation of Cdh13 in or around

5-HT neurons, thus increasing the specificity of the results by distinction between overlay and real co-expression. Like this more detail on Cdh13 function and protein distribution pattern could be learned.

Furthermore, in order to determine the proportion of immature to mature 5-HT cells at certain stages, as well as to visualise the migration of 5-HT cells from the floor plate to their final destinations in hind- and midbrain during their maturation, Cdh13 WT, HZ and KO brains will be double stained with Tph2 and doublecortin (DCX), a marker for serotonergic precursor cells. Additionally, the amount and distribution of mature, as well as of immature cells will be quantified in the different genotypes, in order to carve out a possible Cdh13 influence.

Hopefully, the achieved results will contribute to a better understanding of ADHD on a molecular and cellular level and help to create new opportunities for its effective treatment in the future.

2. Materials and Methods

2.1 Materials

2.1.1 Oligodeoxynucleotide primers for mouse genotyping via PCR

CRE-L-F:	5’ – GCG CGG TCT GGC AGT AAA AAC – 3’
CRE-L-R	5’ – CGC CGC ATA ACC AGT GAA ACA – 3’
Cdh13 – F	5’ – TGG TTC TGC TCC AAG ACT CAG – 3’
Cdh13 – R	5’ – CCA GGA AGA GAT AAA GCC AGG – 3’
Cdh13 – RRic	5’ – ATT AGG GAC TAT CCT GGG CTA – 3’
IL-2-F	5’ – CTA GGC CAC AGA ATT GAA AGA TCT – 3’
IL-2-R	5’ – GTA GGT GGA AAT TCT AGC ATC ATC C – 3’
JAX egfp 3	5’ – TCC TTG AAG AAG ATG GTG CG – 3’
JAX egfp 5	5’ – AAG TTC ATC TGC ACC ACC G – 3’

2.1.2 Consumables

Beaker glasses (100/ 150/ 200ml/ 1l/ 2l/ 3l)	DURAN Group GmbH, Wertheim, Main
Biosphere filter tips (0.5-20µl/ 2-100µl/ 2-200µl/ 1250µl)	Sarstaedt, Nümbrecht
Combitips® Plus (2.5ml, 1=50µl)	Eppendorf GmbH, Hamburg
Erlenmeyer flasks (250/300/500/1000ml)	DURAN Group GmbH, Wertheim am Main
Gel combs (12/ 16/ 20 teeth)	Peqlab Biotechnology GmbH, Erlangen
Gel systems	Peqlab Biotechnology GmbH, Erlangen
Multiply®-µStripPro PCR-Tubes 0,2 ml	Sarstedt, Nümbrecht

Pipettes (0.5-10µl/ 10-100µl/100-1000µl)	Eppendorf GmbH, Hamburg
Reagent and centrifuge tubes (15ml/ 50ml)	Sarstaedt, Nümbrecht
Safe-lock Eppendorf tubes (1.5/ 2ml)	Eppendorf GmbH, Hamburg
SuperFrost®Plus Slides	R.Langenbrinck, Emmendingen

2.1.3 In-house produced Buffers and Solutions

All purchased ready-made substances that have been applied in these experiments are listed in 5.4 of the appendix.

Buffers and solutions for cell lysis, polymerase chain reaction and gel electrophoresis

Lysis-Buffer for mouse-tail tips	3,33ml of 1,5M Tris-HCl (pH 8.5) + 0,5ml of 0,5M EDTA (pH 8) + 2,0ml of 5,0M NaCl + 0,5ml of 20% SDS ad 50ml with Merck H_2O
Ethanol (70%)	35ml of 100% EtOH ad 50ml with Merck H_2O
25xTAE-Running-Buffer (stock solution)	121g Tris-Base + 50ml EDTA (pH 8) + 28,5ml Acetic Acid ad 1l with ddH_2O
1xTAE-Running-Buffer (working solution)	400ml 25xTAE-Buffer ad 10l with ddH_2O

Gel loading Buffer ("blue buffer")	10mM Tris-HCl (pH 7.6) 0.25% Bromine phenol blue 0.25% Xylene cyanol dye 15.0% Glycerol	
10mM/ *25mM* $MgCl_2$	1M KCl 1M Tris-HCl, pH 8,3 0,1M $MgCl_2$ 10%Tween 20 ad 1ml with ddH_2O	500µl 100µl **100µl**/*250µl* 25µl
10x Goldstar	750mM Tris-HCl (pH 7.6) 200mM Ammonium sulphate 0.1 % Tween-20	
2,5mM Nucleotides	each 40mM stock solution for dATP, dGTP, dCTP and dTTP was diluted 1:4 and these 10mM solutions were mixed in equal shares to get a 2.5mM working solution	

Buffers and solutions for immunohistochemistry

Gelatine solution	1,05mg Gelatine A (3%) solubilised in 350ml ddH_2O (stirred at 60°C until completely dissolved) + 0,175mg chrome (III) potassium sulphate (0.5%)
Citrate Buffer (pH 6)	1,92g of 10mM Citric Acid dissolved in 1000ml of ddH_2O + 0.5ml of Tween 20 (pH 6,0 titrated with 1M NaOH/ storage at 4°C)
1xTBS (pH 7,5)	60,5g TRIS + 43,8g NaCl solubilised in 4500ml ddH_2O, pH 7,5 titrated with about 80ml of 5M HCl, ad 5000ml with ddH_2O

1xPBS	200ml 10xPBS ad 2000ml with ddH_2O
H_2O_2 (0.3%)	30% H_2O_2 diluted 1:100 with MetOH
NHS/ NGS/ NDS (10%)	1.5ml NHS/ NGS/ NDS ad 15ml with 1xTBS
NHS/ NGS/ NDS (5%)	10% NHS/ NGS/ NDS diluted 1:2 in 1xTBS
ABC solution	reagent A and reagent B each diluted 1:100 in 1xTBS
Fluorophore tyramide (working solution)	stock solution diluted 1:100 in 1x amplification diluent (out of TSA-Kit)
DAB solution	DAB diluted 1:10 in DAB Substrate
DAPI (14.3mM) (stock solution)	10mg of DAPI were dissolved in 2mL of ddH_2O
DAPI (300nM) (working solution)	DAPI stock solution was diluted to 300nM in 1xPBS
EtOH (70%)	15ml Merck H_2O + 35ml 100%-EtOH
Xylene (50%)	40ml Isopropanol + 40ml 100%-Xylene

Buffers and solutions for mouse tissue preparation

PFA (4%)	3,2g PFA dissolved in 80ml 1xPBS (at 60°C/ pH 7.5)
Sucrose solution (20%)	16g Sucrose solubilised in 80ml 1xPBS
Sucrose solution (10%)	25ml Sucrose solution (20%) + 25ml 1xPBS

2.1.4 Antibodies for Immunohistochemistry

Primary antibodies

Table 2.1 Primary antibodies used for immunohistochemical staining

Antibody	Host species	Clonality	Reactivity	Supplier
Anti-DCX	Goat	Polyclonal	Mouse, rat, Human	Santa Cruz Biotechnology, Inc., Santa Cruz, U.S.A.
Anti-Cdh13	Goat	Polyclonal	Human, mouse	R&D Systems GmbH, Wiesbaden-Nordenstadt
Anti-Tph2	Rabbit	Polyclonal	Human, rat, mouse	In-house production
Anti-eGFP	Chicken	Polyclonal	Aequorea victoria	Abcam pic, Cambridge, UK
Anti-5-HT	Rabbit	Polyclonal	Mouse, rat	Merck-Millipore KGaA, Darmstadt

Secondary antibodies

Table 2.2 Secondary antibodies used for immunohistochemical staining

Antibody	Host species	Dilution	Supplier
Anti-goat Alexa 555	Donkey	1:400	Life Technologies GmbH, Darmstadt
Anti-goat biotinylated	Horse	1:400/ 1:800	Vector Laboratories Inc., Burlingame, U.S.A
Anti-rabbit Alexa 488	Donkey	1:400	Life Technologies GmbH, Darmstadt
Anti-rabbit DyLight 488	Donkey	1:400	Jackson ImmunoResearch Laboratories, Inc., West Grove, PA, U.S.A
Anti-rabbit Alexa 555	Goat	1:400	Life Technologies GmbH, Darmstadt
Anti-chicken Alexa 488	Goat	1:400	Life Technologies GmbH, Darmstadt
Anti-chicken Alexa 488	Donkey	1:1000	Life Technologies GmbH, Darmstadt

2.1.5 Equipment

Benchtop centrifuge MIKRO 220 R (for lysis)	Hettich Lab Technology, Tuttlingen
Biometra Electrophoresis Powerpack P24	Biometra GmbH, Göttingen
Cryostat CM 1950	Leica Mikrosysteme Vertrieb GmbH, Wetzlar
Consort Electrophoresis Power Supply E835	Sigma-Aldrich Chemie GmbH, Steinheim
Consort Electrophoresis Power Supply E844	Peqlab Biotechnology, Erlangen
Gene Power Supply GPS 200/400	Pharmacia, Freiburg
FluoView FV1000 confocal microscope	Olympus GmbH, Hamburg
Hot Plate/ Magnetic Stirrer IKAMAG®RCT	IKA®-Werke GmbH & Co. KG, Staufen
Hot Plate/ Magnetic Stirrer MR Hei-Tec	Heidolph Instruments GmbH & Co. KG, Schwabach
Hot Plate/ Magnetic Stirrer Model L-81	Labinco BV, DG Breda, NL
Microspin FV-2400	Schmidt Laborgeräte und Umweltsimulationen, Wien, A
Microwave R-239	Sharp Electronics GmbH, Hamburg
Molecular Imager ChemiDoc XRS System (Gel documentation System)	BioRad Laboratories GmbH, München
NanoDrop® ND-1000 Spectrophotometer	Peqlab Biotechnology, Erlangen
Neurolucida Microscopy System	MicroBrightField, Magdeburg
Olympus BX51 Fluorescence Microscope (CX9000 Camera)	Olympus GmbH, Hamburg
Olympus IX81 Microscope (XM10 Camera)	Olympus GmbH, Hamburg
PCR-Gradient-Professional Thermocycler	Biometra GmbH, Göttingen
PCR-T1-Thermocycler	Biometra GmbH, Göttingen
pH/ORP-Meter HI 2211	HANNA Instruments GmbH, Kehl

Shaker HS 501 digital (in 4°C storage room)	IKA®-Werke GmbH & Co. KG, Staufen
Shaker VXR basic Vibrax®	IKA®-Werke GmbH & Co. KG, Staufen
UNO II Thermoblock	Biometra GmbH, Göttingen
Water bath	Memmert GmbH, Schwabach
Weighing balance BP 1200	Sartorius AG, Göttingen
Weighing balance Mettler PM300	Mettler-Toledo GmbH, Gießen

2.1.6 Software

Adobe® Photoshop®	Adobe Systems GmbH, München
CellSens Dimension 1.4 (2010)	Olympus GmbH, Hamburg
Graphic Converter 9.7.1 (2045)	Lemke Software GmbH, Peine
Microsoft Office 2010	Microsoft Deutschland GmbH, Unterschleißheim
Microsoft PowerPoint for mac 14.0 (2011)	Microsoft Deutschland GmbH, Unterschleißheim
Neurolucida 10.52 (32 bit)	MicroBrightField, Magdeburg
NanoDrop-1000 V 3.8.1	Peqlab Biotechnology, Erlangen
Quantity One-4.3.1	BioRad Laboratories, München
ImageJ 1.42q	RSB/ NCBI, Rockville Pike, USA
LAS AF 2.6.0 7266	Leica Mikrosysteme Vertrieb GmbH, Wetzlar
LAS AF lite	Leica Mikrosysteme Vertrieb GmbH, Wetzlar

2.2 Methods

2.2.1 Animals

Animal protocols have been approved by the boards of the University of Würzburg and the government of Lower Franconia, and performed according to the European Community guidelines for animal care and use (DL 116/92, application of the European Communities Council Directive 86/609/EEC). They were kept in the Animal Core Facility at the University Hospital of Würzburg on a regular 12h light/12h dark cycle in a temperature (21±1°C) and humidity (50±5%) controlled environment. Food and water were provided *ad libitum*.

For the experiments animals from the B6.Cdh13ko-hCMV and the B6.Pet1-cre.eGFP lines were used. In order to breed mice with varying Cdh13 genotypes, a $Cdh13^{+/+}/eGFP^{+}/Cre^{-}$ male from the B6.Pet1-cre.eGFP line and a $Cdh13^{-/-}$ female from the B6.Cdh13ko-hCMV line were chosen to form the parental generation (P). Their offspring (referred to as the F1 generation) consisted of twenty-three mice, among them seven $Cdh13^{+/+}$ (WT) and sixteen $Cdh13^{+/-}$ (HZ) mice. From the latter, six females were consecutively crossbred with one Cdh13 HZ male, building the F2 generation. The use of heterozygote animals for the breeding allows controlling for any potential effects of genotype on maternal care, and ensures an appropriate distribution of the different genotypes among the litters to be used for experiments. Pregnancy was confirmed by the presence of a vaginal plug after copulation and the embryonic age of the offspring was determined with the day of plug detection being defined as 0.5d. In this way, E13.5 and E17.5 embryos, as well as P7 mice were bred. Figure 2.1 illustrates the described pedigree. Unfortunately, only four of the resulting litters could be

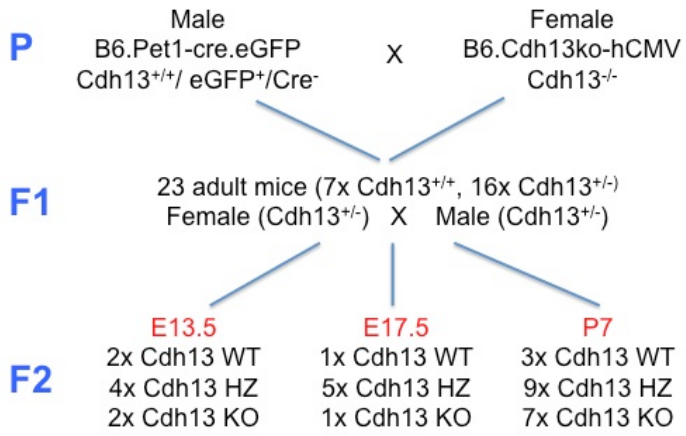

Figure 2.1 Pedigree of the experimental mice

used due to aggressive perfusion techniques, which damaged the tissue. From each of the E13.5 and E17.5 collectives four embryos (1xWT, 1xKO, 2xHZ) were sectioned and used for staining. From P7 seven mouse brains (2xWT, 4xHZ, 1xKO) were treated alike. Additionally, several single slides from eGFP+/Cre+ mouse brains were used for staining.

2.2.2 Generation of the knockout mouse lines

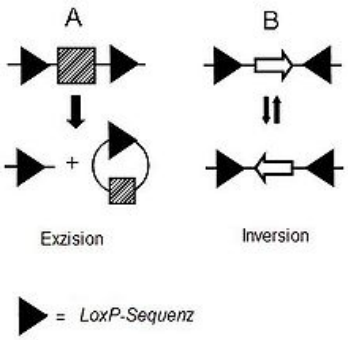

Figure 2.2 The cre recombinase. It acts differently dependent on the orientation of the loxP-sites. (https://de.wikipedia.org/wiki/Cre/loxP-System; 8.7.15)

The two sorts of transgenic black six (B6) mouse lines used for the experiments (B6.Cdh13 ko-hCMV line and B6.Pet1-cre.eGFP line) have both been generated using the Cre-loxP-method. This method allows to permanently replace a *floxed* (flanked by loxP-recognition-sites of 34bp) genetic locus by genes of interest with the help of the Cre recombinase and thus to generate *constitutive* knockout mice. Cre stands for "causing recombination" and it is able to perform site-specific DNA excisions or inversions dependent on the orientation of the loxP sites (cf. Figure 2.2).

For the generation of constitutive *Cdh13* KO mice loxP sites were introduced next to exon 3 of the *Cdh13* gene by homologous recombination technologies. In these *Cdh13* mutant mice *Cre* is expressed under the control of a human cytomegalovirus (hCMV) promoter (cf. Figure 2.3), which is expressed ubiquitarily. Thus a general *Cdh13* knockout via loxP-site specific recombination is possible. In our experiments Cdh13 KO mice were generated via breeding of two transgenic Cdh13 HZ mice. Viability, life expectancy and development of *Cdh13* mutant mice were not affected.

For the B6.Pet1-cre.eGFP line the same principle has been applied, but the expression of Cre and as a consequence of the enhanced green fluorescent protein (eGFP) were put under the control of the tissue-specific Pet1-promoter (cf. Figure 2.4), so that the expression of eGFP only occurred in 5-HT-synthesizing neurons and their postmitotic precursors.

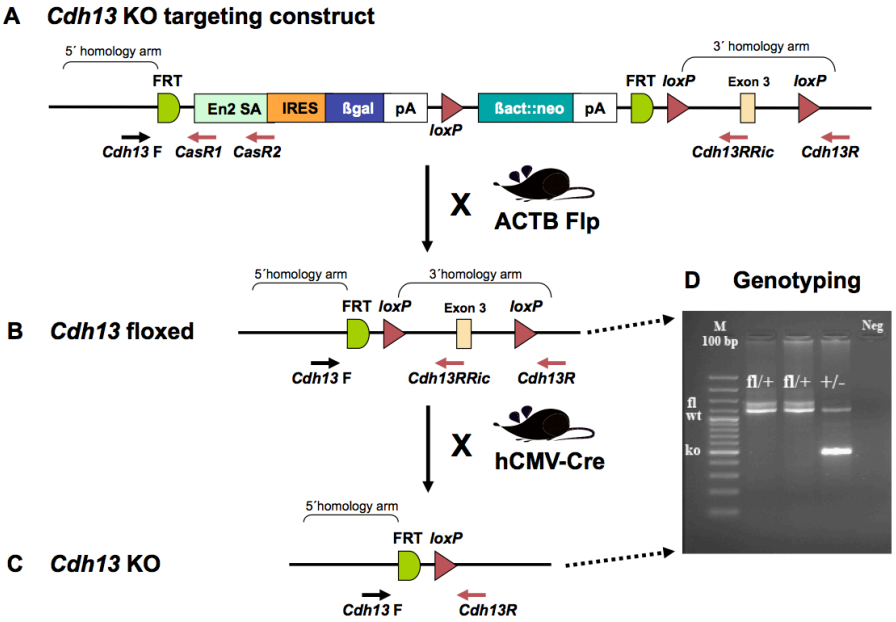

Figure 2.3 Schematic presentation of the *Cdh13* KO strategy (kindly provided by Olga Rivero, Molecular Psychiatry, Würzburg, Germany). Design of the *Cdh13* KO construct (A), as well as the resulting *Cdh13 floxed* (B) and *Cdh13* KO alleles (C), Generated via breeding of *Cdh13* KO mice with the deleter lines expressing hCMV-Cre. D shows PCR-based genotyping allowing the differentiation between wild type (WT) (1190bp bands), *floxed* (1380bp bands) and KO alleles (478bp bands).

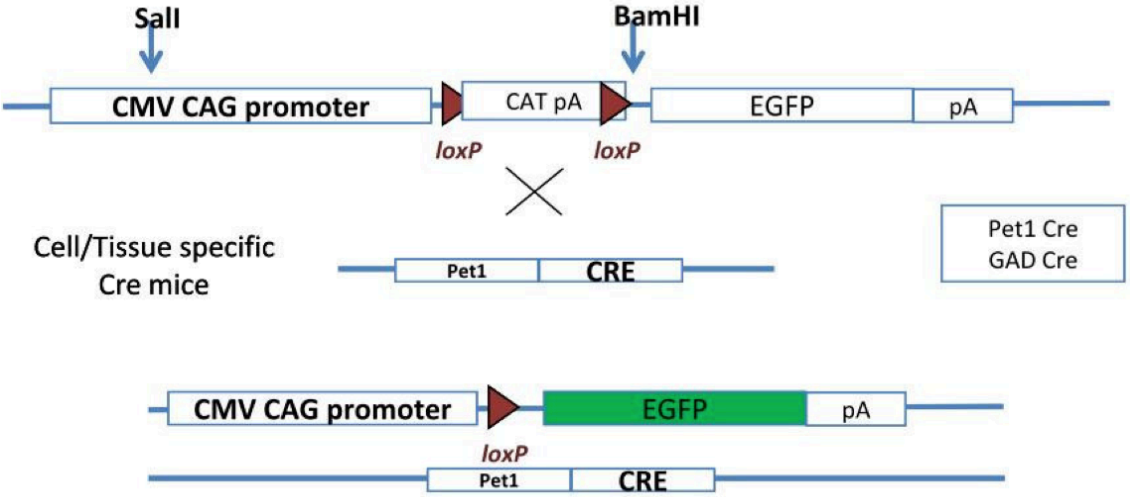

Figure 2.4 Genetic modifications in the B6.Pet1-cre.eGFP mouse line. A Pet1-Cre deleter line is crossed with a mouse line expressing a *floxed* gene followed by the eGFP-coding DNA-sequence. Under Cre expression the floxed CAT pA gene is excised and eGFP expression takes place in 5-HT-synthesizing neuronal cells (Waider, J., doctoral thesis, 2012)

2.2.3 Dissection of murine brains

The following procedure was applied in order to obtain the brains of seven-day-old mice (P7). They were euthanized with an overdose of inhaled isoflurane before being decapitated. The skin of the head was carefully parted in the middle and shifted aside so that the skull was visible. Then it was cut with small dissection scissors starting at the crossing point of the lambdoid suture and the sagittal suture in ventral direction up to the interocular bone, which also was divided. In the following the skull was cut alongside the lambdoid suture in both directions to the sides and from the foramen magnum to the lateral ending points of the lambdoid suture, allowing the gentle removal of the bone from the brain. After having cut off the pituitary gland and the cranial nerves leading from the brain stem to the deeper head regions, the brain could be separated from the rest of the mouse. During this whole process great attention was paid to avoid damaging the neuronal tissue.

Contrary to P7, embryonic mice where killed and fixed via transcardial perfusion of the mother with 4% PFA in phosphate buffered saline (PBS; 8min, pH 7.5). During dissection of 13.5- or 17.5-day-old embryos (referred to as E13.5 or E17.5), their skull could not be separated form the brain, because of the fragility of the organisms. As a result either the whole embryos (E13.5) had to be post-fixed in paraformaldehyde (PFA) or the heads where dissected and put in PFA (E17.5). Since the embryonic tissue is still very soft at that stage of development, this did not affect the future slicing of the tissue (cf. 2.2.5).

Finally small pieces of the tail tips were cut of for future genotyping following the protocol described in 2.2.7.

2.2.4 Fixation and storage of murine brains

The dissected brains and embryos were put in 4% PFA for immersion fixation over one (E13.5) or two nights (E17.5/ P7) at 4°C under constant shaking. After that they were washed three times in 1x PBS and then transferred into 10% sucrose solution. After another one-night-incubation period they were washed again in 1xPBS and transferred in 20% sucrose solution. Sucrose acts as a cryoprotectant by preventing the formation of ice crystals during freezing. The

next day the brains and embryos, respectively, were washed one last time as described above and then frozen in dry ice cooled isopentane (-80°C). This snap freezing technique is widely used because at this temperature the risk of crystal formation is rather low. Furthermore isopentane tends not to degas when the tissue is dipped. Thus the risk for breaks in the tissue and as a consequence for degradation is eliminated and the best morphological and molecular quality of the tissue can be obtained. The specimen were stored at -80°C until further use.

2.2.5 Sectioning at the cryostat

In order to prepare the brain tissue for immunohistochemistry (IHC) it had to be sectioned and placed onto gelatine covered glass slides (cf. 2.2.6). Therefore the brains, respectively the embryos were glued to a carrier plate using cryo-gel. The tissue then was cut into 20µm sections in a sagittal or coronal orientation with the orientation of the cutting regularly being adjusted according to a mouse brain atlas. During the cutting process, the ambient temperature in the cryostat was regulated between -16 and -21°C, avoiding too cold temperatures and thus ripping of the tissue, as well as too warm temperatures and degradation. The brain slices where regularly distributed on six series of microscopic slides (A-F), with each series comprising up to nine slides (e.g. A1-A9). Like this, future staining could be performed on comparable series with the distance between two brain sections in one series always being 120µm.

2.2.6 Coating of slides with gelatine

For better adhesion of the sections to the slides, these were coated with a 3% gelatine solution containing 0.5% of chrome (III) potassium sulphate. Chromium

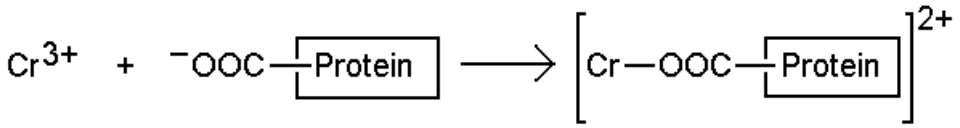

Figure 2.5 Reaction of gelatine with chromium ions. Chromium (III) ions are able to form covalent bonds with oxygen atoms, e.g. of carboxyl groups in proteins like gelatine (http://www.ihcworld.com/_technical_tips/prevent_section_fall.htm; 3.6.2013).

(III) ions are able to form up to six strong covalent bonds with oxygen atoms, preferentially in carboxyl groups of proteins or in water (cf. Figure 2.5).

Gelatine is a collagen derivative and thus a polypeptide consisting mainly of amino acids like glycine, proline and hydroxyproline, i.e. it is rich in carboxyl groups and thus able to be bound covalently by chromium (III). In addition to that, trivalent chromium can bind to carboxyl groups in the tissue sections as well as to oxygen atoms in the glass slides. This allows the formation of a stable gelatine coat, reinforcing the normal non-ionic forces (e.g. hydrogen bonds or

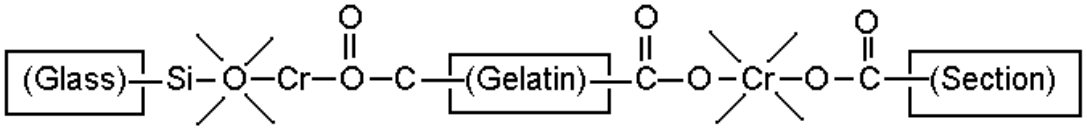

Figure 2.6 Chemical structure of the slide coating. The covalent bounds provided by the chromium (III) ions lead to the formation of a densely cross-linked slide coating, which prevents the sections from being washed away during the staining process. (http://www.ihcworld.com/_technical_tips/prevent_section_fall.htm; 3.6.2013)

van der Waals forces) between tissue and slide with strong covalent bonds and thus providing better stability during the staining process (cf. Figure 2.6).

Gelatine powder was completely dissolved in ddH_2O. This was achieved by heating the suspension up to 60°C under constant stirring. Subsequently chrome (III) potassium sulphate was mixed in. Racks of clean slides were then immersed for 30s into the 50°C gelatine solution. Finally they were lifted out and posed onto paper tissues that soaked up the surplus liquid. The racks were covered with wrapping film over night to prevent dust accumulation.

2.2.7 Isolation of DNA out of mouse-tail tips

Each tail tip (3-5mm) was put in a 1.5ml Eppendorf (Epi) tube and stored on dry ice until use. In the following they were covered with 500µl lysis buffer and 5µl Proteinase K and incubated over night while being constantly shaken at 55°C in a water bath. Being active in the presence of denaturing agents, such as sodium dodecyl sulphate (SDS), and chelating agents, like ethylenediaminetetraacetic acid (EDTA), Proteinase K effectively inactivates DNAses threatening the DNA integrity (Hilz et al., 1975). The next day the samples, containing lysed mouse-tail tips, were vortexed briefly and centrifuged for 10min at 14000rpm (4°C). The supernatant was transferred to 1.5ml Epi

tubes with 500µl of cold isopropanol. Thus the DNA was separated from the residual cell debris. The tubes were gently inverted until precipitated DNA filaments could be observed. Centrifugation for 10min at 14000rpm (4°C) led to the formation of a DNA pellet, which was washed once with 500µl of cold 70% ethanol (EtOH; centrifugation for 10min at 14000rpm/ 4°C) in order to remove remaining isopropanol, cell debris or salts. After having let the samples air-dry for about 1h, 50-100µl of 1x Tris EDTA (TE) buffer were added to each Epi tube and they were incubated for two days at 4°C under constant shaking.

2.2.8 Quantification of DNA using NanoDrop

In order to make sure that comparable amounts of DNA were applied in the polymerase chain reaction (PCR; cf. 2.2.9), the DNA samples were quantified using NanoDrop. After having cleaned (ddH_2O) and blanked (1xTE-Buffer) the Spectrophotometer, the samples were shortly vortexed and the DNA concentrations were determined in representative volumes of 1.5µl. Finally the samples were diluted with different volumes of 1xTE-Buffer, aiming for DNA concentrations between 50-60ng/µl.

2.2.9 Polymerase chain reaction

This broadly used method, which was invented in the 1980's, allows the exponential amplification of a specific DNA fragment and is based on the cyclic repetition of three basic steps: denaturation, annealing and elongation of double-stranded DNA at different temperatures. The following components are required for a successfully performed PCR: a DNA-template, a DNA-dependent DNA-polymerase, deoxynucleotide triphosphates (dNTPs; deoxyadenosine triphosphate (dATP), deoxyguanosine triphosphate (dGTP), deoxycytidine triphosphate (dCTP), deoxythymidine triphosphate (dTTP)), a magnesium chloride ($MgCl_2$)-containing buffer, special forward and reverse primers and a thermal cycler where the reaction can take place.

The initial denaturation is carried out at a temperature of 95°C. Since all components of a PCR react very sensitively to heat, it is recommended to keep the denaturation step as short as possible. The high temperature leads to the

separation of the two DNA strands, allowing the primers to hybridise with the single-stranded DNA in the annealing step.

The annealing temperature, which in most cases lies at 55-60°C, is dependent on the melting temperature (T_m) of the primers, which is determined by their guanosine/ cytosine (GC) content in a directly proportional manner. Since the melting temperature defines the point where 50% of the primers do not bind the template any more, usually the optimal annealing temperature lies 5-10°C below T_m. and can be identified empirically by a preliminary gradient PCR.

The final elongation step is carried out at 72°C, which provides an optimal environment for the *Taq-DNA* polymerase, leading to a working speed of 2800 nucleotides/min. This special thermally stable enzyme, which has been isolated from *Thermus aquaticus* (Taq), a bacterium inhabiting 70°C hot springs, possesses a 5'-3'-DNA-polymerase activity as well as a 5'-3'-exonuclease activity. It is lacking a 3'-5'-exonuclease activity and is thus not capable of proofreading. In order to optimise the efficiency of the enzyme $MgCl_2$ is added to the buffer. This molecule has a great impact on primer annealing, DNA-strand separation, product specificity, the formation of primer dimers and the error rate. Moreover free Mg^{2+} is required in the buffer for *Taq*-polymerase activity. The duration of the elongation step depends on the length of the template (usually 0.5-1min/kb when *Taq* is applied).

Most PCRs run through 30-40 cycles, until the reaction is ended with a final elongation step, ensuring complete DNA-synthesis. The multiplication factor for the produced amount of DNA actually lies at 1.6-1.7 (and not at 2). Good primer design is essential for a successful PCR-run. Usually these are oligonucleotides of 18-30bp in length, with a GC-content of no more than 40-60%, corresponding to the 3'-ends of the two DNA-strands. They should not contain any secondary structures like hairpins since this lowers the hybridisation probability. Moreover the two primers should not be able to bind to each other since this would lead to the formation of primer dimers and thus inhibit the amplification reaction.

In this thesis PCR was used to determine the genotype of the experimental mice. The mice have been tested on the presence of Cdh13 (cf. 2.2.9.1), eGFP (cf. 2.2.9.2) and Cre (cf. 2.2.9.3).

2.2.9.1 Cdh13 gene detection

This PCR protocol had to be optimised at the beginning of this thesis. Originally it was conducted using two different PCR approaches, separately detecting the WT allele and the KO allele of Cdh13. In the following the two approaches could be combined to one single PCR protocol using three different primers (cf. 2.1.1). In this context Cdh13-F and Cdh13-R were amplifying the KO allele and Cdh13-F and Cdh13-RRic would bind to the WT allele. The optimal annealing temperature for this reaction was determined preliminarily by a PCR Gradient approach and lies at 59°C. The amplified fragments had a length of 233bp for the WT allele, respectively 478bp for the KO allele. The applied PCR approach and the thermal cycler protocol are shown in Table 2.3 and Table 2.4 below.

Table 2.3 PCR approach for amplification of the Cdh13-gene-fragments

Components	**Volume [µl]**
$MgCl_2$ (10mM)	2.5
dNTPs (2.5mM)	1.0
Cdh13-R	1.0
Cdh13-F	1.0
Cdh13-RRic	0.5
Taq-Polymerase	1.0
Template	1.0
ddH_2O	17.0
Total volume	**25.0**

2.2.9.2 EGFP reporter gene detection

EGFP is derived from the jellyfish *Aequorea victoria*, where it is responsible for its natural green bioluminescence (Okabe et al., 1997). For this PCR a well-established protocol could be applied, using the JAX-3 and the JAX-5 primers (cf. 2.1.1). The amplified DNA fragment amounts to 173bp. The applied PCR approach and the thermal cycler protocol are shown in Tables 2.4 and 2.5.

Table 2.4 Conditions for PCR-amplification of the Cdh13-alleles/ *eGFP reporter*

Step	Temperature [°C]	Time [s]	Number of cycles
Initial denaturation	95	900	1
Denaturation	95	30	30
Annealing	59 / *55*	30	
Elongation	72	60	
Final elongation	72	600	1
Termination and storage	10	∞	1

Components	Volume [µl]
Goldstar (10x)	2.5
$MgCl_2$ (25mM)	1.0
dNTPs (2.5mM)	1.0
JAX-3	1.0
JAX-5	1.0
Taq-Polymerase	0.5
Template	1.0
ddH_2O	17.0
Total volume	**25.0**

Table 2.5 PCR approach for the PCR-amplification of the eGFP reporter

2.2.9.3 Cre transgene detection

In this protocol four different primers (cf. 2.1.1) were applied. The Il-2-F and IL-2-R primers served as internal positive control, leading to a 324bp long PCR product. In case of absence of a Cre-specific band in gel electrophoresis, the internal control helps to distinguish between a failed experiment and an absent CRE transgene in the DNA. The CRE-L-F and CRE-L-R primers amplified an 117bp long DNA fragment. A PCR Gradient approach was conducted in order to determine the optimal annealing temperature, which was set at 61,2°C. For the optimised PCR approach and thermal cycler protocol cf. Tables 2.6 and 2.7.

Table 2.6 PCR approach for the PCR-amplification of the Cre transgene

Components	Volume [µl]
Goldstar (10x)	2.5
$MgCl_2$ (25mM)	1.0
dNTPs (2.5mM)	0.5
Cre-R	1.0
Cre-F	1.0
IL-2-F	0.5
IL-2-R	0.5
Taq-Polymerase	0.5
Template	1.0
ddH_2O	16.5
Total volume	**25.0**

Table 2.7 Cycler conditions for the PCR-amplification of the Cre transgene

Step	Temperature [°C]	Time [s]	Number of cycles
Initial denaturation	95	300	1
Denaturation	95	40	36
Annealing	61,2	40	
Elongation	72	50	
Final elongation	72	300	1
Termination and storage	10	∞	1

2.2.10 Agarose Gel electrophoresis

Gel electrophoresis was applied for analysis of the PCR products in order to assess target DNA amplification. This method takes advantage of the multiple negative charged properties in the chemical structures of DNA and RNA molecules, enabling their separation in an electric field. Agarose gel is a galactose polymer, which is well suited for the separation of 0.5-25kb long nucleic acids. Its pore size is dependent on the agarose concentration in the gel in an indirectly proportional manner. Moreover an increase of the agarose gel concentration decreases the migration speed and allows the separation of smaller nucleic acid molecules. Although big DNA molecules experience a stronger force dragging them to the positive anode than smaller ones, their size disables them to move fast through the narrow pore matrix, whereas the small

molecules can diffuse without much resistance and thus travel farther, but experience a weaker attractive force. These differences lead to the separation of the molecules in distinctive gel bands. For these experiments 3% agarose gels were used, allowing the separation of molecules between 50-1000bp.

2.2.10.1 Preparation of the agarose gels

Agarose (3g per 100ml) was solubilised in 1x Tris-Acetate-EDTA-Buffer (TAE-Buffer) under constant heating in a microwave for 3-5min. TAE has a rather low buffer capacity, which necessitates a lower voltage and more time for the process. But its addition to the reaction allows a better resolution of bigger DNA fragments. In the following this clear solution was cooled down to hand temperature under constant stirring for 30-40min. This was necessary in order to avoid the formation of toxic vapours when ethidium bromide (EtBr) was added (3µl per 100ml of agarose gel). Finally the solution was disposed in a specific mould equipped with combs (to form slots). EtBr is an organic DNA intercalating agent, which emits orange fluorescence light of 590nm after being exited by ultraviolet (UV) light (wavelength 300-380nm). This signal is 20x enhanced when EtBr is bound to DNA. It thus enables the detection of clear DNA bands under UV light after successful gel electrophoresis.

2.2.10.2 Gel electrophoresis

A gel chamber containing running buffer (1xTAE) was prepared and the agarose gel was placed in it. Then in each PCR tube 3µl of blue loading buffer were added. After that 12µl of each sample were filled into the slots, one slot containing 10µl of a DNA ladder going from 100bp-1500bp in 100bp steps, indicating the size of the wandering DNA fragments. Then the gel chamber was connected to an electric field (120V), leading the DNA fragments to move dependent on their size and electric charge. After 20-30min the gel could be evaluated under the UV light.

2.2.11 Immunohistochemistry

When in 1941 Albert H. Coons and his colleagues started to use fluorescently labelled antibodies in order to detect specific antigens in tissue sections, IHC was born (Coons et al., 1941). Today this method is used in all fields of research to attain an understanding of the distribution and localisation of biomarkers in biological tissues. It relies on the specificity of antibody-antigen-interactions, which can be visualised via fluorescence, enzymatic colour-producing reactions or radioactivity. It can be distinguished between direct IHC (cf. Figure 2.7) and indirect IHC (cf. Figure 2.8).

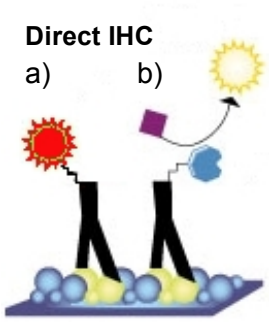

Figure 2.7
Direct IHC using
a) Fluorophores and
b) Enzyme reactions

Direct IHC involves only one staining step with a labelled primary antibody (AB) and can thus be performed very quickly. However, it only works well for the detection of abundant proteins since this method is lacking a signal amplification step and thus provides lower sensitivity. Nowadays the indirect method is more commonly used.

Indirect IHC follows a more complex protocol, involving an unlabelled primary AB binding to the protein of interest (first layer) and a labelled secondary AB reacting with the F_c-fragment of the latter (second layer). This leads to higher sensitivity since signal amplification is achieved via multiple binding of secondary antibodies to different antigenic sites on the primary AB. Therefore the secondary AB needs to recognise specifically the IgG of the animal species the primary AB was raised in. Usually the secondary AB is conjugated with a fluorescent stain (or fluorophore), e.g. cyanine 3 (Cy3) or Alexa 488, with an enzyme, mostly horseradish peroxidase (HRP) or alkaline phosphatase (AP), or with biotin (vitamin H). The HRP-labelled biotin plays a role in the avidin-biotin complex (ABC) method described in 2.2.11.2.

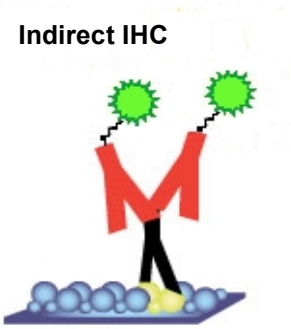

Figure 2.8
Indirect IHC using fluorophores

There are several ways to significantly improve the intensity and specificity of the obtained signal. Dependent on the fixation it might be necessary to pre-treat

the tissue sections with heat using antigen retrieval (AR) in order to break protein cross-links formed during formalin fixation and thus uncover hidden antigenic sites. In addition to that, the cell membrane can be permeabilised using Triton X-100, which diminishes the surface tension and facilitates the attachment of antibodies to intracellular targets. This detergent should, however, not be used for the detection of membrane antigens since it damages the membrane integrity. In order to prevent unspecific background staining, which is caused by non-immunological binding of the secondary antibodies (via hydrophobic and electrostatic forces), these binding sites can be previously blocked with normal serum coming from the secondary antibody's animal of origin. If HRP or AP is applied in the course of the experiment, it is obligatory to quench the tissue's endogenous enzyme activity with hydrogen peroxide prior to the incubation with the first AB. If double staining is planned, it is important to make sure that the applied antibodies do not cross-react and derive from different host animals. The following IHC staining protocols have been applied in this thesis.

2.2.11.1 Indirect immunohistochemistry using antigen retrieval

IHC was performed using AR for Tph2-doublecortin (DCX)-double staining and 5-HT-eGFP-double staining. For information about the applied primary antibodies see 2.1.4/ Table 2.8. The following staining protocols were applied:

- Slides with frozen sections were thawed and air-dried for 20-30min.

Antigen retrieval

- Hidden epitopes were uncovered using AR. For this the slides were placed in a cuvette with citrate buffer, which had been preheated to 80°C (Tph2-DCX), respectively to 70°C (5-HT-eGFP), in a water bath. In this solution the slides were scalded to 90°C (Tph2-DCX), or 80°C (5-HT-eGFP) respectively, and left to incubate at this temperature for 10min.

Blocking and permeabilisation

- After the slides had cooled down to about 40°C they were washed three times for 5min in 1x Tris buffered saline (TBS) under gentle shaking at room temperature (RT).
- Subsequently the sections on each slide were covered with 300µl of blocking solution (BS, 5% normal horse serum (NHS), 0,25% Triton X-100 in 1xTBS for Tph2-DCX, and 10% normal goat serum (NGS), 0,25% Triton X-100 in 1xTBS for 5-HT-eGFP respectively) and incubated for 1h in a wet chamber at RT.

Primary antibodies

- The BS was dripped of and replaced with 300µl of primary antibodies, diluted in BS. The applied concentrations are listed in Table 2.8.
- The slides then were incubated over night in a wet chamber at 4°C.

Secondary antibodies

- The next day the slides were washed three times 5min in 1xTBS at RT in order to remove the primary antibodies and then the sections were covered with 300µl of the secondary antibodies, diluted in half-concentrated BS (2,5% NHS, 0,125% Triton X-100 in 1xTBS (Tph2-DCX), respectively 5% NGS, 0,125% Triton X-100 in 1xTBS (5-HT-eGFP)). The sections then were left to incubate at RT for 1,5h in a wet dark chamber. The utilised secondary antibodies and their dilutions are listed in Table 2.8.

Counter staining

- After having washed the slides three times for 5min in 1xTBS at RT they were counterstained with 300µM 4',6-diamidino-2-phenylindole (DAPI) and incubated for 10min.
- Finally the slides were washed three times for 5min in 1xTBS at RT followed by mounting of the sections in Fluorogel.

Table 2.8 Antibodies and dilutions in Tph2-DCX- and 5-HT-eGFP-staining. The optimal dilutions were determined in preliminary experiments. For information about their origin cf. 2.1.4.

Antibody			**Dilution**
Anti-DCX	Primary antibody	Made in goat	1:300
Anti-goat Alexa 555	Secondary antibody	Made in donkey	1:400
Anti-Tph2	Primary antibody	Made in rabbit	1:300
Anti-rabbit Alexa 488	Secondary antibody	Made in donkey	1:400
Anti-eGFP	Primary antibody	Made in chicken	1:500
Anti-chicken Alexa 488	Secondary antibody	Made in goat	1:400
Anti-5-HT	Primary antibody	Made in rabbit	1:5000
Anti-rabbit Alexa 555	Secondary antibody	Made in goat	1:400

2.2.11.2 Indirect immunohistochemistry using the ABC method

This method was applied in Cdh13 single staining, as well as in fluorescent double staining of Cdh13 in combination with 5-HT or eGFP. For single staining, Cdh13 was detected via an enzyme-coupled colour reaction involving HRP and 3,3'-diaminobenzidine (DAB). Using the ABC method, four-fold higher signal amplification and sensitivity compared to direct IHC could be achieved.

Avidin is a glycoprotein with four high-affinity binding sites for biotin allowing the formation of macromolecular complexes during the reaction (cf. Figure 2.9). Three of its binding sites are previously conjugated to HRP-labelled biotin molecules, enabling the enzyme-triggered colour reaction. The fourth site then binds to the biotinylated AB, thus marking the epitope of interest. Finally the HRP is developed using DAB or detected via tyramide signal amplification (TSA).

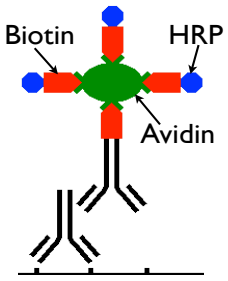

Figure 2.9 Indirect IHC using ABC

The TSA Plus reaction kit, which has been used for every fluorescent Cdh13 (single or double) staining, provides a signal amplification technology, leading up to 1000-fold increased sensitivity compared to other methods, without affecting resolution or background clarity. This is achieved via HRP–triggered transformation of TSA reagents into highly reactive radicals binding covalently to electron-rich amino acids, e.g. tryptophan or tyrosine, in direct vicinity of the target of interest. The TSA reagent itself is

labelled with a fluorophore (in this experiment Cy3), thus enabling direct fluorescent detection. The applied antibodies are listed in Table 2.9.

Antibody			Dilution
Anti-Cdh13	Primary antibody	Made in goat	1:500
Anti-goat biotinylated	Secondary antibody	Made in horse	1:400/ 800
Anti-5-HT	Primary antibody	Made in rabbit	1:5000
Anti-rabbit DyLight 488	Secondary antibody	Made in donkey	1:400
Anti-eGFP	Primary antibody	Made in chicken	1:500
Anti-chicken Alexa 488	Secondary antibody	Made in donkey	1:1000

Table 2.9 Antibodies used for Cdh13-DAB- and Cdh13-5-HT/-eGFP double staining. The optimal dilutions were determined in preliminary experiments. For information about their origin cf. 2.1.4. It needs to be mentioned, that in all figures the colour of the eGFP-staining was artificially changed to red (originally labelled with Alexa 488=green) and the one of the 5-HT-staining to green (originally stained with Alexa 555=red). This was necessary because of the Cdh13-5HT-double-staining where Cdh13 was also stained red.

The following staining protocol was applied:

- The frozen sections were thawed and dried for about 30min.

Blocking of endogenous peroxidase activity

- In the next step they were washed three times for 5min in 1xTBS under constant shaking at RT.
- Subsequently the slides were put into a cuvette filled with 0,3% H_2O_2 and incubated for 10min in order to block endogenous peroxidase activity.

Blocking and permeabilisation

- After having washed them again three times for 5min in 1xTBS, unspecific binding sites were blocked by incubating the slides with 300µl of BS (10% NHS in 1xTBS, in case of Cdh13-eGFP double-staining +0.25% Triton X-100) for 1h at RT in a wet chamber.

Primary antibody

- Finally the BS was removed using tissue paper and replaced with 300µl/slide of the primary AB solution containing the Cdh13 AB diluted 1:500 alone or in combination with either the anti-5-HT AB diluted 1:5000

in 1xPBS or the anti-eGFP AB diluted 1:500 in 1xPBS dependent on the staining. They then were stored over night at 4°C in a wet chamber.

Cdh13 Secondary antibody

- The next day the slides were washed following the same procedure. Then the sections were covered with biotinylated horse anti-goat AB (for the detection of Cdh13), which had been diluted 1:400 (for DAB staining and 5-HT double staining) respectively 1:800 (for eGFP double-staining) in half-concentrated BS (5% NHS in 1xTBS (+0.125% Triton X-100)).

ABC reaction

- After an incubation time of 1.5h the slides were washed (see above) and then treated for another 1.5h with an ABC solution. This solution had been prepared exactly 30min before its application to the sections in order to guarantee its optimal reactivity with the biotinylated AB.

Tyramide signal amplification

- Having washed the slides again, they were covered with the fluorophore tyramide (Cy3) and incubated for 10min at RT in a dark and wet chamber.
- In case of Cdh13 double staining the second secondary AB was added after another washing step. Either donkey anti-rabbit DyLight diluted 1:400 in half-concentrated BS (5% NHS in 1xTBS) or donkey anti-chicken diluted 1:1000 in half-concentrated BS (5% NHS and 0.125% Triton X-100 in 1xTBS) were applied (300µl/slide). The slides then were left to incubate for 1.5h at RT in a wet chamber.
- Before counter staining the sections with DAPI, they were washed 3x 5min with 1xTBS at RT. Then 300µl of 300µM DAPI was put on each slide and left there for 5min.
- After a final washing step the slides were embedded with Aquatex and coverslips. Fluorogel cannot be used with the TSA-Kit because it interferes negatively with Cy3.

DAB staining

- Finally the slides were incubated for 10min with DAB solution under the hood (300µl/ slide).
- Subsequently, the slides were shortly rinsed with 1xTBS, washed 2x 5min with 1xTBS and 1x 4min in ddH_20 before being dehydrated in an ascending alcohol series (short swaying in 70% EtOH, then in 96% EtOH before treating the slides 2x 3min with 100% EtOH and 2x 4min with Xylene). In the end they were mounted in VitroClud, covered with a cover slip and left to dry.

2.2.12 Nissl staining

This method is used to visualise the cytoarchitectonics of cerebral regions. In these experiments it was performed on one series of each developmental stage

(E13.5, E17.5, P7), representing the three different genotypes of interest, i.e. Cdh13 WT, HZ and KO mice. First the slides were incubated for 5min in cresyl violet acetate, an alkaline dye staining the negatively charged RNA or DNA of the cell nucleus and of the so-called *Nissl substance* (=rough endoplasmatic reticulum) blue. Then the slides were treated with different concentrations of EtOH (70%, 96%, 100%) in order to remove surplus dye, fixate and differentiate the staining. Meanwhile they were regularly controlled under the light microscope so as to prevent exaggerated dye removal and guarantee optimal staining success. Finally the slides were swayed in a xylene-propanol solution (50:50), treated 2x 5min with pure xylene, mounted and coverslipped using VitroClud.

2.2.13 Counting of serotonergic cell clusters

For each developmental stage (E13.5/ E17.5/ P7) one out of six Tph2-stained series has been quantitatively analysed using Cell Counting in ImageJ. The ABA and the anatomic classifications by Alonso et al. (2013) served as references (cf. 1.3.3).

The tissue has been cut into 20µm thick sections and distributed on a whole of six series, so that the distance between each section of one series lies at 120µm (cf. 2.2.5) Only cells with a discernible DAPI-stained nucleus were included in the counting, in order to reduce the possibility of double counts. For E13.5 and E17.5 Tph2-ir cells were assigned to the following groups: fp, migrating, DR/ CLi and MnR. In these stages the caudal clusters could not be properly analysed due to lack of cells and poor tissue quality. For P7 cells were assigned to being located in DR, DRW, CLi, CLiW, MnR, SuLR, PPnR/PnR and the caudal cluster. Fibres have not been included in the analysis. If single cells could not be reliably assigned to a specific cell cluster, they were defined as being part of the group at the same level of the brainstem.

2.2.14 Picture Processing

Light microscopic images were obtained with an Olympus BX51 microscope using Neurolucida software. Fluorescence images were obtained using an

inverted epifluorescence Olympus IX81 microscope and cellSens Dimension software. Confocal images were acquired using a FluoView FV1000 confocal microscope. Pictures were taken with a 10x (light-/fluorescence), 40x or 63x objective (confocal) processed with Graphic Converter or ImageJ. Figures containing images were composed using PowerPoint.

2.2.15 Immunohistochemical controls

In order to double-check the specificity of the staining protocols, each double-staining protocol included a negative control, where the primary antibody was left out. Since staining was performed simultaneously on all three genotypes, normally slides from the HZ genotypes were used for the controls (because of their higher prevalence in the litters). Furthermore, the stained Cdh13-KO slides were also considered as negative controls.

3. Results

3.1 The different genotypes

In order to breed knockout mice and to identify the required genotypes, three different PCR protocols had to be established and refined (cf. 2.2.8.1-3): one for the B6.Cdh13 ko-hCMV line (cf. (a)) and two for the B6.Pet1-cre.eGFP line (cf. (b)/(c)). The resulting electrophoresis gels are displayed in Figure 3.1.

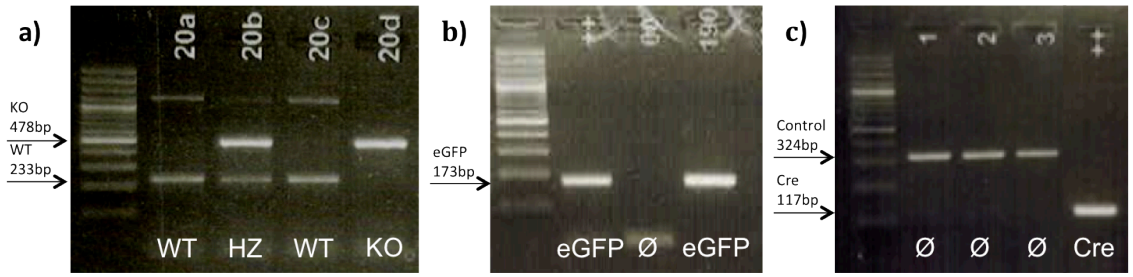

Figure 3.1 Electrophoresis results from three different PCRs. (a) Cdh13 gel: Cdh13 WT mice possess two of the 233bp alleles, like normal mice, whereas the HZ mouse has only one functional allele and the KO mouse shows two abnormal copies at 478bp. The signals at about 1200bp are unspecific or constitute slicing products of the WT allele. (b) eGFP reporter gel: Compared to the positive control on the left (++) it is evident that sample 190 contains an eGFP gene. (c) Cre transgene gel: None of the tested mice (1-3) contains Cre.

3.2 Cdh13

Before focussing on the central 5-HT system and possible influences of Cdh13, the latter will be regarded in terms of staining (cf.3.2.1), protein distribution pattern (cf. 3.2.2) and Cdh13-containing fibre tracts (cf. 3.2.3), as well as its protein compared to mRNA distribution (cf. 3.2.4).

3.2.1 Staining of Cdh13

Fluorescent IHC staining of Cdh13 was achieved using TSA (cf. 2.2.10.2). In order to test the staining specificity and to confirm the successful knockout of Cdh13, staining was compared on mid-sagittal planes of WT, HZ and KO mouse brains (cf. Figure 3.2). In image (c) the absence of Cdh13-immunoreactivity (IR) in KO mouse brains is documented. The few visible unspecific staining sites lie clearly outside the CNS in the nasopharyngeal area.

Consequently, the Cdh13-immunoreaction in image (a) and (b) has been assessed as specific. In comparison they might even suggest a quantitative difference in Cdh13 presence, which would be consistent with the different displayed genotypes.

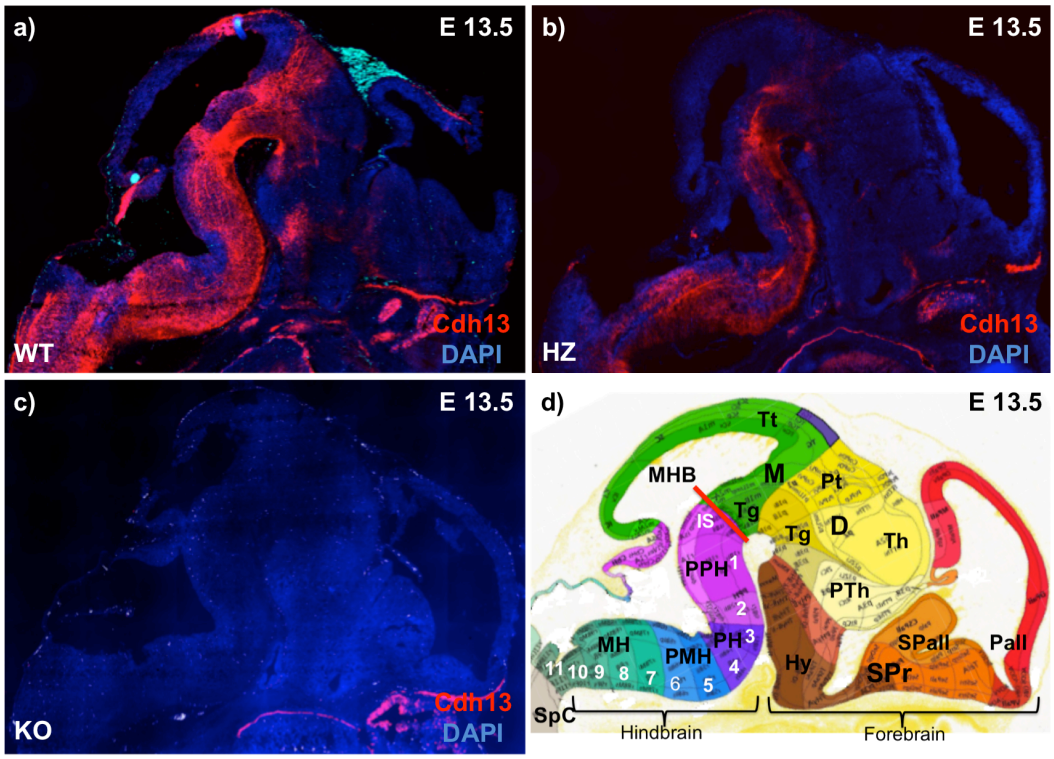

Figure 3.2 Fluorescent Cdh13-staining. It is shown on 20µm paramedian sections of embryonic WT, HZ and KO mouse brains of the B6.Cdh13 ko-hCMV line (reference picture (d) is adapted from the ABA, Developing Mouse Brain, E13.5, image 10/15). (a) and (b) show Cdh13-IR in hindbrain and adjacent spinal and midbrain areas. In (c) no signals are visible in the CNS, which proves the successful knockout, as well as the specificity of the Cdh13-signals above. The few unspecific staining sites lie clearly outside the CNS in the nasopharyngeal area. Tt= tectum, Tg= tegmentum, D= diencephalon, Pt= pretectum, PTh= prethalamus, Th= thalamus, SP= secondary prosencephalon, Hy= hypothalamus, SPall= subpallium, Pall= pallium, MHB= midbrain-hindbrain-boundary, 1-11= rhombomeres, PPH= prepontine hindbrain, PH= pontine hindbrain, PMH= pontomedullary hindbrain, MH= medullary hindbrain (medulla).

Concerning the DAB-staining (cf. 2.2.10), it has been conducted successfully (data not shown) on sagittally sectioned E13.5 and E17.5 murine brains of all three genotypes. The tissue quality, however, was mediocre, so that no additional information could be drawn from this staining.

3.2.2 Cdh13 distribution over murine development

The Cdh13 protein distribution pattern was examined over three developmental stages in WT mice (cf. Figure 3.3).

At E13.5 (cf. (a), for full view also see Figure 3.2.a) the majority of Cdh13-IR seems to be located in hindbrain and adjacent spinal and midbrain areas. There is, however, additional evidence of simultaneously occurring Cdh13-IR in outer layers of the forebrain pallium (Pall, data not shown). Given that the fluorescence signals predominantly show on filamentary structures, Cdh13 seems to be mostly located on axonal membranes. Image (a) shows a multitude of Cdh13-ir fibres running parallel to the brainstem axis towards or from the spinal cord and through the midbrain Tg, where two bundles can be distinguished (cf. 3.2.3). Strikingly, the only area in the hindbrain, which is completely devoid of Cdh13-IR, seems to be the (peri-) ventricular zones of and around r4. Furthermore, it looks like it is more concentrated near the fp than towards the ventricular side of the brainstem, with only the isthmus and r1 (cf. (c)) being exempt from this rule. It is evident, that in these areas Cdh13-ir fibres no longer run parallel to the hindbrain axis, but interlink superficial and ventricular zones, thus having the same orientation as migrating 5-HT neurons in this area. They thus build a sharp border to the midbrain with the MHB being indicated by a small dent above the Is at the ventricular side of the brainstem.

Figure 3.3 Cdh13 protein distribution pattern over development (cf. next page). Staining was performed on 20µm thick sagittal (E13.5, E17.5, P7) and coronal (P7) sections. Reference pictures (b)/(e)/(h) were adapted from the ABA, Developing Mouse Brain: E13.5 (image 10/15)/ E17.5 (HP Yellow, image 135/313)/ P7 (Nissl, image 169/397), (l) from Alonso et al. (2013). (a) At E13.5 Cdh13-IR is mainly localised in fibres running parallel to the hindbrain axis. (c) shows a more lateral section of area c in (a): in Is and r1 Cdh13-ir fibres run between superficial and ventricular layers. (d) At E17.5 Cdh13 protein occurs in the forebrain pallium and in isocortical layers (higher magnification of area I in (d) shown in (i)). In the higher magnification it looks like Cdh13-immunoreaction occurs in all layers and that it is mostly localised on the neuropil than in cell bodies. Region f of (d) is shown in (f), again in a more lateral section: Fan-shaped Cdh13-containing fibres reach the cortex from the sides. (p) and (q) show magnifications the area of transition from 6-layered isocortex (Iso) to 3-layered allocortex (Allo) and of the hippocampus (Hippo). (g) At P7 Cdh13-IR is homogenously distributed in the CNS. No distinct fibre tracts can be distinguished any more. (n) In Hippo and Allo (cf. star), however, only the molecular layer of the dentate gyrus and the lacunosum-molecular layer of CA2/3 (white arrow) show fluorescence signal. Furthermore, the cerebellum (cf. (m)), apart from white matter in the vermis (cf. star), seems to be devoid of Cdh13-IR. Image (k) presents a coronal view of hindbrain Cdh13-IR at P7. The most striking Cdh13-containing structures (arrow) are magnified in (o). They correspond to the dopaminergic anterior tegmental nuclei (ATg). Tel= (alar plate of the exvaginated) telencephalic vesicle, C= cerebellum

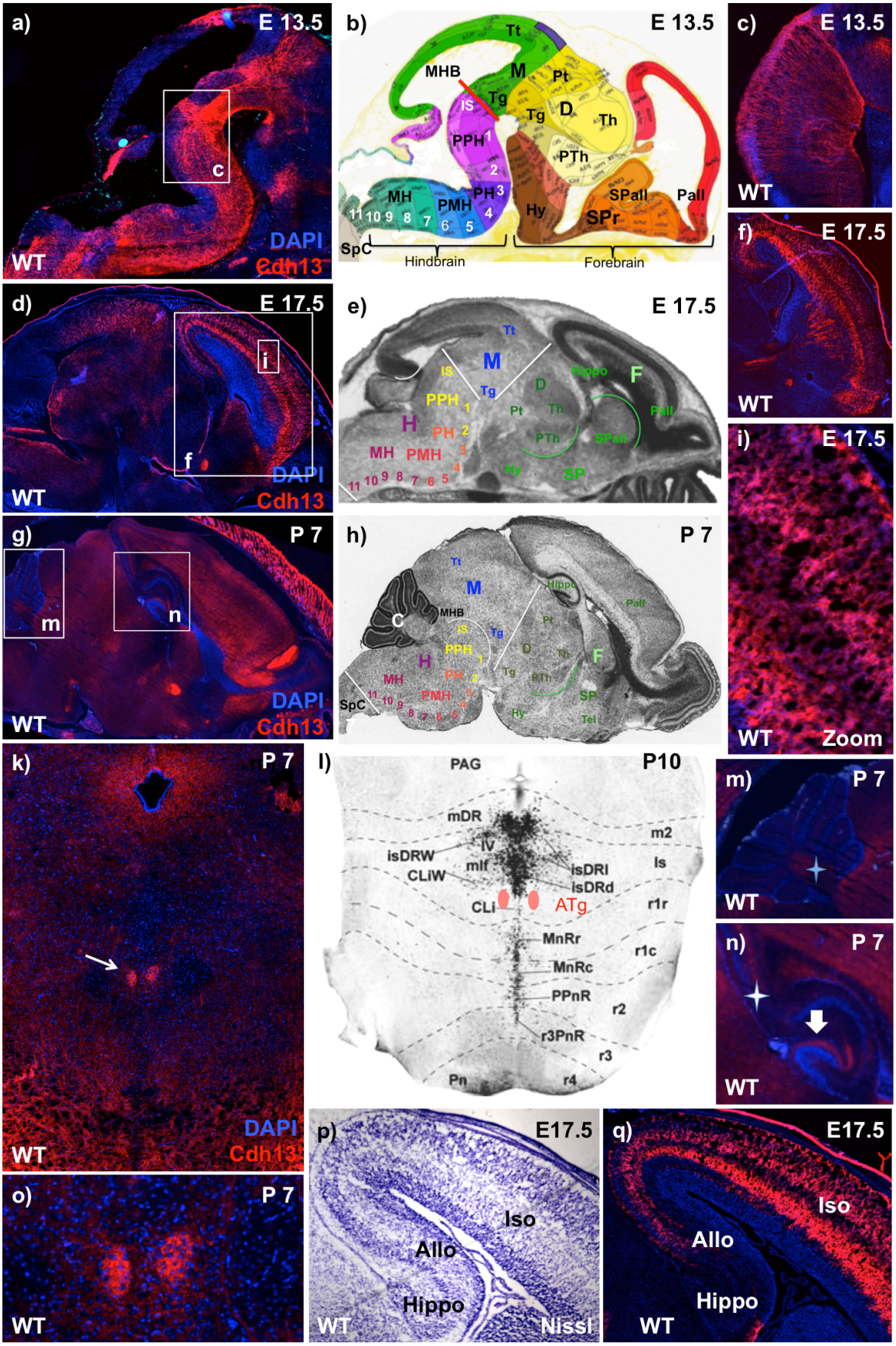
a)
E 13.5
c
WT
DAPI
Cdh13
b)
E 13.5
Tt
MHB
M
Pt
IS
Tg
Tg
D
Th
PPH 1
PTh
2
MH
PMH
PH 3
4
Hy
SPall
Pall
SPr
11 10 9 8 7 6 5
SpC
Hindbrain
Forebrain
c)
E 13.5
WT
f)
E 17.5
WT
d)
E 17.5
i
f
WT
DAPI
Cdh13
e)
E 17.5
Tt
M
IS
Hippo
F
D
Tg
PPH 1
Pt
Th
Pall
H
PH 2
PTh
SPall
MH
PMH 3
4
Hy
SP
11 10 9 8 7 6 5
i)
E 17.5
WT
Zoom
g)
P 7
m
n
WT
DAPI
Cdh13
h)
P 7
Tt
M
Hippo
Pall
C
MHB
IS
Pt
Tg
D
Th
F
PPH 1
H
PH 2
Tg
MH
PMH 3
PTh
SP
SpC
11 10 9 8 7 6 5
4
Hy
Tel
k)
P 7
WT
DAPI
Cdh13
l)
P10
PAG
mDR
IV
m2
isDRW
mlf
Is
CLiW
isDRl
isDRd
CLi
ATg
r1r
MnRr
r1c
MnRc
PPnR
r2
r3PnR
r3
Pn
r4
m)
P 7
WT
n)
P 7
WT
o)
P 7
WT
p)
E17.5
Iso
Allo
Hippo
WT
Nissl
q)
E17.5
Iso
Allo
Hippo
WT

Later developmental stages (cf. (d) and (g)) do not show this specific orientation of Cdh13-ir fibres any more. At E17.5 (cf. (d)) Cdh13-IR shows a more homogenous distribution and the intense signals noted in the hindbrain at earlier stages seem to have decreased. Instead, some layers of the forebrain Pall appear particularly enriched with Cdh13-IR. Comparing images (p) and (q), which show the transition zone from six-layered isocortex (Iso) to three-layered allocortex (Allo), the cell-rich Nissl-stained layers (V and III) seem to correspond to the most intensely Cdh13-ir ones. Image (i) shows a higher magnification of the cortical layers. As at E13.5, Cdh13-IR seems to emanate more from cell membranes than from the cytoplasm. It is present in all layers, though in some more intensely than in others. Image (f) shows a more lateral section of the forebrain with Cdh13-ir fibres crossing the subpallium (SPall) and entering the cortex bilaterally in a fan-like manner. In both displayed views of the forebrain cortex (cf. (f)/ (d)) the intensity of Cdh13-IR diminishes towards the upper margin of the Pall, where the Iso turns into the hippocampal Allo (cf. star in (n)). The hippocampus (Hippo) itself seems to be nearly devoid of Cdh13-IR at this age.

Contrary to the earlier developmental stages, at P7 (cf. (g)) Cdh13 shows a homogenous distribution all over the brain, without any sites of specific signal enrichment. Only the cerebellum (cf. (m)) and the Hippo (cf. (n)) show reduced Cdh13-IR. In the three-layered hippocampal allocortex immunoreaction is missing, apart from the molecular layer of the dentate gyrus and the adjacent lacunosum-molecular layer of CA2/3 (cf. (n) white arrow). The cerebellar hemispheres look completely devoid of Cdh13-IR, only the white matter of the vermis (cf. (m) star) shows positive signals. Image (k) contributes a coronal view, taken from rostral hindbrain. Analogous to the observations in sagittal sections described above, Cdh13 protein occurs mainly on fibres. Furthermore, IR shows a higher intensity towards the superficial side of the brainstem (corresponding to the lower part of the image), as well as around the aqueduct (Aq). The most striking Cdh13-ir structures (cf. arrow; magnified in (o)), appear to correspond to the anterior tegmental nuclei from the dopaminergic system, which are located bilaterally to the raphe nucleus constellation shown in (l).

3.2.3 Cdh13-immunoreactive fibre tracts

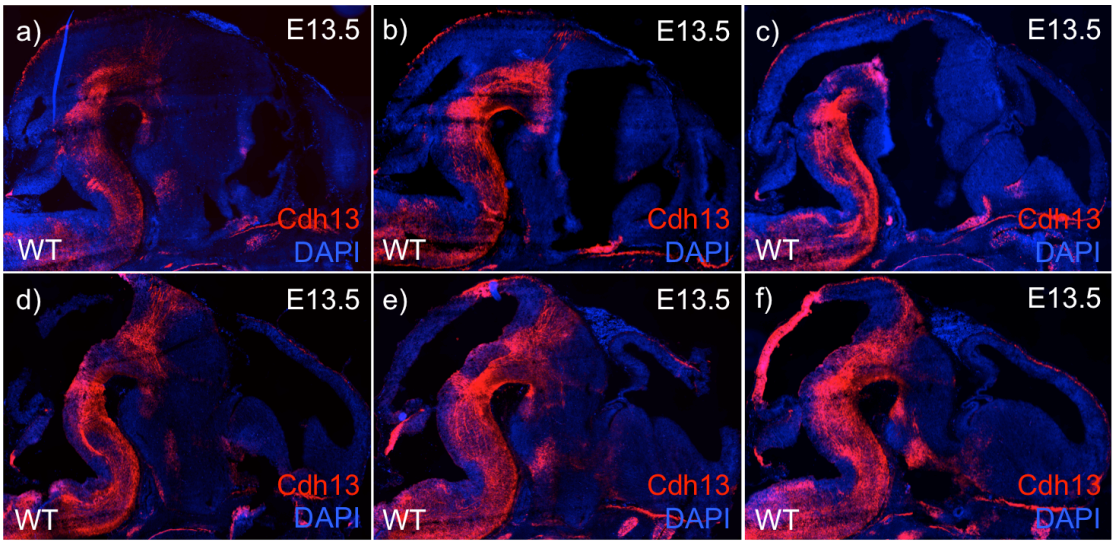

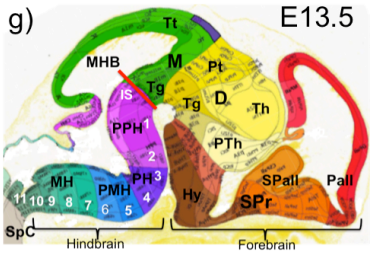

Figure 3.4 Developing Cdh13-containing fibre tracts at E13.5. B6.Cdh13 ko-hCMV mice were used ((g) adapted from the ABA, Developing Mouse Brain, E13.5, image 10/15). The sagittal sections (20µm) start from lateral (a) and proceed towards paramedian sections (e/f). Cdh13-IR is most concentrated at paramedian levels and can be found on two fibre tracts: the upper one interlinks the hindbrain with dorsal tectal areas, the lower one travels through midbrain tegmentum and fans out in the subpallium (cf. (f)).

As described above, at E13.5 Cdh13-IR occurs mainly on filamentary structures, running through murine hind- and midbrain. Figure 3.4 shows the course of Cdh13-containing fibres on a series of sagittal sections, starting with the most lateral (a) and proceeding towards paramedian sections (e/f). The density of Cdh13-ir fibres running parallel to the hindbrain axis augments with proximity to the midline. In the midbrain fibres divide into two broad tracts. The upper one, which appears on medial and paramedian sections (d-f), crosses to the midbrain tectum (Tt). It is, however, not clear whether these fibres arise from hindbrain regions and travel towards this area or vice versa. The lower tract runs through pretrectal Tg, as well as hypothalamic areas and fans out in the subpallium (SPall) region (cf. d-f). On its way this tract takes a gentle curve through lateral regions (cf. c/d), even though most of its fibres keep near the midline (cf. f). There is no conclusive evidence for the orientation of these fibres as well. They, however, very much look like they take their source somewhere in the hindbrain and aim for forebrain structures.

3.2.4 Comparison of Cdh13 protein and mRNA distribution

In Figure 3.5 the Cdh13 protein distribution is compared to the mRNA pattern at E13.5 old mice. Image (a) is taken from the ABA and shows mid-sagittally sectioned hindbrain reacted with CDH13-mRNA in-situ-hybridisation (ISH). Cell bodies with *Cdh13* mRNA presence are highlighted as black dots. In (b) Cdh13 protein locations are marked by red immunofluorescence.

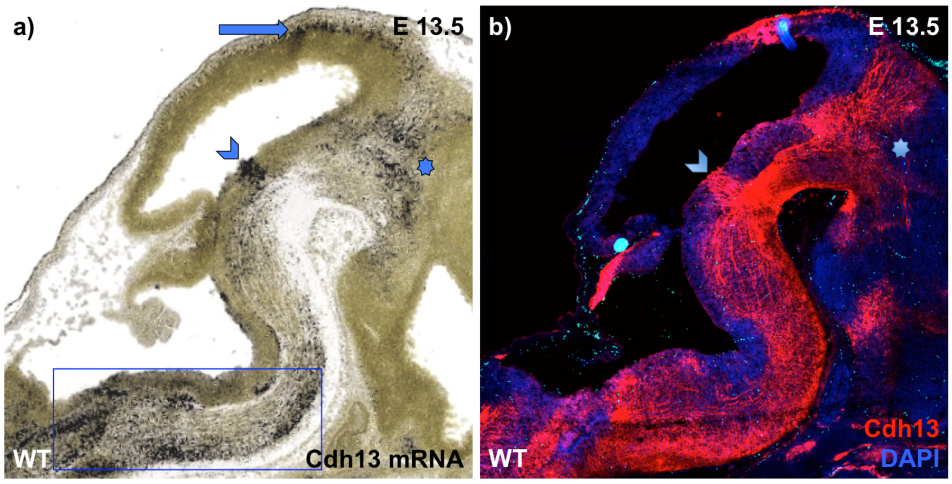

Figure 3.5 Comparison of Cdh13 in-situ-hybridisation (adapted from the ABA, http://developingmouse.brain-map.org/experiment/show/100042196, Image 12/17) and fluorescent staining. In (a) Cdh13 mRNA is labelled with ISH; reactive cells appear as black dots. In (b) Cdh13 protein is labelled by fluorescence IHC on a sagittal section (20µm) of E13.5 mouse brain. Apparently the distribution of RNA-containing cells and the Cdh13-ir filamentary structures are congruent. The isthmus shows a particularly high presence of Cdh13 mRNA, as well as protein (see arrowheads). The stars emphasise the separation into the two Cdh13-containing pathways in the midbrain. Comparison of the two images indicates that these pathways are intermingled with CDH13-mRNA-reactive cells.

The two images look rather congruent in their distribution patterns. In (a) remarkable mRNA-containing cell aggregates can be found in the region of the Is (arrowhead), in superficial and ventricular layers of the caudal rhombomeres r5-11 (square), around the separation point of the two fibre bundles visible in (b) (star), as well as in tectal midbrain or the superior colliculus (arrow), respectively. These cell groups might represent the sources of the Cdh13-ir fibres visible in (b), since these tracts interlink the above mentioned cell accumulations and show more intense CDH13-IR at these sites. Given that the isthmic cell group lies in the area of the serotonergic DR, it might well be possible, that fibre tracts arising from this site belong to the 5-HT system

described in 3.3.4. Apart from the above-mentioned locations, at E13.5 *Cdh13*-expressing cells can only be found in superficial layers of the forebrain pallium (cf. ABA, data not shown). At this age, however, there is no evidence of Cdh13-ir fibres in this area. These cells could be the aim of the fibre tract, which runs through diencephalon and hippocampus before fanning out in the SPall region. In consequence it can be stated that at E13.5 hind- and midbrain constitute the principal sites of *Cdh13* expression.

3.3 The central serotonergic system

Having analysed the Cdh13 distribution pattern over different developmental stages, the next chapter will focus upon the central 5-HT-system, exploring the developmental processes (cf. 3.3.1), which with the aid of somal translocation (cf. 3.3.3) lead to the mature raphe nuclei constellation (cf. 3.3.2), as well as to the establishment of its ascending fibre tracts (cf. 3.3.4).

3.3.1 Formation of the raphe nuclei

In order to detect aberrations in development and structure of the 5-HT system due to Cdh13 absence, it is important to first retrace and understand the natural undisturbed processes. Consequently, we analysed the formation of the raphe nuclei in WT mice (cf. Figure 3.6) before paying attention to other genotypes. Anti-5-HT immunostaining was performed on B6.Pet1-cre.eGFP brains (cf. a-c, g-i) in order to distinguish between mature 5-HT neurons and their Pet1-expressing precursors. With Pet-1 being strictly limited to hindbrain 5-HT neurons and showing a particularly high expression in differentiating postmitotic precursors (cf. 1.2.3), eGFP is only expressed in this collective of cells. Tph2 and DCX were labelled on WT B6.Cdh13 ko-hCMV mouse brains (cf. d-f).

Image (a) displays a paramedian section showing eGFP-containing young serotonergic cells in (pre-) pontine hindbrain (Is-r3). As expected, the majority is located at the “birthplace” of 5-HT neurons alongside the superficial stratum next to the fp. Some cells, however, are still eGFP-ir after having migrated to the periventricular location of the future DR, as well as to the intermediately located CLi, which together form quite a sharp border to the midbrain. Comparing (a) to (b), it is evident, that 5-HT follows the inverse rule, being predominantly present in the area of the future rostral cluster, namely the DR and MnR regions, and thus in more mature serotonergic neurons. Only few 5-HT-ir cells can be found at the fp. The assumption that 5-HT expression starts only after migration (Wallace and Lauder, 1983), however, could not be confirmed, since some neurons already produced 5-HT during migration (cf. Figure 3.6.b/k).

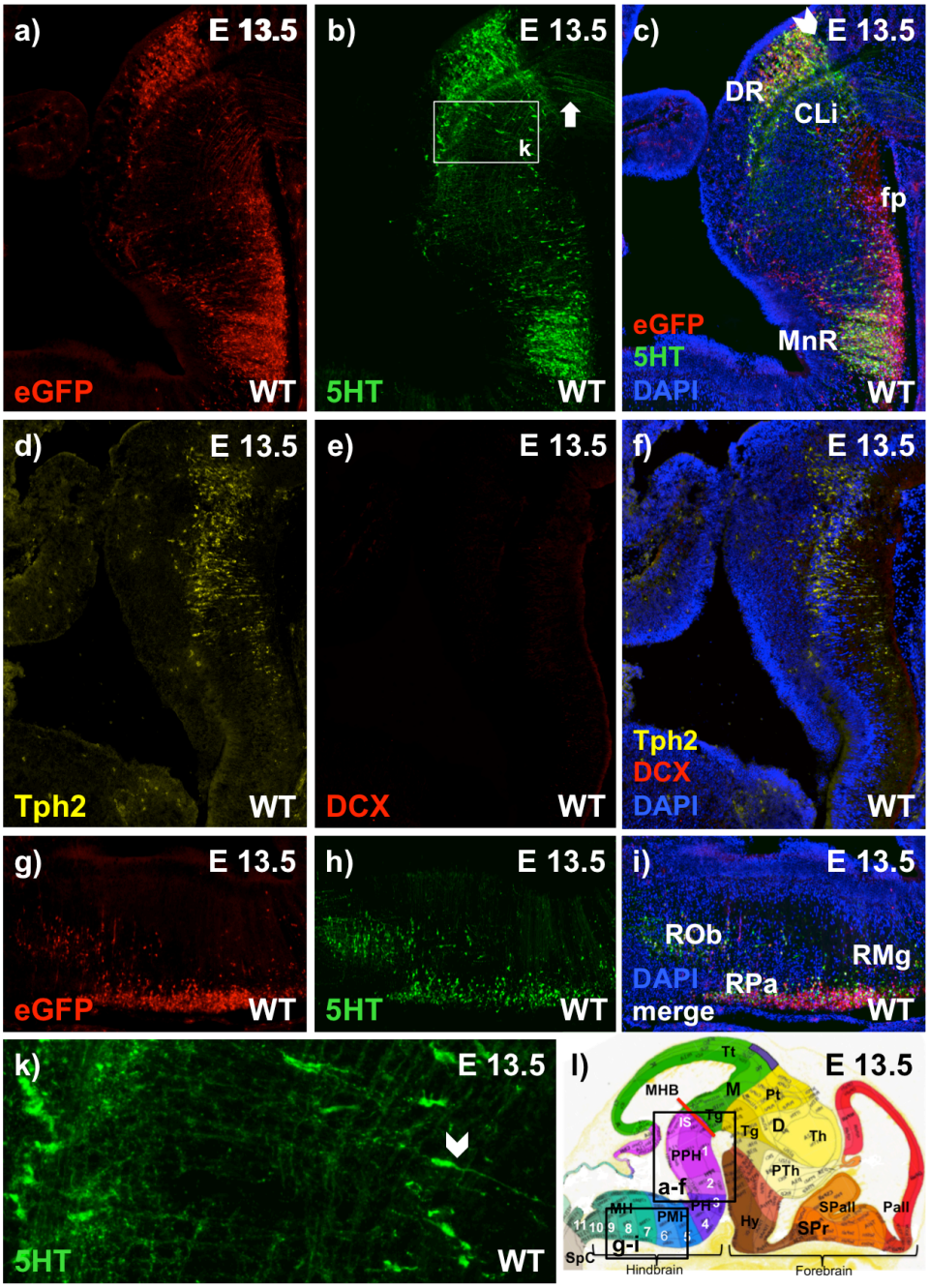

Figure 3.6 Development of the rostral and caudal raphe nuclei. The images show hindbrain of B6.Pet1-cre.eGFP (a-c/ g-i) and B6.Cdh13ko-hCMV (d-f) mice at E13.5 (20µm paramedian sections). (a)-(c) Pet-1 dependent eGFP expression (a) – here artificially changed to red – starts the earliest and is mainly visible at the superficial stratum near the floorplate of the hindbrain. Only after eGFP and Tph2 expression, neurons are able to produce 5-HT (artificially changed to green), which thus is detected on slightly more mature cells (b). By E13.5 the majority has already finished their migration towards the future positions in DR and MnR. Behind the MHB (c, arrowhead), interlinking fibre bundles to mid- and forebrain can be seen ((b), arrow). (d)-(f) Tph2 (d) occurs before 5-HT, but after Pet-1 expression. Unfortunately, staining for DCX has failed. (g)-(i) these images show the above explained (cf. a-c) differentiation and migration processes for the caudal cluster, which develops about 1d after the rostral one. (k) The arrowhead points at a serotonergic cell during somal translocation. Its ventricular process is nicely visible. (l) Anatomic reference adapted from the Allen Brain Reference Atlas for E13.5.

Furthermore, outgrowing 5-HT-containing fibres (cf. arrow in (b)) can be seen, crossing the MHB (arrowhead in (c)) and aiming for mid- and forebrain regions. They will be treated in more detail under 3.3.4. Given the above-mentioned observations, Tph2 distribution would be expected to take an intermediate position. In accordance with this expectation, image (d) shows its presence in cells migrating towards the DR, MnR and CLi, respectively, as well as in some cells near the fp. On adjacent sections (data not shown), however, Tph2 was also found in the area of the future rostral cluster, as would be expected.

Since DCX is a microtubule binding protein (Brown et al., 2003) and serves as a marker for immature neurons, its expression would be anticipated throughout their proliferation, differentiation and migration (Rao and Shetty, 2004; Francis et al., 1999). Unfortunately, apart from little unspecific red staining on the superficial stratum of the hindbrain, no fluorescent signal could be detected.

Images (g)-(i) display eGFP and 5-HT staining of the caudal cluster and thus help to retrace its formation. Comparable to (a)-(c), eGFP-containing cells are predominantly visible near the ventrally located fp at the superficial stratum of r5-9 and only the minority of migrating cells still show a red signal. As it is the case in the rostral cluster, more and more cells become 5-HT-ir when they mature and start migrating towards their final destinations in the areas of ROb and dorsal RMg. The fact that the RPa and ventral RMg are located superficially, explains why a remarkable collective of 5-HT-expressing cells stays in the surroundings of the fp (cf. (h)).

3.3.2 Somal translocation

Hawthorne et al. (2010) suggest somal translocation as the main migratory mechanism for 5-HT-ir neurons in rostral murine hindbrain. Hawthorne states that “the expression of 5-HT coincided with the completion or near completion of radial somal migration”. Figure 3.6.k shows a still migrating, but already 5-HT-ir neuron with a radially aligned, elongated cell body and a cellular process pointing to the fp (arrow), whose morphology might be consistent with this theory (cf. 4.1.2).

3.3.3 Constellation of the mature raphe nuclei

According to Levitt and Moore (1978), the nine bilaterally located groups of serotonergic neurons are first discernible around E17-18. From this time on, their fusion and thus the formation of the mature raphe nuclei continue, terminating with the midline-fusion of the caudal ROb and RMg around P6 (cf. 1.2.3). Consequently, from P7 on the raphe nuclei can be observed in their mature constellation, even when the precise cell locations might still shift a little due to brain growth, which is not terminated until P21. Figure 3.7 shows the rostral raphe cluster in midbrain and pons in a coronal (a-b) and sagittal (c-d) section, as well as rostral parts of the caudal cluster.

The xscp (b) lies in the caudal Is and marks the border to r1. It is the most rostrally located of the three connections between cerebellum and hindbrain

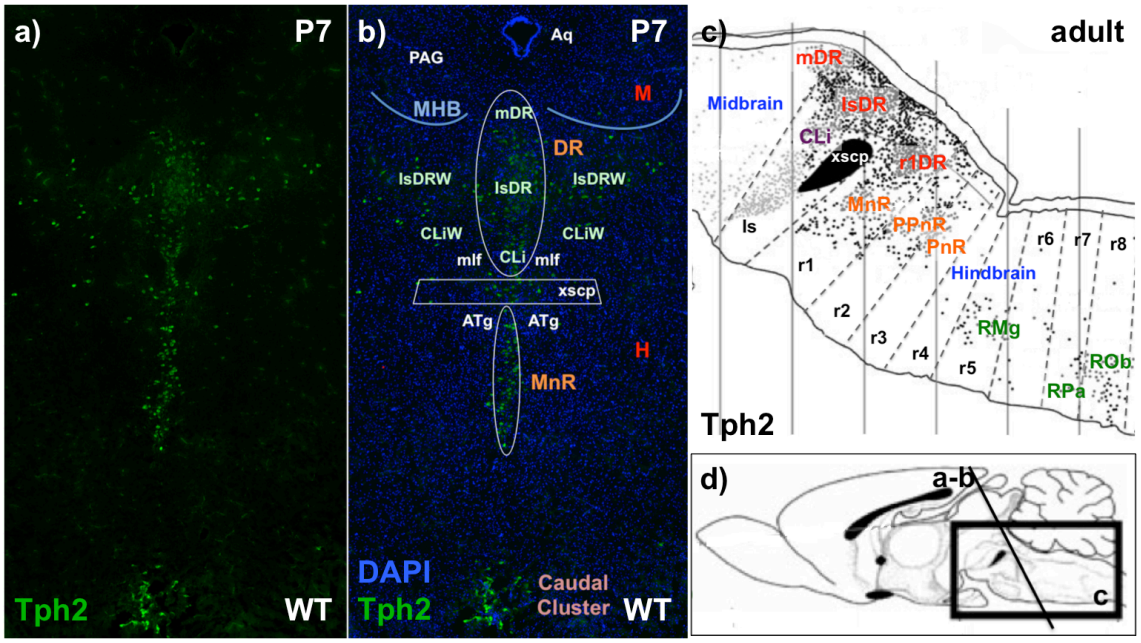

Figure 3.7 Constellation of the mature rostral and caudal raphe nuclei. Coronal (a/b) and mid-sagittal (c/d) sections of P7 WT B6.Cdh13ko-hCMV hindbrain are displayed (images (c)/ (d) adapted from Lowry et al. (2008)/ Alonso et al. (2013)). Each dot represents a single Tph2-ir neuron within a 20µm (a/b) and 30µm (c/d) section, respectively. The rostral cell cluster with DR, MnR and CLi, as well as parts of the caudal one are displayed. The xscp, which marks the Is-r1 transition, contains the cerebellothalamic, as well as the cerebellorubral tract. The mlf is the major motor association tract running medially through the brainstem and interlinking motor brain nerve nuclei (e.g. III, IV and VI). Not far from it, in pontine Tg lies the dopaminergic ATg. Since (c) shows a mid-sagittal view, the lsDRW and CLiW are not visible there. Image (d) visualises the planes displayed in the preceding images in relation to the whole brain. MHB= midbrain-hindbrain-boundary, Aq= aqueduct, PAG= periaqueductal grey, mlf= medial longitudinal fasciculus, xscp= decussation of the superior cerebellar peduncle, ATg= anterior tegmental nucleus,

and contains the cerebellothalamic and cerebellorubral tracts. The adjacent medial longitudinal fasciculi (mlf), which constitute the major motor association tracts, run medially parallel to the brainstem axis and interlink motor brain nerve nuclei. Caudal to the xscp in pontine tegmentum lie the anterior tegmental nuclei (ATg), which belong to the dopaminergic system (Benninghoff and Drenckhahn, 2008) and have been suspected to contain Cdh13 (cf. 3.2.2).

3.3.4 Outgrowing 5-HT projections

Since the serotonergic system in the hindbrain supplies many other brain regions with 5-HT, an extensive interlinking fibre tract system is required.

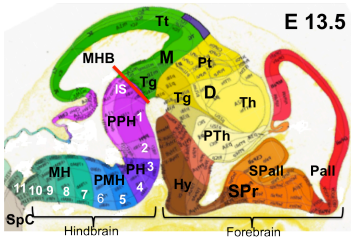

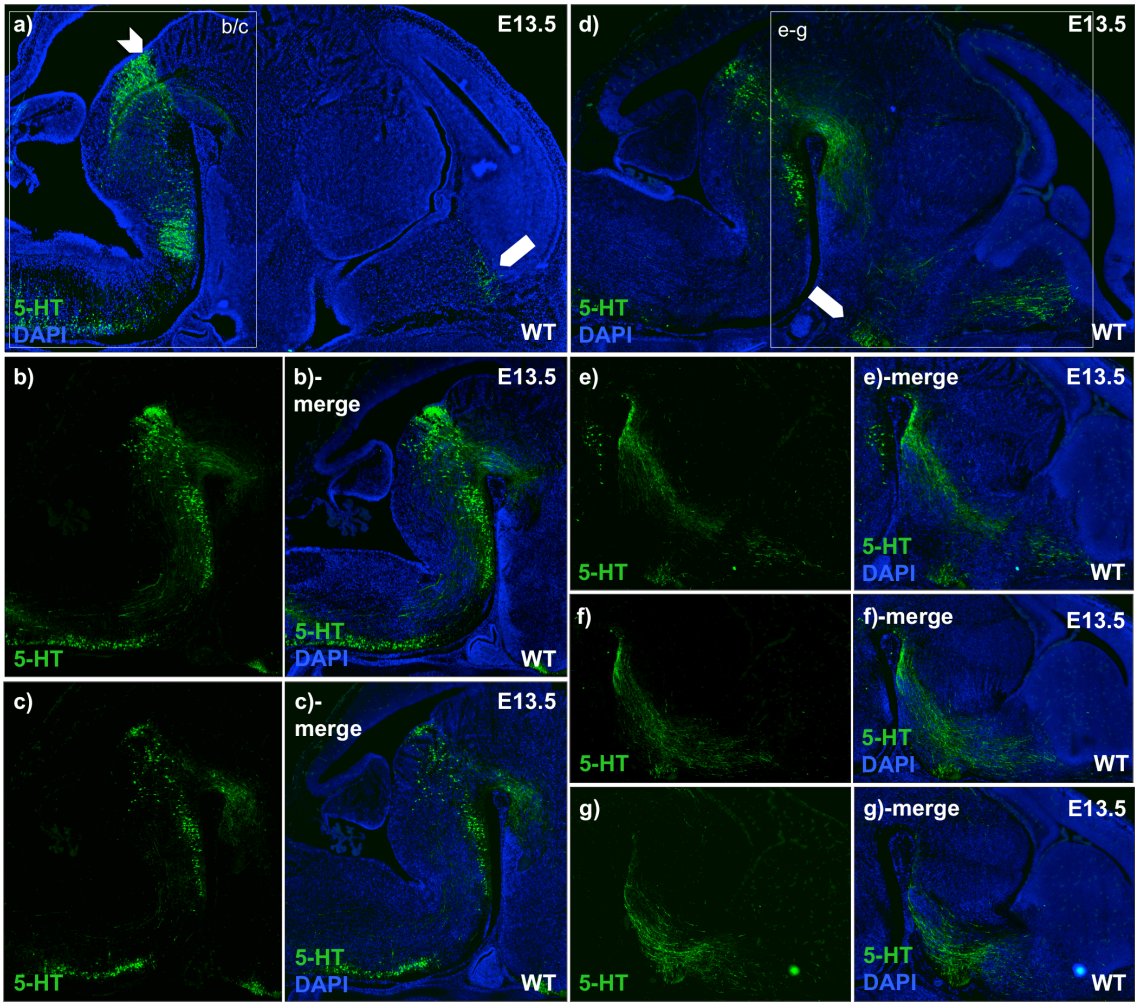

Figure 3.8 5-HT-ir fibres ascend from the anterior raphe nuclei. EGFP^{+} E13.5 mice from the B6.Pet1-cre.eGFP line were used (for anatomic reference see above). The displayed sagittal brain sections (20µm) show the serotonergic nuclei and fibres starting with a paramedian section (a) and proceeding towards more and more lateral sections (b-g). The frames in (a) and (d) show the details the images below refer to. In (a-c) it becomes evident that the 5-HT cell bodies, which are about to form the raphe nuclei, are restricted to the midline (a) and its direct proximity (b-d). At this age the 5-HT cell groups are not yet fused and thus more widely distributed. Apparently, some connecting tracts, i.e. to the Pall and the hypothalamus (Hy), are already established at E13.5. The 5-HT-ir fibres start in the midline at the MHB (arrowhead in (a)) and run through pretectal Tg. Then the tract follows a bent course, drifting more and more to the side, while traversing Hy and basal forebrain. Only when arriving at the SPall and Pall it relocates towards the midline (cf. arrow in (a)). The Hy (cf. arrow in (d)) looks extensively rich in 5-HT fibres, with its area being stained in nearly all of the sections (b-g). Furthermore it is worth mentioning that the fibres start as a circumscribed bundle, which fans out more and more, when entering forebrain areas. Finally, some fibres run medially alongside the hindbrain axis (cf. (b)), linking the rostral and caudal clusters. The colour of the 5-HT-staining was artificially changed to green (originally stained with Alexa 555=red; cf. comment to Table 2.9).

According to Azmitia and Segal (1978) there are at least six symmetrically laid out serotonergic fibre tracts ascending from the rostral raphe nuclei (mainly DR/ MnR) and running towards mid- and forebrain regions, with the DRFT and MRFT travelling within the MFB (cf. 1.2.3). As can be seen in Figure 3.8, at E13.5 the serotonergic cell bodies are located in proximity to the midline (cf. paramedian sections a-d) and just migrating from the fp towards their future locations in the caudal or rostral cluster. At this point in development, the cell groups are still separate and thus more widely distributed (cf.1.2.3). Apparently some of the 5-HT fibre tracts are already forming at E13.5 (cf. (d)). It is obvious, that they only emerge from mature 5-HT cell bodies located in the area of the future DR, CLi and MnR or Is and rh1-4, respectively. The fibres appear to be united in a quite circumscribed bundle crossing the MHB and running through the midbrain. As soon as they enter the diencephalon, whilst surrounding prethalamus (PTh) and thalamus (Th), the fibres start to fan out more and more, following a bent course through latero-basal parts of the forebrain (cf. e-g). Only when they arrive at the SPall they draw back to the midline (cf. (a) arrow). The cortical layers themselves look devoid of 5-HT. The hypothalamic area, however, seems to be especially rich in 5-HT fibres, since it shows stained fibres in nearly all of the sections (b-g; arrow in (d)). Given the above-described course of the 5-HT fibres they could very well correspond to the DRFT and MRFT. At this point in development there is no visible sign of the other fibre tracts described by Lowry et al. (2008), i.e. the DRCT, DRPT, DRAT and RMT.
We would have liked to compare these observations to the situation at E17.5, but unfortunately the 5-HT staining failed for this very stage. Referring to the results from Zhou et al. (2000), we would have expected to see new 5-HT-ir projections beyond the MFB, reaching for example for fascicularis retroflexus, (hypo-) thalamus, habenular nucleus and mammillary bodies.

After having analysed the Cdh13 distribution pattern and the 5-HT system separately in two murine developmental stages, in a next step the influence of reduced Cdh13 presence on the developing 5-HT system has to be examined.

3.4 Influence of Cdh13 deficit on the central serotonergic system

3.4.1 Cdh13 in serotonergic neurons

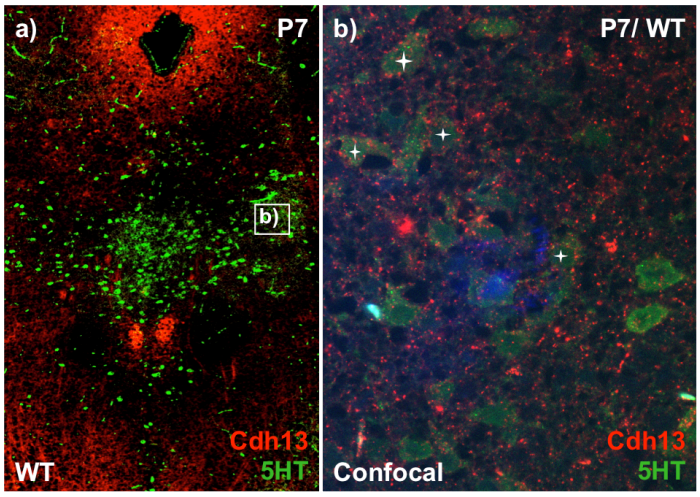

Figure 3.9 Evidence for co-expression of Cdh13 and 5-HT in confocal microscopy. Image (a) shows coronally sectioned rostral hindbrain from the B6.Cdh13ko-hCMV mouse line, which was double-stained for Cdh13 and 5-HT. In (b) the highlighted square is 40x magnified (layers 2µm), using confocal microscopy. It seems that Cdh13, which can be seen as a red punctate pattern in the neuropil, is located along the plasma membranes of 5-HT cells (cf. stars). 5-HT is here shown in green (cf. comment to Table 2.9).

Using confocal microscopy, it is possible to differentiate between overlay and co-expression of Cdh13 and 5-HT (cf. Figure 3.9). Image (a) displays a coronal section through rostral hindbrain, which was double-stained for Cdh13 and 5-HT. In (b) a 40x magnified detail is shown. Cdh13 is known to show a punctate distribution pattern all over cell bodies (cf. 1.2.3), which agrees with our observations. In (b) it appears as irregularly distributed red fluorescent dots on the plasma membranes of 5-HT-ir cells (cf. stars). In consequence, it can be stated that Cdh13 is co-expressed in (at least some) serotonergic neurons. Apart from this location, the protein seems also to be present on non-5-HT-ir fibre tracts in the hindbrain (cf. (a)). These observations agree with findings from ISH double staining (Cdh13/ Tph2) performed in our research group (Rivero et al., 2013).

3.4.2 Comparison of 5-HT- and Cdh13-immunoreactive fibre tracts

The 5-HT- (cf. 3.3.4) and Cdh13-containing fibre tracts (cf. 3.2.3) have already been treated in detail. In the following their paths will be compared in order to find possible similarities.

As can be seen in Figure 3.10.a, Cdh13 is present on fibres running parallel to the brainstem axis, before dividing in two fibre tracts: the upper one travels

between hindbrain and tectum, the lower one comes from the hindbrain and then runs through diencephalon and hypothalamus, before fanning out in the SPall region. Since the upper tract does not contain 5-HT (cf. (c)), the following comparison will concentrate on the lower one. The 5-HT fibres (cf. (c)/(d)) run in only one circumscribed bundle (supposedly as part of the MFB). Furthermore, they arise from the rostral raphe nuclei (i.e. DR, CLi and MnR) and thus do not appear in more caudal hindbrain regions like it is the case for Cdh13 fibres. The serotonergic bundle travels through midbrain, diencephalon and hypothalamus, whereat it describes a gentle curve through more lateral regions, before returning to the midline and fanning out in SPall regions.

Given the comparability of the two tracts, there might very well be an overlap, if not co-localisation of the Cdh13-containing fibres and the serotonergic tracts to

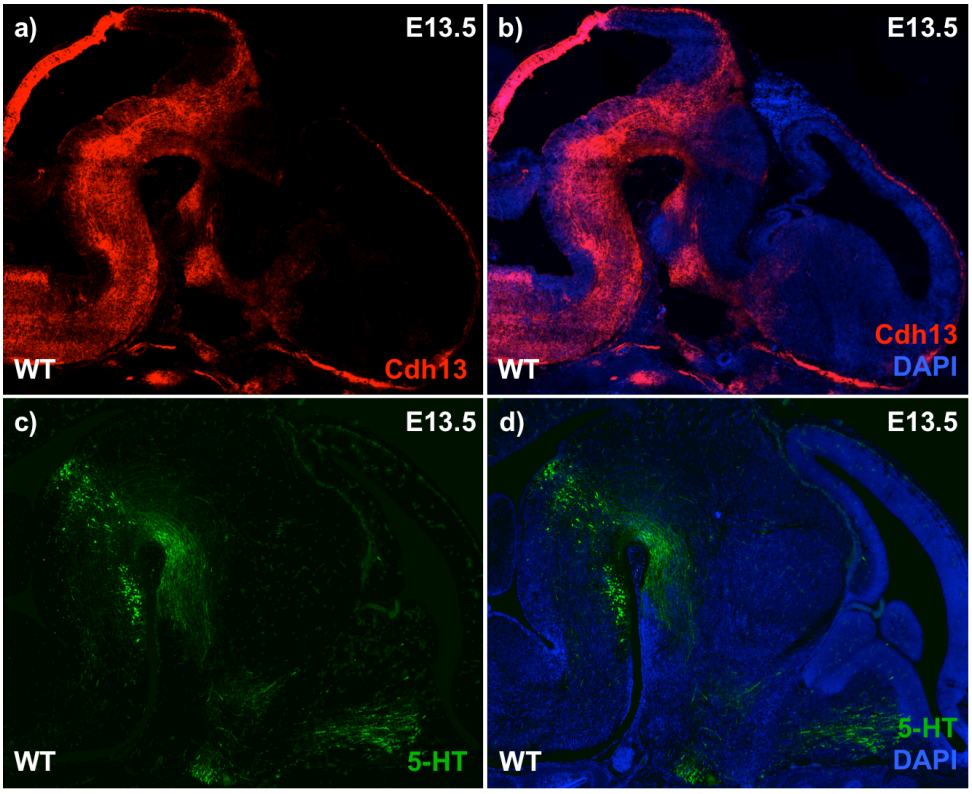

Figure 3.10 Comparison of Cdh13- and 5-HT-ir fibre tracts. Images (a)/(b) show a paramedian sagittal section (20µm) of B6.Cdh13ko-hCMV mouse brain. In (c)/(d) staining was performed on matching sections of B6.Pet1-cre.eGFP mouse brain. As can be seen in (a) Cdh13 is present in two fibre tracts. Only the lower one takes a similar course as the serotonergic tract. The serotonergic fibres (cf. (c)/(d)) run in only one circumscribed bundle, which probably lies within the MFB. In contrast to the Cdh13-containing fibres, they are not present in the hindbrain area between the rostral and caudal raphe cluster. Given the similarities of the fibre courses, there might well exist some fibres containing 5-HT and Cdh13. The 5-HT colour was artificially changed to green (cf. comment to Table 2.9).

the forebrain. The described lateral deviation of the Cdh13-containing fibres, however, does not seem as marked as for the 5-HT bundle: the Cdh13-ir tract can be retraced in its full length on stained paramedian sections (cf. Figure 3.10.a) with only parts of it showing on more lateral sections (cf. Figure 3.4). The serotonergic one, however, clearly deviates completely to the lateral (cf. Figure 3.8). Furthermore, the Cdh13-bundle gives the impression of being less densely packed than the serotonergic one, since the latter appears much thinner at the mesencephalic flexure and seems to fan out in a more restrictive manner.

3.4.3 Distribution of Tph2-immunoreactive cells in the raphe nuclei

Tph2-ir cells have been quantified in WT, HZ and KO mice for all three ages (E13.5, E17.5 and P7), in order to look for aberrations concerning development or distribution of serotonergic cells dependent on reduced Cdh13 expression (Figure 3.11). For better comparability between the genotypes only the relative amounts of cells are displayed.

Compared to the KO, at E13.5 (cf. (a)) the WT sample contains more cells in the act of migration, as well as at the DR/CLi and MnR sites – which are the migratory destinations – and in consequence less cells at the fp. In contrast to that, the result for E17.5 (cf. (b)) seems to point in the opposite direction. There the WT shows fewer cells at the fp and during migration than at E13.5, but still more than the KO at E17.5. In the KO all cells seem to have reached the raphe nuclei already and thus exceed the WT cell numbers in this area. The HZ appears to take an intermediate position between WT and KO. It contains near to no cells at the fp and during migration, but comparable numbers at the raphe nuclei sites. Yet its MnR shows a much higher cell density (near the KO value) than its DR/ CLi (near the WT value). At P7 (cf. (c)) data points from all genotypes lie very close to each other so that no significant deviations between them can be stated. Table 3.1 gives an overview of the absolute numbers resulting of the quantitative analysis.

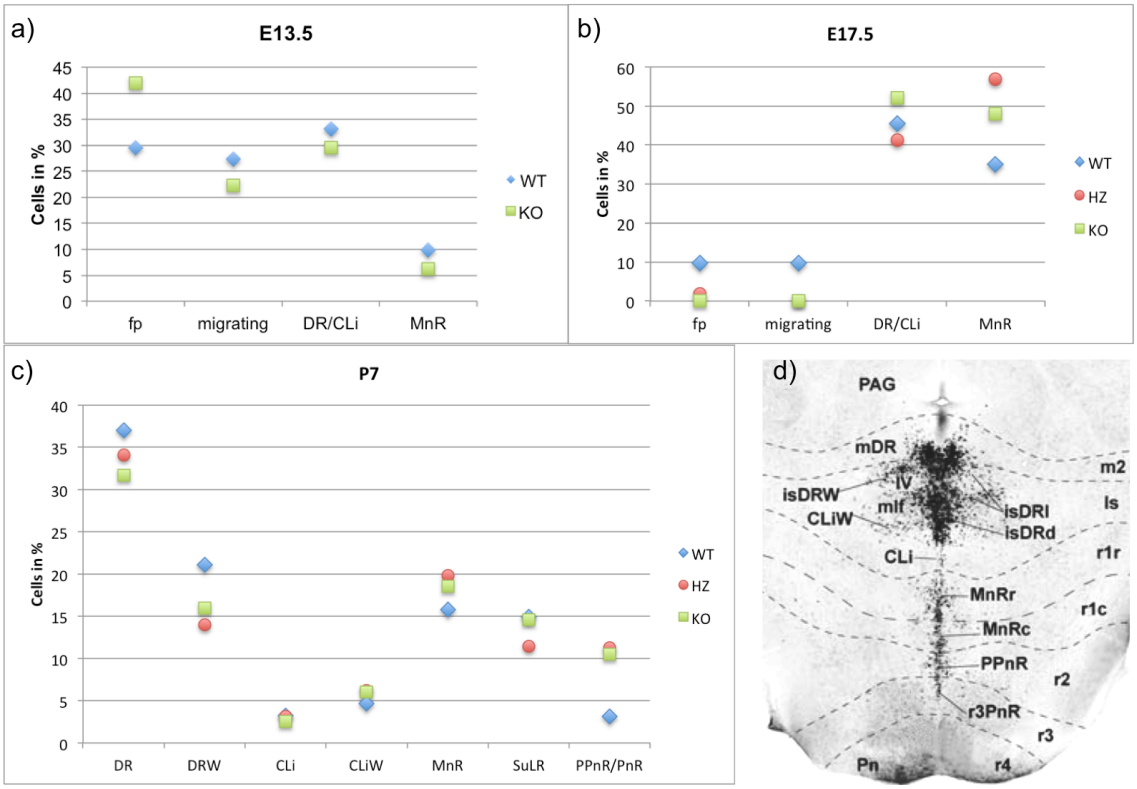

Figure 3.11 Diagrammatic presentation of the counting results. Cells have been counted on sagittally (E13.5/ E17.5), as well as coronally sectioned (P7) 20µm murine hindbrain from B6.Cdh13ko-hCMV mice of three genotypes (WT, HZ, KO). The ABA and Alonso et al. (2013) served as anatomic references for correct cell assignment to the nuclei (cf. (d)). The SuLR is only visible rostral to the section shown and lies bilateral to the MnR. Due to bad tissue quality of the HZ E13.5 series and difficulties with cell classification in the caudal cluster, this data has been excluded from the statistics. For better comparability, a-c display the cell count relative to the absolute number of counted cells per genotype and age (cf. Table 3.1 for the raw data). For each genotype and age only one series of sections has been analysed. For E13.5 and E17.5 cells have been assigned to the following groups: fp, migrating, DR/CLi and MnR. In (a) it is striking that in the KO there are more cells at the fp than the WT. In the latter the majority has already reached the raphe nuclei. Image (b) gives a different impression, with the WT still showing more cells at the fp than the KO, whose cells seem to have reached the raphe already. In (c) most of the data point lie very close to each other so that no trend is showing.

Categories for E13.5, E17.5 and P7 were chosen differently, since in earlier stages the raphe nuclei were more difficult to differentiate and at P7 migration has already finished. The amount of sections is meant to give an idea of the lateral extensions of the nuclei. It is striking that at E13.5 and E17.5 the WT sections always contain more cells than the HZ and KO ones. Only at P7 the values lie closer together. Since the DR is known to be the most extensive one of the raphe nuclei, it is not surprising that it claims the highest proportion of

cells after finished migration, apparently more or less unaffected by the Cdh13 deficit.

	fp	migrating	DR	DRW	CLi	CLiW	MnR	SuLR	PPnR/ PnR	Amount of Sections	Total
E13.5											
WT	215	199		241				72		6	727
In %	29,6	27,4		**33,1**				9,9			100
HZ	80	32		74				30		8*	216
In %	**37,0**	14,8		34,3				13,9			100
KO	87	46		61				13		7 (2)	207
In%	**42,0**	22,2		29,5				6,3			100
E17.5											
WT	89	89		415				319		14 (1)	912
In %	9,8	9,8		**45,5**				35,0			100
HZ	10	0		218				300		13	528
In %	1,9	0		41,3				**56,8**			100
KO	0	0		298				275		9	573
In %	0	0		**52,0**				48,0			100
P7											
WT	-	-	891	509	78	113	381	361	77	13	2410
In %	-	-	**37,0**	21,1	3,2	4,7	15,8	15,0	3,2		100
HZ	-	-	773	317	72	141	450	260	255	10	2268
In %	-	-	**34,1**	14,0	3,2	6,2	19,8	11,5	11,2		100
KO	-	-	746	376	61	143	437	344	247	12 (8)	2354
In %	-	-	**31,7**	16,0	2,6	6,1	18,6	14,6	10,5		100
* Half of the sections could not be analysed due to bad tissue quality. Therefore this data is not included in the chart.											

Table 3.1 Numeric presentation of the counting results. The head row lists the categories cells were assigned to in the different developmental stages. The latter are visible in the first column and further differentiated in the three genotypes. Since cell migration has already been finished at P7, the first two categories were not considered for this age. In earlier ages the raphe categories could not be differentiated as reliably as for P7, so that cells were only assigned to being part of DR/CLi and MnR. Counting results are given in absolute numbers, as well as in relation to the total amount of counted cells per genotype, which is always listed below the absolute values. The category with the biggest proportion of cells is highlighted in bold. Furthermore, the amount of sections with visible cells of the rostral cluster is given in row 10. The bracketed numbers give the number of additional sections containing only cells from the caudal cluster. This information is thought to help estimating the volume of the raphe nuclei in the hindbrain. At E13.5 and E17.5 WT samples contain more cells than the HZ and KO ones. Only at P7, they show comparable amounts. The DR as the biggest of the nuclei contains most cells more or less independent of the Cdh13 expression.

3.4.4 Morphologic comparison of the raphe constellation

In order to examine possible influences of a Cdh13 deficit on the morphologic occurrence of the mature raphe complex comparable sections of rostral murine hindbrain were selected and can be seen in Figure 3.12. The size of the aqueduct and landmarks like the ATg ((d)/ arrow) were used for the selection of matching sections. In Figure 3.12.n another confocal image is

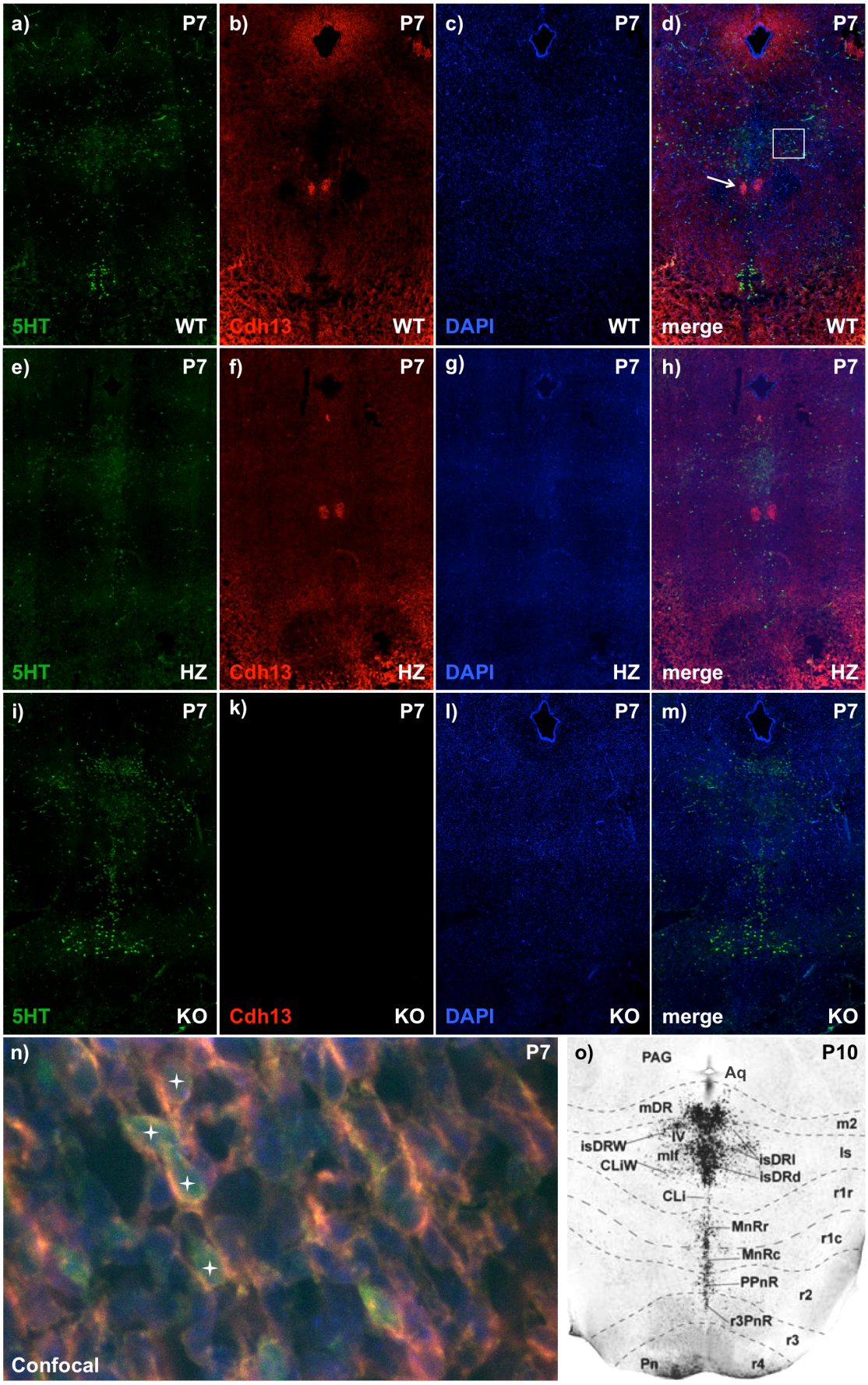
a)
P7
5HT
WT
b)
P7
Cdh13
WT
c)
P7
DAPI
WT
d)
P7
merge
WT
e)
P7
5HT
HZ
f)
P7
Cdh13
HZ
g)
P7
DAPI
HZ
h)
P7
merge
HZ
i)
P7
5HT
KO
k)
P7
Cdh13
KO
l)
P7
DAPI
KO
m)
P7
merge
KO
n)
P7
Confocal
o)
P10
PAG
Aq
mDR
m2
lV
isDRW
CLiW
mlf
isDRl
isDRd
ls
r1r
CLi
MnRr
r1c
MnRc
PPnR
r2
r3PnR
r3
Pn
r4

Figure 3.12 Morphologic comparison of the raphe formation in rostral hindbrain at P7 (cf. previous page). Comparable Cdh13 and 5HT double-stained sections (20µm) from rostral hindbrain of B6.Cdh13ko-hCMV mice are displayed. Comparability was achieved, using the size of the aqueduct, as well as the presence of the ATg as markers. One row of images shows all three channels and the merge for one genotype. The arrow points to the structure suspected to be the dopaminergic ATg (cf. Figure 3.3). The frame in (d) is magnified under a confocal microscope (cf. (n)). It provides further proof for the co-expression of Cdh13 and 5-HT (visible as yellow signal), even though the punctate pattern of Cdh13 is not as evident as in Figure 3.9. Image (o) provides the anatomic reference adapted from Alonso et al. (2013). Staining for 5-HT occurred with high background in our experiments, which is why cells are not as easily discernible as with Tph2 staining. Between the WT and the HZ no big difference is evident. In the KO, however, cells seem to be more widely scattered and the raphe nuclei less tightly packed than in WT or HZ. 5-HT colour was changed to green (cf. comment to Table 2.9).

shown. It provides further evidence for the co-expression of Cdh13 and 5-HT, which is visible at the outer zones of the serotonergic cells where red and green signals appear together, thus giving a yellow impression.

In addition to that it can be stated that the complete absence of Cdh13 (cf. i-m) does not prevent the formation of the raphe nuclei. They seem to be all in place and the overall structure of the raphe constellation also looks unaffected. The comparison to the WT and HZ, however, gives the impression that serotonergic cells are more scattered in the KO and that the raphe nuclei are less tightly packed (cf. i/ m). In order to get a better impression of the raphe constellation in its whole extent, Figure 3.13 provides coronal series of Tph2-stained sections of rostral hindbrain from the three genotypes.

When comparing the three genotypes, their morphological appearances seem to be slightly different. Throughout the whole series, the WT raphe nuclei give the impression of being more tightly packed than the other genotypes, meaning that cells are less scattered and lie nearer to the midline. The WT sections correspond to the anatomic references (cf. 3.12.o and Alonso et al. (2013)). The HZ and even more the KO give a different impression. There, many Tph2-ir cells lie far from the midline and are sometimes not easy to assign to a distinct raphe nucleus (e.g. in 3.13.s/r). The rough constellation of the raphe is, however, conserved.

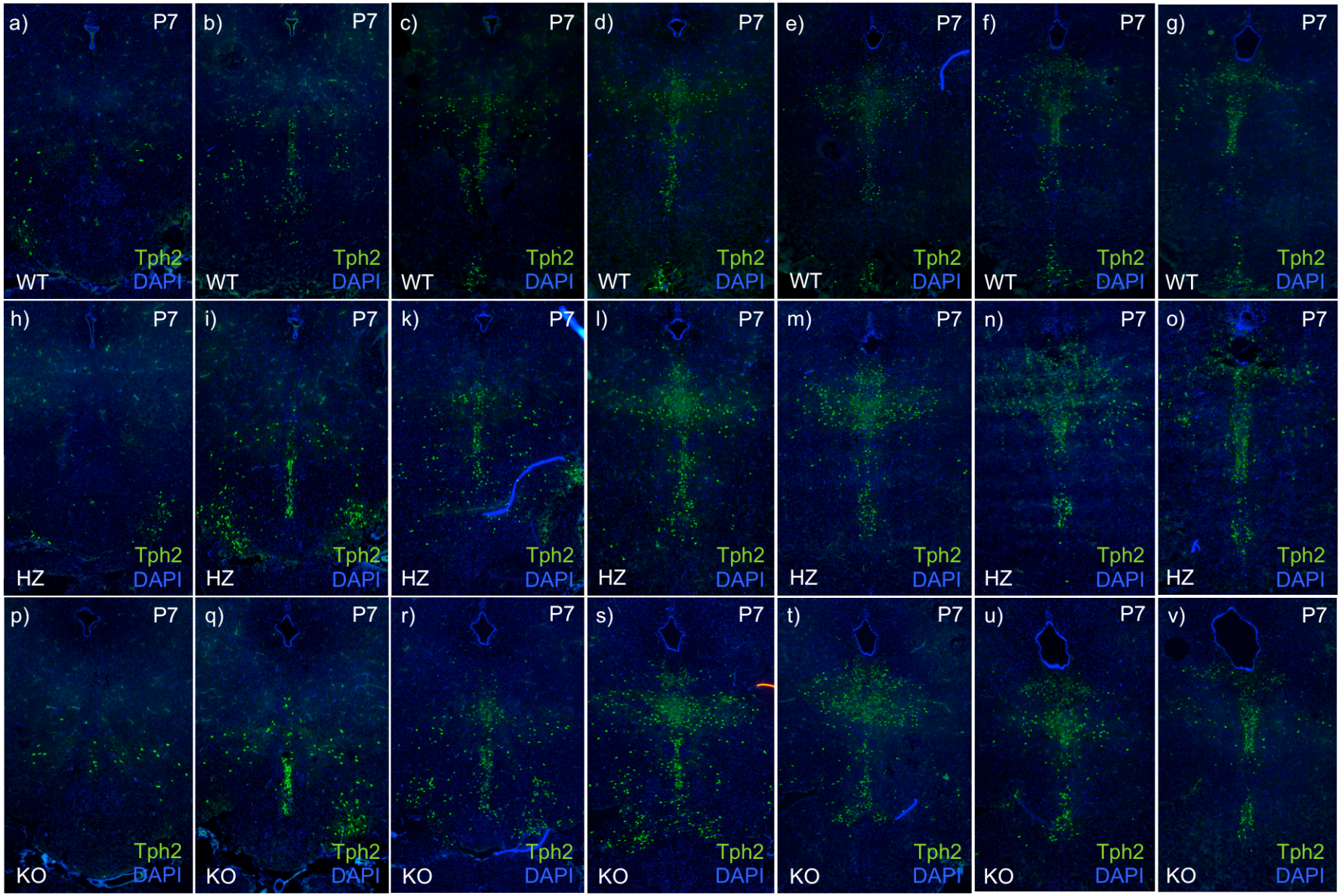
a) P7
WT
Tph2
DAPI
b) P7
WT
Tph2
DAPI
c) P7
WT
Tph2
DAPI
d) P7
WT
Tph2
DAPI
e) P7
WT
Tph2
DAPI
f) P7
WT
Tph2
DAPI
g) P7
WT
Tph2
DAPI
h) P7
HZ
Tph2
DAPI
i) P7
HZ
Tph2
DAPI
k) P7
HZ
Tph2
DAPI
l) P7
HZ
Tph2
DAPI
m) P7
HZ
Tph2
DAPI
n) P7
HZ
Tph2
DAPI
o) P7
HZ
Tph2
DAPI
p) P7
KO
Tph2
DAPI
q) P7
KO
Tph2
DAPI
r) P7
KO
Tph2
DAPI
s) P7
KO
Tph2
DAPI
t) P7
KO
Tph2
DAPI
u) P7
KO
Tph2
DAPI
v) P7
KO
Tph2
DAPI

Figure 3.13 Morphologic comparison of the raphe constellations in coronal series (cf. previous page). Three series of sections, one for each genotype, of P7 murine hindbrain from the B6.Cdh13ko-hCMV line are displayed. These Tph2-stained series (together with the ones for E13.5 and E17.5) have been the basis for the quantitative analysis (cf. 3.4.3), since this staining showed less background signals than the one for 5-HT. In comparison to the other genotypes, the WT raphe nuclei appear more tightly packed and keep near to the midline. On the HZ sections the DR gives a more scattered impression and in the KO cells from both, the DR and MnR, seem to be more widely distributed to the lateral.

4. Discussion

Considering the results of the present study, it is evident that the absence of Cdh13 does not *prevent* the 5-HT system from forming. Whether the lack of Cdh13, however, impacts its development or the establishment of its fibre tracts still needs to be discussed.

Beforehand, it has to be stated that our experiments only have the ability to determine mere trends or observations and the results should be considered as preliminary. With only one animal having been examined per genotype and age and every staining only having been performed once, the results lack statistical power. All experiments should be repeated at least twice and more transgenic mice will have to be examined in order to sufficiently increase the reliability and to be able to calculate the standard deviations. Nevertheless, the findings are highly plausible, for instance with regard to the restriction of CDH13- and 5-HT-immunoreactivity to specific developmentally determined regions at the different ages, with regard to the changes in the patterns from one developmental stage to the next, and with regard to the localization and organization of the different serotonergic cell groups. Therefore, they represent a valid basis for the following discussion as well as for future investigations.

Furthermore it has to be mentioned that not all results obtained for mice must be 100% applicable to humans. The chemical neuroanatomy of the DRN for example varies considerably between species (Fu et al., 2010).

4.1 Cdh13

4.1.1 Protein distribution pattern

Our staining protocol detects Cdh13-IR as early as E13.5, where it already shows quite an elaborate distribution pattern. This agrees with the observation

of Redies (2000), stating that the expression of most cadherins starts early in development right after brain segmentation. In brain development they are known to play a fundamental role in cell sorting and aggregation within the various brain regions (Redies, 1995). In this process cadherins often occur in a gradient-like manner within one distinct brain subdivision (e.g. a rhombomere), although their expression often abruptly changes at the borders between the subdivisions (Redies, 2000). This is consistent with our observations concerning Cdh13 (cf. 3.2.2): In hindbrain rhombomeres it appears in a gradient-like manner between ventricular and superficial zones and the MHB is quite pronouncedly marked.

According to Philippova et al. (2005), Cdh13 shows a punctate distribution all over cell body membranes, not with preference to synapses or intercellular junctions like classical cadherins, but to membrane lipid rafts. This pattern is only abandoned during development or in case of tissue damage when Cdh13 accumulates at the leading ends of processes, possibly steering their migration (Philippova et al., 2009; Mavroconstanti et al., 2013). In our experiments the distribution of Cdh13-IR only appeared punctate on coronal sections of P7 murine hindbrain (cf. Figure 3.9). This might, however, also be an effect of transversal cutting of fibres since at E13.5 and E17.5 Cdh13 is predominantly present on (hindbrain) fibres, showing a very high intensity.

At E17.5 the focus of Cdh13 seems to have shifted from hindbrain to cerebral cortex (cf. Figures 3.3.d/f). Takeuchi et al. (2000) observed Cdh13 to be present in pyramidal, as well as in non-pyramidal cortical cells. This theory cannot be confirmed reliably in this thesis, since further staining would have to be performed in order to distinguish properly between both cell types. In addition to that, Cdh13 occurs in all cortical layers with preference to what appears to be layers III and V. Given that these layers are very rich in pyramidal cells, this distribution could point towards an augmented concentration in these cells. The higher intensity of the Cdh13 signal could, however, also result from an increased cell density in these layers.

In our experiments Cdh13-immunoreaction did not label the nuclei, since there were no overlaps with DAPI staining (cf. Figure 3.3.i). Furthermore, it could not

be seen in neural cytoplasm, contrasting the statements of Takeuchi et al. (2000). These aberrations, however, could be due to the use of differing antibodies, consequently detecting different splice variants or uncleaved propeptides of Cdh13 (Philippova et al.; 2009). It is evident that membrane proteins like Cdh13 need to be processed in cytoplasm before being inserted into the membranes, so that sensitive methods might be able to detect it there as well.

4.1.2 Cdh13 as a developmental guiding molecule

The distribution pattern of Cdh13 in murine CNS changes over development. At E13.5 Cdh13-IR is limited to certain fibre tracts and cell aggregates (cf. Figure 3.5.a), which mainly reside in hindbrain and adjacent areas. It is striking that Cdh13 is present at the starting points, as well as at the final destinations of the visible fibre tracts, thus confirming the observation of Redies et al. (2012), that "grey matter structures, their fibre projections and their target areas have matching cadherin profiles". This strengthens a role of cadherins (and presumably also of Cdh13) in the process of migration and path finding of neural processes with the aid of low-adhesive homo- or heterophilic interactions (Rivero et al., 2015). Presupposing the Cdh13 deficiency is associated with ADHD, this would imply mislead or malfunctioning neuronal circuits, as has been described recently in frontal, striatal and cerebellar white matter connectivity in ADHD patients (Hong et al., 2014). In order to examine possible tract deviations, it would be helpful to determine the type of neurotransmitter in these tracts, so that specific staining protocols could be performed.

At advanced stages of development (E17.5/ P7) the Cdh13 signal decreases in the hindbrain and becomes more homogenously distributed all over the CNS (cf. Figure 3.3.g). As Rivero et al. (2013) stated for human brain, Cdh13 is present in developing, as well as in adult CNS, showing higher expression in the latter. Cdh13 mRNA expression has been found to reach a peak concentration in rat brains between P7 and P21, coinciding with increasing synaptogenesis in the neocortex (Rivero et al., 2015). These observations would be consistent with our findings, since Cdh13 is more widely spread in

mouse brains at P7 than at E13.5, even if it appears to be more concentrated in immunoreactive structures at the younger stage. The above-mentioned changes of Cdh13 appearance over development and its wide-spread but dampened presence after birth (i.e. P7) agree with Cdh13 being a developmental guiding molecule, as well as with its suggested role in the maintenance of developed circuits (Takeuchi et al, 2000; Rivero et al., 2013).

According to Hawthorne et al. (2010) embryonic 5-HT neurons in the hindbrain use somal translocation when they migrate from the fp to form the rostral and caudal clusters of the raphe nuclei. Typical for this special form of locomotion is the transient persistence of the *ventricular* (towards the fp) and *pial* (towards the raphe clusters) processes of the migrating cell. In this way the cells align radially, showing a bipolar morphology, and move by shifting their soma through the pial process. Finally, the ventricular process, which is at least present until E13.5, is retracted. The Cdh13-ir fibres, which connect superficial and ventricular layers of the Is/r1 area at E13.5 (cf. Figures 3.3.a/c), need to be considered in this context. They might play a role in somatic translocation. Since in this area Cdh13 could not be detected on 5-HT fibres themselves, the immunoreactive fibres might correspond to radial glia (cf. Redies, 2000), serving as rail-like framework for these dynamic processes.

The sharp border these fibres form towards the midbrain (cf. Figure 3.3.c) might be considered in the context of Cdh13 possibly playing a role in the segregation of CNS compartments (Philippova et al., 2009). At E17.5 or P7 these fibres are not discernible any more (cf. Figures 3.3.d/g), which strengthens the suggestion that they play a transient role during development of murine hindbrain structures.

4.1.3 Cdh13 and other neurotransmitter systems

In the course of our experiments it could be confirmed that Cdh13 is localised within Tph2-ir cells, an observation that has already been reported for Cdh13 mRNA in ISH staining by our research group (Rivero et al., 2013). This observation is crucial for the theory that Cdh13 has an impact on the (developing) serotonergic system. There is, however, evidence towards Cdh13

not being exclusively present in the 5-HT system, but also playing a role in other neural networks. For instance it has also been detected in GABAergic and glutamatergic synapses, as well as in catecholaminergic, dopaminergic and noradrenergic CNS structures, like ventral tegmental area, substantia nigra and locus coeruleus (Rivero et al, 2013).

Concerning our experiments, it is obvious that the Cdh13 protein distribution pattern and the 5-HT system are incongruent in some parts. To be mentioned are the Cdh13-containing fibre tracts between hindbrain and tectum, as well as the extensive fibre tracts running alongside the hindbrain axis below the rostral raphe cluster (cf. Figure 3.4). In addition to that the dopaminergic ATg in the area of r1 show strong Cdh13-IR (cf. Figure 3.3.k). These observations could be interpreted in accordance with the long-pursued dopaminergic theory in the context of ADHD (Roman et al., 2009). It was based on the existence of effective therapeutics like MPH, blocking DA transporters, as well as on the association of ADHD with defect frontostriatal dopaminergic pathways (Banaschewski et al, 2010). The DA transporters (e.g. DAT1/SLC6A3) and receptors (DRD1-5), the DDC, as well as the dopamine-β−hydroxylase (DBH) ranging among the top susceptibility genes in genetic studies (Roman et al., 2009; ADHDgene) also support this theory. The idea of abnormal DA levels being the exclusive cause of ADHD, however, was quickly abandoned, due to insufficient statistical significance of the candidate genes and the huge amount of upcoming susceptibility genes, which were unrelated to the DA system. Given that DDC is involved in the production of DA *and* 5-HT, as well as that DBH also catalyses the conversion of DA to noradrenaline, these transmitter systems seem to be closely linked. Montalbano et al. (2015) further stressed these connections by stating that in absence of Tph2 mice show abnormal brain development resulting in “reduced numbers of noradrenergic neurons in the locus coeruleus and lower epinephrine content”. The relevance of these other transmitter systems for ADHD is strengthened by the existence of strong catecholaminergic (e.g. NET1/SLC6A2 and ADRA2A/2C; Banaschewski et al., 2010), as well as cholinergic (CHRNA4; ADHDgene) susceptibility genes.

With Cdh13 being present not only in the 5-HT system, but also in dopaminergic and noradrenergic neurons, its absence could impact these systems just as the serotonergic one and thus contribute to the occurrence of ADHD-like phenotypes. A link between Cdh13 and the other neurotransmitter systems could help to explain why all of them show strong associations with ADHD, without being significant on their own. Since several constituents the Cdh13 expression pattern, e.g. the tectal fibre tract, could not yet be associated to a certain neurotransmitter system, it would be a promising task to explore possible connections to the above mentioned candidates.

4.2 Cdh13 and the 5-HT system

4.2.1 Similarities in 5-HT- and Cdh13-containing fibre tracts

Referring to the observations in 3.3.4 and 3.4.2 there is one 5-HT-containing fibre bundle, which travels between brain stem and prefrontal cortex. Based on the analysis of Lowry et al. (2008), it was suggested that this bundle consists of the DRFT and MRFT, which lie within the MFB. DRFT/ MRFT lie in its ventrolateral/ ventromedial aspect, respectively, and project to lateral/ medial forebrain areas. The MFB is known to comprise ascending, as well as descending fibres (Azmitia & Segal, 1978), thus connecting the forebrain to basal olfactory regions, to the periamygdaloid region, to the septal nuclei and to brainstem regions like the ventral tegmental area. It runs through the lateral hypothalamus and the basal forebrain in a rostro-caudal direction (Anthofer et al., 2015). This description corresponds very well to the course of the serotonergic fibre bundle described in 3.3.4. In consequence, it can be assumed that this bundle is equivalent to the MRFT and DRFT.

In 3.4.2 the course of these tracts has been compared to the Cdh13-ir fibre bundle, which follows approximately the same trajectory. As has been stated before that the two tracts are well comparable, only that the Cdh13-ir one gives the impression of not deviating as lateral as the serotonergic one and of being less tightly packed. There are three possibilities of interpretation: First, this could be interpreted as the Cdh13- and 5-HT-containing tracts corresponding to

each other. When considering the proportions of the Cdh13 tract, it might, however, correspond to only one of the 5-HT containing tracts, most likely the more medially located MRFT. Second, since no co-localisation of the fibres could be proven so far, the Cdh13-ir fibres might as well correspond to other bundles within the MFB, like for example dopaminergic ones. According to Azmitia and Segal (1978), these fibres, as well as noradrenergic ones, should occupy the dorsal aspect of the MFB, whereas serotonergic fibres occupy the ventral one. Since the ATg has been proven to contain Cdh13 (cf. 3.3.n) and the MFB is known to contain fibres from the ventral tegmental area, this does not seem too far-fetched. Finally, it is possible that the Cdh13-containing fibres constitute rail-like guiding assistants for the outgrowing 5-HT fibres, as has been suggested for the isthmic hindbrain (cf. 4.1.2). The first two theories, however, can only be confirmed with evidence for co-localisation of Cdh13 and 5-HT (or DA) in these fibres, which should be addressed in future experiments using confocal microscopy and further double staining.

4.2.2 Interpretation of the quantitative analysis

It has been suggested in literature that ADHD might result from errors in synaptic formation and connectivity, leading to “delays in maturation of cortical neurocircuits” (Lesch et al., 2008), which impact cognition and emotional control. The aim of this analysis was to explore the dynamics of the developing serotonergic system and to determine a possible impact of absent Cdh13.

Comparing the differences in cell distribution between WT and KO seen in Figure 3.11.a, these observations could be interpreted in the sense of a migratory delay of serotonergic cells due to the Cdh13 deficit, thus confirming the above-mentioned theory. Figure 3.11.b, however, gives a different impression, which can be interpreted in two different ways: Either migration starts earlier and takes longer in WT than in KO B6.Cdh13ko-hCMV mice. This would, however, imply that serotonergic cells in KO mice were able to catch up their deficit and furthermore overtake the WT cells in development within four days. Or the low number of analysed samples just does not allow a consistent interpretation of the results. Concerning the results for P7 (Figure 3.11.c), the

data points lie very close together without showing any clear deviations between the genotypes. Either this is also resulting from the low sample size, or at this point in development the Cdh13 deficit does no longer impact the cell distribution in the serotonergic system. This would lead to the intriguing conclusion that a Cdh13 deficit only changes the dynamics of the developing serotonergic system, yet not the (quantitative) result itself.

Concerning the results in Table 3.1, there are some issues in the experimental setup that might influence the results and thus will be discussed in the following. Brains from all developmental stages have been sectioned with the same thickness of 20µm. Obviously, this implies a higher number of resulting sections for P7 than for E13.5, due to different brain volumes. It would have been better to reduce the size of the sections for the younger stages relatively to their brain volume, so that the number of sections would have been identical. Given that the sections were equally distributed to six series (cf. 2.2.4) and only one series has been stained for each genotype and age, this procedure would have levelled the error, resulting from the proportion of uncounted cells on the five adjacent series. This would have led to a better comparability of the absolute total cell numbers between the three ages. Evidently, staining and analysis of all series from one genotype could have eliminated this error. It has, however, to be stated, that the fact of serotonergic cells at E13.5 and E17.5 not being yet as widely distributed as at P7 still increases the above-mentioned error for these younger stages. Furthermore, the closer the cells lie together, the more difficult it is to reliably determine their number, due to cell overlap. Finally, some series showed rather bad tissue quality, e.g. E13.5 HZ, which of course also hindered reliable cell counting. These thoughts have been at the origin for the calculation of the relative cell proportions and their display in the graphs.

These limitations, however, do not touch the comparability between the three genotypes of one age. For E13.5 and E17.5 the absolute number vary immensely between the WT and the two others. Reduced amounts or absence of Cdh13 might thus very well cause reduced serotonergic cell numbers as has been suggested by Arias-Vasquez et al. (2011). The proportions at the various sites (cf. Table 3.1), though, stay comparable to the WT. The DR/CLi for

example is meant to contain the better part of 5-HT cells, which is fulfilled for all stages apart from the migration phase, where the raphe nuclei are still forming. Considering the statements of Gaspar et al. (2003) and Alonso et al. (2013), which imply that the generation of serotonergic neurons takes place between E10-E12 and should have been finished by E12.5, the growing absolute cell numbers between E13.5 and P7 (cf. Table 3.1) could not be attributed to development and thus growth of the raphe nuclei in the hindbrain. The number of serotonergic cells in the hindbrain would have been set at E12.5 and should stay stable over development. In this case the detected aberrations would have to be explained by the above-mentioned errors, as well as the change from sagittal to coronal slicing between E17.5 and P7, which improved the counting conditions. Even if Alonso and Gaspar were wrong, this would only impact the interpretation of the E13.5 results, since it is very unlikely that serotonergic neurons, being part of the earliest appearing neurotransmitter system (Zhou et a., 2000), should still be born as late in development as between E17.5 and P7.

4.2.3 The development of the raphe nuclei

Concerning the time frame of raphe nuclei development, Hawthorne et al. (2010) name E10.0 as date of first appearance for Pet1-expressing 5-HT-precursor cells. With Pet1-expression always preceding the occurrence of 5-HT-expression by half a day and the rostral cluster developing about 1d before the caudal one, serotonergic cells were then to be expected around E10.5 for the rostral and around E11.5 for the caudal cluster. Deng et al. (2007), however, give divergent information, dating the first detection of serotonergic neurons at E11.5. In the following maturation process, the cells start to produce Tph2, the key enzyme for 5-HT production. Naturally, serotonin itself can only be detected after that. According to Alonso et al. (2013), the majority of 5-HT raphe neurons should have been born by E12.5. Using DCX as a marker for immature neurons in combination with 5-HT staining, we aimed to determine the exact time in development for 5-HT-cell maturation. According to the Allen Brain Atlas, during embryogenesis and at E13.5 in particular, DCX should be found in a dense

expression pattern all over the hind- and midbrain, which is not the case in our experiments. Most likely this has to be assigned to a failed staining protocol.
When taking a look at Figure 3.12, it is striking that the raphe nuclei have developed in all genotypes and even show a more or less comparable constellation. In comparison to each other, the cells appear to be the more scattered, the fewer the Cdh13 expression, i.e. the WT looks more tightly packed than the KO with less cells being difficult to assign to certain raphe nuclei. It has been stated before that “altering cadherin expression [can induce a change in the migratory path of, L.P.] early migrating neurons” (Redies et al., 2012), so that the final placing of the neurons deviates from their original destination points. If Cdh13 really was involved in the outgrowth and formation of the serotonergic system, its absence might influence this system accordingly.
Although with the serotonergic system developing in spite of Cdh13 absence, it is likely that other molecules exist with at least partially overlapping functions. According to Bekirov et al. (2002), “most anatomical groups are associated with more than one cadherin”. In consequence, the loss of Cdh13 might be compensated in parts by a different cadherin. This would not be surprising, given their important role during neurogenesis (cf. 1.2.3).
Apart from these explanations the differences between the genotypes could also be a question of varying section planes. In order to differentiate more reliably between these possibilities more series will need to be analysed.

4.3 Conclusion

4.3.1 Pleiotropy

It has been suspected before that “deficits in single cadherins are likely to result in *minor* changes in neural connectivity and synaptic function” (Redies et al., 2012), due to redundant distribution and function of the diverse cadherins. In consequence, defective cadherins probably have an impact on a multitude of neural subcircuits. This is consistent with the concept of *pleiotropy*, which implies that molecules can have a “number of distinct roles in the CNS at different times in development” (Redies, 1995). This would explain why alterations in the genetic sequence of Cdh13 could contribute to several distinct

psychiatric phenotypes, like autism, alcohol dependence or ADHD (Redies et al., 2012). Considering these thoughts, it is not surprising that in our experiments the serotonergic system develops in spite of the Cdh13 KO without showing more pronounced disturbances. Furthermore, pleiotropy might be one reason for the huge amount of candidate molecules in ADHD pathophysiology.

4.3.2 Decanalization

Even with the limitations of our study it can be stated that the observed trends concerning the characteristics of the cadherin system agree with formerly suggested theories. The changing Cdh13 distribution over time, as well as its presence in more than one neurotransmitter system (5-HT, DA) give the impression of Cdh13 influencing neurogenesis and/ or neuronal differentiation continuously on a broad scale. The impact of its absence on singular neural subsystems like the raphe nuclei, however, has not been too pronounced. It could only be observed that under deprivation of Cdh13 the development of the serotonergic system was transiently delayed and the absolute numbers of serotonergic cells were reduced, even though their distribution to the single nuclei stayed constant. It was striking that after birth the raphe constellation, as well as the total amount of serotonergic cells seemed more or less approximate between the genotypes. The observed deviations in raphe morphology were assigned to its role as guiding molecule in migration. Taken together, these experiments suggest a subtle but nonetheless existent influence of CDH13 deficiency on the serotonergic system, which is underlined by the demonstrated co-localisation of the two molecules. This could be explained considering inbuilt compensatory systems like the concept of pleiotropy (cf. 4.3.1), as well as “genetic redundancy and homeostatic mechanisms” (Loke et al., 2015). In consequence the knockout of a specific gene only results in subtle phenotypic changes, which is referred to as *decanalization*.

4.3.3 Dysfunctional pathways

Considering the huge variety of candidate genes as well as the interconnection between the single affected systems (cf. 1.4.3), it seems only consequent to

search for candidate genes, which are involved in very early stages of development. Contrary to former expectations GWAS reported growing evidence for candidate genes related to basic developmental processes like neuronal migration and plasticity, cell division and adhesion (via cadherin and integrin systems), gene transcription and cytoskeletal remodelling (Franke et al., 2009), like genes for nerve growth factor (NGF) and its receptor (NGFR), glial cell line-derived neurotrophic factor (GDNF), brain derived neurotrophic factor (BDNF), synaptosome-associated protein of 25,000Da (SNAP25) and many more (Banaschewski et al, 2010). This would imply that pathways developing in dependence of these early molecular cues were involved in the pathogenesis of ADHD, without the alteration of the involved molecules exerting a significant influence. This very much reflects the current situation of genetic studies for ADHD, where only very little evidence points to a direct involvement of neurotransmitters or regulators. It thus seems plausible to think that ADHD does not result from specific dysfunctional genes, but from dysfunctional pathways, as it was proposed for autism (Loke et al., 2015).

4.3.4 Epigenetics

Considering the still minor effect of Cdh13 deficiency in our experiments, with it being one of these early developmental factors, it might, however, be a good idea to expand the focus of research on other levels, e.g. the epigenetic one. Given that “early development is accompanied by rapid epigenetic change” (Loke et al., 2015), many of the early developmental candidate genes mentioned above might be affected in this context, too. In fact, in the last few years several authors started to consider the influence of epigenetics on neurodevelopmental disorders, among the first ones Redies et al. (2012), as well as Lesch and Waider (2012). Since adopted siblings of ADHD patients showed the same risk as real relatives (Schuch et al., 2015), this idea does not seem too far-fetched and was growing subject of discussion (e.g. Abdolmaleky et al., 2015; Kiser et al., 2015). Only recently several studies on epigenetics have been conducted for ADHD and its candidate genes like DRD4 and SERT (Wong et al., 2010), as well as for related psychiatric diseases like bipolar and

autism spectrum disorders (Perroud et al., 2015; Loke et al., 2015). The future will show, whether the epigenetic level will turn out to be more rewarding than the genetic one.

5. Appendix

5.1 Abbreviations

	VII/X/XII	cranial nerve nuclei (facial, vagal, hypoglossal)
A	AB	antibody
	ABA	Allen Brain Atlas
	ABC	avidin-biotin complex
	AC	adenylate cyclase
	ADHD	attention deficit/ hyperactivity disorder
	ADRA2A	adrenergic receptor alpha 2A gene
	Allo	allocortex
	AP	alkaline phosphatase
	Aq	aqueduct
	AR	antigen retrieval
	ATg	anterior tegmental nucleus
	ATP	adenosine triphosphate
	ATX	atomoxetine
B	B6	black 6
	BDNF	brain derived neurotrophic factor
	bp	base pairs
	BS	blocking solution
C	c	caudal
	C	cerebellum
	Ca^{2+}	calcium
	cAMP	cyclic adenosine monophosphate,
	Cdh13	cadherine 13
	cf.	confer
	(Is) CLi	(isthmic) caudal linear nucleus
	(Is) CLiW	(isthmic) caudal linear wing nucleus
	CNV	copy number variation
	CNS	central nervous system
	Cre	„Causes Recombination“ (a recombinase enzyme)
	Cy3	cyanine 3

D	d	day
	D	diencephalon
	DA	dopamine
	DAB	3,3'-Diaminobenzidine
	DAG	diacylglycerol
	DAPI	4',6-diamidino-2-phenylindole
	DAT1	dopamine transporter gene
	DBH	dopamine-β-hydroxylase
	DCX	doublecortin
	DDC	dopamine decarboxylase gene
	ddH_2O	double distilled water
	DNA	deoxyribonucleic acid
	DOPA	3,4-dihydroxyphenylalanine
	DRAT	dorsal raphe arcuate tract
	DRC	dorsal raphe nucleus, caudal part
	DRCT	dorsal raphe cortical tract
	DRD	dorsal raphe nucleus, dorsal part
	DRD1-5	dopamine receptor D1-5 gene
	DRFT	dorsal raphe forebrain tract
	DRI	dorsal raphe nucleus, interfascicular part
	(m/ls) DR	mesencephalic/ isthmic dorsal raphe nucleus
	DRL	dorsal raphe nucleus, lateral part
	DRPT	dorsal raphe periventricular tract
	DRV	dorsal raphe nucleus, ventral part
	DRVL	dorsal raphe nucleus, (ventro-) lateral part
	DSM-V	Diagnostic and Statistical Manual of Mental Disorders, 5^{th} edition
	dATP	deoxyadenosine triphosphate
	dCTP	deoxycytidine triphosphate
	dGTP	deoxyguanosine triphosphate
	dNTP	deoxynucleotide triphosphate
	dTTP	deoxythymidine triphosphate
E	E11/ 13.5	embryonic day 11/13.5
	E15/ 17.5	embryonic day 15/17.5
	EDTA	ethylenediaminetetraacetic acid

	e. g.	for example (lat.: exempli gratia)
	eGFP	enhanced green fluorescent protein
	ES	embryonic stem
	EtOH	ethanol
	EtBr	ethidium bromide
F	f	feminine
	F	forebrain
	Fgf 2/ 4/ 8	fibroblast growth factor 2/ 4/ 8
	F(or)	forward
G	GAP-43	growth-associated protein 43
	GC content	guanosine/ cytosine content
	GDNF	glial cell line-derived neurotrophic factor
	GeR	Supragenual raphe nuclei
	GFOD1	glucose-fructose oxidoreductase domain containing protein 1
	GPI	glycosylphosphatidylinositol
	GWAS	genome-wide association study
H	H	hindbrain
	HCl	hydrochloric acid
	hCMV	human cytomegalovirus
	5-HIAA	5-hydroxyindoleacetic acid
	Hippo	hippocampus
	HRP	horseradish peroxidase
	5-HT	5-hydroxy-tryptamine = serotonin
	5-HTP	5-hydroxytryptophan
	5-HTT	5-hydroxy-tryptamine transporter
	Hy	hypothalamus
	HZ	heterozygous
I	i. e.	that means (lat.: id est)
	IHC	immunohistochemistry
	IO	inferior olivary nucleus
	IP3	inosin triphosphate
	Ir	immunoreactive
	IR	immunoreactivity
	Is	isthmus/ isthmic

	Iso	Isocortex
	ISH	in situ hybridisation
K	KO	knockout
L	LAS AF	Leica Application Suite Advanced Fluorescence
M	m	masculine
	M	midbrain
	MAO-A	monoamine oxidase A
	MetOH	methanol
	MFB	medial forebrain bundle
	$MgCl_2$	magnesium chloride
	MH	medullary hindbrain (medulla)
	MHB	midbrain-hindbrain-boundary
	mlf	medial longitudinal fasciculus
	MnR	median raphe nucleus
	MPH	methylphenidate
	MRFT	median raphe forebrain tract
N	n. / nn.	nucleus/ nuclei
	NaCl	sodium chloride
	NC	negative control
	NE	norepinephrine
	NGF	nerve growth factor
	NGFR	nerve growth factor receptor
	NGS	normal goat serum
	NHS	normal horse serum
P	P	parental generation
	P7	postnatal day number seven
	PAG	periaqueductal grey
	Pall	pallium
	PBS	phosphate buffered saline
	PC	positive control
	PCB	polychlorinated biphenyl
	PCR	polymerase chain reaction
	PDR	posterodorsal part of the dorsal raphe nucleus
	PFA	paraformaldehyde
	PFC	prefrontal cortex

	PH	pontine hindbrain
	PIP2	phosphatidylinositol 4,5-biphosphate
	PM	plasma membrane
	PMH	pontomedullary hindbrain
	PNS	peripheral nervous system
	PPH	prepontine hindbrain
	PPnR	Prepontine raphe nucleus
	Pt	putamen
	PTh	prethalamus
R	r	rostral
	r 1-9	rhombomere(s)
	R(ev)	reverse
	RF	reticular formation
	RMg(D/V)	Raphe magnus nuclei (dorsal/ ventral)
	RMT	raphe medial tract
	RNA	ribonucleic acid
	ROb	Raphe obscurus nuclei
	RPa	Raphe pallidus nuclei
	RPPy	Parapyramidal raphe nuclei
	RT	room temperature
S	SDS	sodium dodecyl sulphate
	SERT	serotonin transporter
	Shh	sonic hedgehog
	SNAP25	synaptosome-associated protein of 25,000 Da
	SNP	single-nucleotide polymorphisms
	SP	secondary prosencephalon
	SPall	subpallium
	SpC	spinal cord
	SSRI	selective serotonin reuptake inhibitors
	SuLR	Supralemniscal raphe nuclei
T	TAE-Buffer	Tris-Acetate-EDTA-Buffer
	Taq	Thermus aquaticus (thermophilic bacteria)
	TBS	Tris buffered saline
	TE	Tris EDTA
	Tel	(alar plate of the exvaginated) telencephalic vesicle

	Tg	tegmentum
	Th	thalamus
	Tph2	tryptophan hydroxylase 2
	Tris	tris(hydroxymethyl)aminomethane
	Tt	tectum
U	UV	ultraviolet
V	VMAT 1/2	vesicular membrane transporters 1/2
W	WT	wild type
X	xscp	decussation of the superior cerebellar peduncle,

cm/ mm/ µm/ nm	centimetre/ millimetre/ micrometre/ nanometre
cM	centimorgan
h/ min/ s	hour/ minute/ second
kb	kilobase (=1000bp)
kg/ g/ mg/ µg	kilogramme/ gramme/ milligramme / microgramme
l/ ml/ µl	litre/ millilitre/ microlitre
bp/ kbp/ Mb	base pair/ kilo base pairs/ mega base pairs
mM/ µM	millimolar/ micromolar
mol	mole
rpm	rounds per minute
V/A	volt/ ampere
Da/ kDa	dalton/ kilodalton

5.2 List of figures and tables

Introduction

Materials and methods

Results

5.3 Bibliography

Abdolmaleky, H.M., Horizons of Psychiatric Genetics and Epigenetics: Where are we and where are we heading? *Iran J Psychiatry Behav Sci* **8(3)**: 1-10 (2014).

Akins, M.R., Benson, L.D. & Greer, C.A., Cadherin expression in the developing mouse olfactory system. *J Comp Neurol* **501**: 483-497 (2007).

Alemany, S. et al., New suggestive genetic loci and biological pathways for attention function in adult attention-deficit/ hyperactivity disorder. *Am J Med Genet B Neuropsychiatr Genet* (2015). [Epub ahead of print]

Alonso, A. et al., Development of the serotonergic cells in murine raphe nuclei and their relations with rhombomeric domains. *Brain Struct Funct* **218**: 1229-1277 (2013).

Amin, N., et al., Suggestive linkage of ADHD to chromosome 18q22 in a young genetically isolated Dutch population. *Eur J Hum Genet* **17(7)**: 958-66 (2009).

Andrade, R. & Haj-Dahmane, S., Serotonin neuron diversity in the dorsal raphe. *ACS Chem Neurosci* **4(1)**: 22-25 (2013).

Angst, B.D., Marcozzi, C. & Magee, A.I., The cadherin superfamily: diversity in form and function. *J Cell Sci* **114**: 629-641 (2001).

Anthofer, J.M. et al., DTI-based deterministic fibre tracking of the medial forebrain bundle. *Acta Neurochir* **157**: 469–477 (2015).

Arcos-Burgos, M. et al., Attention-deficit/ hyperactivity disorder in a population isolate: linkage to loci at 4q13.2, 5q33.3, 11q22 and 17p11. *Am J Hum Genet* **75**: 998-1014 (2004).

Arias-Vásquez, A. et al., CDH13 is associated with working memory performance in attention deficit/ hyperactivity disorder. *Genes Brain Behav* **10**: 844-851 (2011).

Asherson, P. et al., A high-density SNP linkage scan with 142 combined subtype ADHD sib pairs identifies linkage regions on chromosomes 9 and 16. *Mol Psychiatry* **13**: 514-521 (2008).

Azmitia, E.C. & Segal, M., An autoradiographic analysis of the differential ascending projections of the dorsal and median raphe nuclei in the rat. *J Comp Neur* **179**: 641-668 (1978).

Bakker, S.C. et al., A whole-genome scan in 164 Dutch sic pairs with attention deficit/ hyperactivity disorder: Suggestive evidence for linkage on chromosomes 7p and 15q. *Am J Hum Genet* **72**: 1251-1260 (2003).

Banaschewski, T. et al., Molecular genetics of attention-deficit/ hyperactivity disorder: an overview. *Eur Child Adolesc Psychiatry* **19**: 237-257 (2010).

Banerjee, T.D., Middleton, F. & Faraone, S.V., Environmental risk factors for attention-deficit hyperactivity disorder. *Acta Paediatr* **96(9)**: 1269-1274 (2007). – Review

Baroni, A. & Castellanos, F.X., Neuroanatomic and cognitive abnormalities in attention-deficit/ hyperactivity disorder in the era of “high definition” neuroimaging. *Curr Opin Neurobiol* **30C**: 1-8 (2014).

Bekirov, I.H. et al., Identification and localization of multiple classic cadherins in developing rat limbic system. *Neuroscience* **115(1)**: 213-227 (2002).

Benninghoff, A. & Drenckhahn, D., Taschenbuch Anatomie, München 2008, 424-436.

Brooks, L.R. et al., Fibroblast growth factor deficiencies impact anxiety-like behaviour and the serotonergic system. *Behav Brain Res* **264**:74-81 (2014).

Brown, J.P. et al., Transient expression of doublecortin during adult neurogenesis. *J Comp Neurol* **467(1)**: 1-10 (2003).

Brüning, G., Liangos, O. & Baumgarten, H.G., Prenatal development of the serotonin transporter in mouse brain. *Cell Tissue Res* **289**: 211-221 (1997).

Coons, A.H, Creech, H.J & Jones, R.N., Immunological properties of an antibody containing a fluorescent group. *Proc Soc Exp Biol Med* **47**: 200–202 (1941).

Cordes, S.P., Molecular genetics of the early development of hindbrain serotonergic neurons. *Clin Genet* **68**: 487-494 (2005).

Cortese, S., Faraone, S.V. & Sergeant, J., Misunderstandings of the genetics and neurobiology of ADHD: moving beyond anachronisms. *Am J Med Genet B Neuropsychiatr Genet* **156B(5**): 513-516 (2011).

Deng, D.R. et al., Embryonic and postnatal development of the serotonergic raphe system and its target regions in $5HT_{1A}$ receptor deletion or overexpressing mouse mutants. *Neuroscience* **147**: 388-402 (2007).

Donovan, S.L. et al., GAP-43 is critical for normal development of the serotonergic innervation in forebrain. *J Neurosci* **22(9)**: 35-43 (2002).

Dorocic, I.P. et al., A whole-brain atlas of inputs to serotonergic neurons of the dorsal and median raphe nuclei. *Neuron* **83 (3)**: 663-678 (2014).

Ebejer, J.L. et al., Genome-wide association study of inattention and hyperactivity-impulsivity measured as quantitative traits. *Twin Res Hum Genet* **16(2)**: 560-574 (2013).

Elia, J. et al., Rare structural variants found in attention-deficit hyperactivity disorder are preferentially associated with neurodevelopmental genes. *Mol Psychiatry* **15(6)**: 637-646 (2010).

Elia, J. et al., Genome-wide copy-number variation study associates metabotropic glutamate receptor gene networks with attention deficit hyperactivity disorder. *Nat Genet* **44(1)**: 78-84 (2011).

Erspamer, V. & Vialli, M., Ricerche sul secreto delle cellule enterocromaffini. *Boll d Soc Med-chir Pavia* **51**, 357-363 (1937).

Erspamer, V. & Asero, B., Identification of enteramine, the specific hormone of the enterochromaffin cell system, as 5-hydroxytryptamine. *Nature* **169**, 800-801 (1952).

Faraone, S.V. & Khan, S.A., Candidate gene studies of attention-deficit/ hyperactivity disorder. *J Clin Psychiatry* **67(8):** 13-20 (2006). – Review

Faraone, S.V. et al., Linkage analysis of attention deficit/ hyperactivity disorder. *Am J Med Genet B Neuropsychiatr Genet* **147B**: 1387-1391 (2007).

Faraone, S.V. & Mick, E., Molecular genetics of attention deficit hyperactivity disorder. *Psychiatr Clin North Am* **33(1)**: 159-180 (2009). – Review

Fisher, S.E. et al., A genome-wide scan for loci involved in attention-deficit/ hyperactivity disorder. *Am J Hum Genet* **70**: 1183-1196 (2002).

Francis, F. et al., Doublecortin is a developmentally regulated microtubule-associated protein expressed in migrating and differentiating neurons. *Neuron* **23(2)**: 247-256 (1999).

Franke, B., Neale, B.M. & Faraone, S.V., Genome-wide association studies in ADHD. *Hum Genet* **126**: 13-50 (2009). – Review

Franke, B. et al., The genetics of attention deficit/ hyperactivity disorder in adults, a review. *Mol Psychiatry* **17**: 960-987 (2012). – Review

Frazer, A. & Hensler, J.G., Serotonin, in: Siegel, G.J., Agranoff, B.W. & Albers, R.W. (Hgg.), Basic Neurochemistry: molecular, cellular and medical aspects. Philadelphia 1999, NCBI bookshelf.

Fu, W. et al., Chemical neuroanatomy of the dorsal raphe nucleus and adjacent structures of the mouse brain. *J Comp Neurol* **518(17)**: 3464-3494 (2010).

Gaspar, P., Cases, O. & Maroteaux, L., The developmental role of serotonin: news from mouse molecular genetics. *Nat Rev Neurosci* **4(12)**: 1002-1012 (2003). – Review

Graeff, F.G. & Zangrossi Jr., H., The dual role of serotonin in defence and the mode of action of antidepressants on generalized anxiety and panic disorders. *Cent Nerv Syst Agents Med Chem* **10**: 207-2017 (2010).

Gutknecht, L. et al., Spatio-temporal expression of tryptophan hydroxylase isoforms in murine and human brain: convergent data from Tph2 knockout mice. *Eur Neuropharmacol* **19(4)**: 266-282 (2009).

Hackenberg, B. & Aichhorn, W., Kinder- und Jugendpsychiatrie, in: Fleischhacker, W.W. & Hinterhuber, H. (Hgg.), Lehrbuch Psychiatrie, Wien 2012, 323-351.

Hamshere, M.L. et al., A shared polygenetic contribution between ADHD and adult schizophrenia. *Br J Psychiatry* 1-5 (2013). [Epub ahead of print]

Hawi, Z. et al., The molecular genetic architecture of attention deficit hyperactivity disorder. *Mol Psychiatry* **20(3)**: 289-297 (2015). – Review

Hawthorne, A.L. et al., Serotonergic neurons migrate radially through the neuroepithelium by dynamin-mediated somal translocation. *J Neurosci* **30(2)**: 420-430 (2010).

Hebebrand, J. et al., A genome-wide scan for attention-deficit/ hyperactivity disorder in 155 German sib-pairs. *Mol Psychiatry* **11**: 196-205 (2006).

Hebebrand, J., Nicht in Erfüllung gegangene Erwartungen in die molekulargenetische Forschung psychiatrischer Störungen: Eine Bestandsaufnahme. *Z Kinder Jugendpsychiatr Psychother* **39(3)**: 157-159 (2011). – review

Hendricks, T. et al, The ETS domain factor Pet-1 is an early and precise marker of central serotonin neurons and interacts with a conserved element in serotonergic genes. *J Neurosci* **19(23)**: 10348-10356 (1999).

Hensler, J.G., Serotonergic modulation of the limbic system. *Neurosci Biobehav Rev* **30**: 203-214 (2006).

Hilz, H., Wiegers, U. & Adamietz, P., Stimulation of proteinase K action by denaturing agents: application to the isolation of nucleic acids and the degradation of 'masked' proteins. *Eur J Biochem* **56(1)**: 103-8 (1975).

Hinney, A. et al., Genome-wide association study in German patients with attention deficit/hyperactivity disorder*. Am J Med Genet B Neuropsychiatr Genet* **156B(8)**: 888-97 (2011).

Hong, S.-B. et al., Connectomic disturbances in Attention-Deficit/ Hyperactivity disorder: A whole brain tractography analysis. *Biol Psychiatry* **76(8)**: 656-663 (2014).

Hudziak, J.J. & Faraone, S.V., The new genetics in child psychiatry. *J Am Acad Child Adolesc Psychiatry,* **49(8)**: 729-735 (2010). – Review

Huntley, G.W., Dynamic aspects of cadherin-mediated adhesion in synapse development and plasticity. *Biol Cell* **94(6)**: 335-344 (2002). - Review

Janusonis, S., Gluncic, V. & Rakic, P., Early serotonergic projections to Cajal-Retzius cells: relevance for cortical development. *J Neurosci* **24(7)**: 1652-1659 (2004).

Jarick, I. et al., Genome-wide analysis of rare copy number variants in attention-deficit reveals PARK2 as candidate gene for attention-deficit/ hyperactivity disorder. *Mol Psychiatry* **19(1)**: 115-121 (2014).

Jensen, P. et al., Redefining the central serotonergic system based on genetic lineage. *Nat Neurosci* **11(4)**: 417-419 (2008).

Jessell, T.M., Adhesion molecules and the hierarchy of neural development. *Neuron* **1**: 3-13 (1988). - Review

Jinno, S. & Kosaka, T., Cellular architecture of the mouse hippocampus: A quantitative aspect of chemically defined GABAergic neurons with stereology. *Neurosci Res* **56(3)**: 229-245 (2006).

Joshi, M.B. et al., Integrin-linked kinase is an essential mediator for T-cadherin-dependent signalling via Akt and GSK3β in endothelial cells. *FASEB J* **21**: 3083-3095 (2007).

Kebir, O. et al., Candidate genes and neurophysiological phenotypes in children with ADHD: review of association studies. *J Psychiatry Neurosci* **34(2):** 88-101 (2009). – Review

Kim, D.-Y. & Camilleri, M., Serotonin: A mediator of the brain-gut connection. *Am J Gastroenterol* **95(10)**: 2698-2709 (2000).

Kiser, D., Rivero, O. & Lesch, K.-P., Annual Research Review: The (epi)genetics of neurodevelopmental disorders in the era of whole-genome sequencing – unveiling the dark matter. *J Child Psychol Psychiatry* **56**: 3 (2015). – Review

Lang, F. & Verrey, F., Hormone, in: Schmidt, R.F., Lang, F. & Heckmann, M. (Hgg.), Physiologie des Menschen mit Pathophysiologie, Heidelberg 2010, 460-489.

Langley, K. et al., Clinical and cognitive characteristics of children with attention-deficit hyperactivity disorder, with and without copy number variants. *Br J Psychiatry* **199**: 398-403 (2011),

Lasky-Su, J. et al., Genome-wide association scan of quantitative traits for attention deficit hyperactivity disorder identifies novel associations and confirms candidate gene associations. *Am J Med Genet B Neuropsychiatr Genet* **147B(8)**: 1345-1354 (2008).

Lesch, K.-P. et al., Molecular genetics of adult ADHD: converging evidence from genome-wide association and extended pedigree linkage studies. *J Neural Transm* **115**: 1573-1585 (2008).

Lesch, K.-P. et al., Genome-wide copy number variation analysis in attention-deficit/ hyperactivity disorder: association with neuropeptide Y gene dosage in an extended pedigree. *Mol Psychiatry* **16**: 491-503 (2011).

Lesch, K.-P. & Waider, J., Serotonin in the modulation of neural plasticity and networks: Implications for neurodevelopmental disorders. *Neuron* **76(1)**: 175-191 (2012).

Lesch, K.-P., Illuminating the dark matter of developmental neuropsychiatric genetics – strategic focus for future research in child psychology and psychiatry. *J Child Psychol Psychiatry* **55(3)**: 201-203 (2014). - Editorial

Levitt P. & Moore, R.Y., Developmental organization of raphe serotonin neuron groups in the rat. *Anat Embryol* **154 (3)**: 241-251 (1978).

Lionel, A.C. et al., Rare copy number variation discovery and cross-disorder comparisons identify risk genes for ADHD. *Sci Transl Med* **3(95)**: 95ra75 (2011).

Liu, Ch., et al., Pet-1 is required across different stages of life to regulate serotonergic function. *Nat Neurosci* **13(10)**: 1190-8 (2010).

Loke, Y.J., Hannan, A.J. & Craig, J.M. The role of epigenetic change in autism spectrum disorders. *Front Neurol* **6**:107 (2015). [eCollection 2015] – Review

Lowry, Ch.A. et al., Topographic organization and chemoarchitecture of the dorsal raphe nucleus and the median raphe nucleus, in: Monti, J.M. et al. (Hgg.), Serotonin and Sleep: molecular, functional and clinical aspects. Switzerland 2008, Birkhäuser Verlag, 25-67.

Mátyás, F., Freund, T.F. & Gulyas, A.I., Immunocytochemically defined interneuron populations in the hippocampus of mouse strains used in transgenic technology. *Hippocampus* **14(4)**: 460-481 (2004).

Mavroconstanti, T. et al., Functional properties of rare missense variants of human CDH13 found in adult attention deficit/ hyperactivity disorder (ADHD) patients. *PLoS One* **8(8)**: e71445 (2013).

Montalbano, A. et al., Cellular resilience: 5-HT neurons in Tph2-/- mice retain normal firing behaviour despite the lack of brain 5-HT. *Eur Neuropsychopharmacol* **25 (11)**: 2022-35 (2015).

Murphy, D.L. & Lesch, K.-P., Targeting the murine serotonin transporter: insights into human neurobiology. *Nat Rev Neurosci* **9(2)**: 85-96 (2008).

Neale, B.M. et al., Genome-wide association scan of attention deficit hyperactivity disorder. *Am J Med Genet B Neuropsychiatr Genet* **147B(8)**: 1337-1344 (2008).

Neale, B.M. et al., Case-control genome-wide association study of attention-deficit/ hyperactivity disorder. *J Am Acad Child Adolesc Psychiatry* **49(9)**: 906-920 (2010a).

Neale, B.M. et al., Meta-analysis of genome-wide association studies of attention deficit/ hyperactivity disorder. *J Am Acad Child Adolesc Psychiatry* **49(9)**: 884-897 (2010b).

Ogdie, M.N. et al., Pooled genome-wide linkage data on 424 ADHD ASPs suggest genetic heterogeneity and a common risk locus at 5p13. *Mol Psychiatry* **11**: 5-8 (2006).

Patnala, R., Clements, J. & Batra, J., Candidate gene association studies: a comprehensive guide to useful in silico tools. *BMC Genet* **14**:39 (2013)

Paul, E.D. & Lowry, Ch.A., Functional topography of serotonergic systems support the Deakin/Graeff hypothesis of anxiety and affective disorder. *J Psychopharmacol* **27(12)**: 1090-1106 (2013). – Review

Perroud, N. et al., methylation of serotonin receptor 3A in ADHD, borderline personality and borderline disorders: Link with severity of the disorders and childhood maltreatment. *Depress Anxiety* (2015). [Epub ahead of print]

Persico, A.M. et al., Reduced programmed cell death in brains of serotonin transporter knockout mice. *Neuroreport* **14(3)**: 341-344 (2003).

Philippova, M. et al., RhoA and Rac mediate endothelial cell polarization and detachment induced by T-cadherin. *FASEB J* **19(6)**: 588-590 (2005).

Philippova, M. et al., Identification of proteins associating with glycosylphosphatidylinositol-anchored T-cadherin on the surface of vascular endothelial cells: Role for Grp78/BiP in T-cadherin-dependent cell survival. *Mol Cell Biol* **28 (12)**: 4004-4017 (2008).

Philippova, M. et al., A guide and guard: The many faces of T-cadherin. *Cell signal* **21**: 1035-1044 (2009).

Pulst, S.M., Genetic linkage analysis. *Arch Neurol* **56**: 667-672 (1999). – Review

Ranscht, B., Cadherins and catenins: Interactions and functions in embryonic development. *Curr Opin Cell Biol* **6**: 740-746 (1994).

Ranscht, B. & Dours-Zimmermann, M.T., T-cadherin, a novel cadherin cell adhesion molecule in the nervous system lacks the conserved cytoplasmic region. Neuron **7**: 391-402 (1991).

Rao, M.S. & Shetty, A.K., Efficacy of doublecortin as a marker to analyse the absolute number and dendritic growth of newly generated neurons in the adult dentate gyrus. *Eur J Neurosci* **19(2)**: 234-246 (2004).

Rapport, M.M., Green, A.A. & Page, I.H., Serum vasoconstrictor, serotonin; isolation and characterization. *J Biol Chem* **176**, 1243-51 (1948).

Redies, Ch., Cadherin expression in the developing vertebrate CNS: from neuromeres to brain nuclei and neural circuits. *Exp Cell Res* **220(2)**: 243-56 (1995). - Review

Redies, Ch., Cadherins in the central nervous system. *Prog Neurobiol* **61(6)**: 611-48 (2000).

Redies, Ch., Hertel, N. & Hübner C.A., Cadherins and neuropsychiatric disorders. *Brain Res* **1470**: 130-144 (2012).

Riccio, O. et al., Excess of serotonin affects embryonic interneuron migration through activation oft the serotonin receptor 6. *Mol Psychiatry* **14**: 280-90 (2009).

Rivero, O. et al., Impact of the ADHD-susceptibility gene Cdh13 on development and function of brain networks. *Eur Neuropsychopharmacol* **23(6):** 492-507 (2013).

Rivero, O. et al., Cadherin-13, a risk gene for ADHD and comorbid disorders, impacts GABAergic function in hippocampus and cognition. *Transl Psychiatry* 5: e655. doi: 10.1038/tp.2015.152 (2015).

Roman, T., Rohde, L.A. & Hutz, M.H., A role for neurotransmission and neurodevelopment in attention-deficit/ hyperactivity disorder. *Genome Med* **1(11)**: 107:1-3 (2009). – Review

Romanos, M. et al., Genome-wide linkage analysis of ADHD using high-density SNP arrays: novel loci at 5q13.1 and 14q12. *Mol Psychiatry* **13**: 522-530 (2008).

Rommelse, N.N. et al., Neuropsychological endophenotype approach to genome-wide linkage analysis identifies susceptibility loci for ADHD on 2q21.1 and 13q12.11. *Am J Hum Genet* **83(1)**: 99-105 (2008).

Saviouk, V. et al., ADHD in Dutch adults: heritability and linkage study. *Am J Med Genet B Neuropsychiatr Genet* **156B(3)**: 352-62 (2011).

Schiebler, T.H., Nervensystem, in: Schiebler, T.H. (Hgg.), Anatomie, Heidelberg 2005, 687-825.

Schneider, F. & Weber-Papen, S., Psychiatrie, Psychosomatik und Psychotherapie… in 5 Tagen. Heidelberg (2010).

Schuch, V.S. et al., Attention deficit hyperactivity disorder in the light of the epigenetic paradigm. *Front Psychiatry* **6**: 126 (2015).

Smoller, J.W. et al., Identification of risk loci with shared effects on five major psychiatric disorders: a genome-wide analysis. *Lancet* **381(9875)**: 1371-1379 (2013).

Soiza-Reilly, M. & Commons, K.G., Unravelling the architecture of the dorsal raphe synaptic neuropil using high-resolution neuroanatomy. *Front Neural Circuits* **8**: 105 (2014). – Review

Sowell, E.R. et al., Cortical abnormalities in children and adolescents with attention-deficit hyperactivity disorder. *Lancet* **362**: 1699-1707 (2003).

Sparta, D.R. & Stuber, G.D., Cartography of serotonergic circuits. *Neuron* **83(3)**: 513-515 (2014).

Stergiakouli, E. et al., Investigating the contribution of common genetic variants to the risk and pathogenesis of ADHD. *Am J Psychiatry* **169**: 186-194 (2012).

Takeuchi, T. et al., Expression of T-Cadherin (CDH13, H-Cadherin) in human brain and its characteristics as a negative growth regulator of epidermal growth factor in neuroblastoma cells. *J. Neurochem* **74**: 1489-1497 (2000).

Twarog, B.M. & Page, I.H., Serotonin content of some mammalian tissues and urine and a method for its determination. *Am J Physiol* **175**, 157-161 (1953).

Twarog, B.M., Responses of a molluscan smooth muscle to acetylcholine and 5-hydroxytryptamine. *J Cell Comp Physiol* **44**,141–163 (1954).

Twarog, B.M., Serotonin: History of a discovery. *Comp Biochem Physiol* **91(1)**: 21-24 (1988).

Uhl, G.R. et al., Molecular genetics of addiction and related heritable phenotypes: genome-wide association approaches identify “connectivity constellation” and drug target genes with pleiotropic effects. *Ann N.Y. Acad Sci* **1141**: 318-381 (2008).

Vegt, R. et al., Genome-wide linkage analysis in a Dutch multigenerational family with attention deficit hyperactivity disorder. *Eur J Hum Genet* **18(2)**: 206-11 (2010).

Waider, J., New insights into the serotonergic system: Spatial and temporal expression pattern of Tph1 and Tph2 in wild type mice and first characterisation of a new mouse model for central serotonin deficiency. Diplomarbeit (2008).

Wallace, J.A. & Lauder, J.M., Development of the serotonergic system in the rat embryo: An immunocytochemical study. *Brain Res Bull* **10(4)**: 459-479 (1983).

Williams, N.M. et al., Rare chromosomal deletions and duplications in attention-deficit hyperactivity disorder: a genome-wide analysis. *Lancet* **376(9750)**: 1401-1408 (2010).

Williams, N.M. et al., Genome-wide analysis of copy number variants in attention deficit hyperactivity disorder: the role of rare variants and duplications at 15q13.3. *Am J Psychiatry* **169(2)**: 195-204 (2012).

Wilson, M.A. & Molliver, M.E., The organization of serotonergic projections to cerebral cortex in primates: regional distribution of axon terminals. *Neuroscience* **44(3)**: 537-553 (1991).

Wong, C.C. et al. A longitudinal study of epigenetic variation in twins. *Epigenetics* **5(6)**: 516–26 (2010).

Wong, D.T., Kenneth, W.P. & Bymaster, F.P., Case history: The discovery of fluoxetine hydrochloride (Prozac). *Nat Rev Drug Discov* **4(9)**: 764-74 (2005).

Wylie, Ch. J. et al., Distinct transcriptomes define rostral and caudal serotonin neurons. *J Neurosci* **30(2)**: 670-684 (2010).

Yang, L. et al., Polygenic transmission and complex neurodevelopmental network for attention deficit hyperactivity disorder: Genome-wide association study of both common and rare variants. *Am J Med Genet B Neuropsychiatr Genet* **162B(5)**: 419-430 (2013).

Zayats, T. et al., Genome-wide analysis of attention deficit hyperactivity disorder in Norway. *PLoS One* **10(4)**: e0122501. doi: 10.1371/journal.pone. 0122501 (2015).

Zhang, L. et al., ADHDgene: a genetic database for attention deficit hyperactivity disorder. *Nucleic Acids Res* **40**: D1003-1009 (2012).

Zhou, F.C., Sari, Y. & Zhang, J.K., Expression of serotonin transporter protein in developing rat brain. *Developmental Brain Research* **119(1)**: 33-45 (2000).

Zhou, K. et al., Meta-analysis of genome-wide linkage scans of attention deficit hyperactivity disorder. *Am J Med Genet B Neuropsychiatr Genet* **147B(8):** 1392-1398 (2008a).

Zhou, K. et al., Linkage to chromosome 1p36 for attention-deficit/ hyperactivity disorder traits in school and home settings. *Biol Psychiatry* **64**: 571-576 (2008b).

Allen Brain Atlas/ Developing Mouse brain: http://www.brain-map.org
http://www.ihcworld.com/_technical_tips/prevent_section_fall.htm
http://www.alphelys.com/alph01/prod/us/snapfrost/snapfrost.php (freezing)
ADHDgene – A genetic database for ADHD: http://adhd.psych.ac.cn/index.do

5.4 List of purchased ready-made substances

(Bio-)/Chemicals	Additional information	Company/ Headquarters
Acetic acid		Merck-Millipore KGaA, Darmstadt
Agarose (Biozym LE)		Biozym Scientific GmbH, Oldendorf
Aquatex		Merck-Millipore KGaA, Darmstadt
A-/ B-Reagent	2 drops = 100µl	Vector Laboratories Inc., Burlingame, U.S.A
Bromine phenol blue		Sigma-Aldrich Chemie GmbH, Steinheim
BSA	Powder	Sigma-Aldrich Chemie GmbH, Steinheim
Citric acid monohydrate	Powder, M= 210.14g/mol	AppliChem GmbH, Darmstadt
Chrome III –Potassium sulphate dodecahydrate	Powder, p.a.	Sigma-Aldrich Chemie GmbH, Steinheim
DAB	Metal 10x concentrate, 3,3-Diaminobenzidine	Roche Diagnostics GmbH, Mannheim
DAB Substrate	Peroxide Buffer	Roche Diagnostics GmbH, Mannheim
DAPI	M=350,3g/mol	Life Technologies GmbH, Darmstadt
EDTA	0,5M, pH 8	AppliChem GmbH, Darmstadt
EtOh	100%	AppliChem GmbH, Darmstadt
EtBr	0.07%, dropper bottle	AppliChem GmbH, Darmstadt
Fluorogel	Without fading agent	Elecron Microscopy Sciences, Hatfield, U.S.A
Gelatine	Powder, from porcine skin	Sigma-Aldrich Chemie GmbH, Steinheim
Gene Ruler 100bp ladder		MBI Fermentas GmbH, St. Leon-Rot
Glycerol		Sigma-Aldrich Chemie GmbH, Steinheim
HCl (1M)		E. Merck KGaA, Darmstadt
HCl (5M)		AppliChem GmbH, Darmstadt
H_2O	M=18,02g/mol, ρ=1.00g/cm^3 (20°C)	Merck KgaA, Darmstadt
H_2O_2 (30%)		E. Merck KGaA, Darmstadt
Isoflurane		CP-Pharma Handelsgesellschaft GmbH, Burgdorf

Isopropanol	= 2-Propanol, 100%	Sigma-Aldrich Chemie GmbH, Steinheim
KCl		Sigma-Aldrich Chemie GmbH, Steinheim
MetOH	100%	Sigma-Aldrich Chemie GmbH, Steinheim
2-Mathylbutane	M=72,15g/mol	AppliChem GmbH, Darmstadt
$MgCl_2$	Magnesium chloride	Sigma-Aldrich Chemie GmbH, Steinheim
NaOH (1M)		E. Merck KGaA, Darmstadt
NaOH (5M)		AppliChem GmbH, Darmstadt
NGS/ NHS/ NRS		Vector Laboratories Inc., Burlingame, U.S.A
dNTP-Mix	dATP, dCTP, dGTP, dTTP	Peqlab Biotechnologie GmbH, Erlangen
PBS (10x)	Without Mg2+ and Ca2+	Lonza Group AG, Verviers, Belgium
PFA	Powder	E. Merck KGaA, Darmstadt
pH calibration solutions	pH 4.01/ 7.01/ 10.01	HANNA Instruments, Kehl am Rhein
Proteinase K	Powder, M=2700g/mol, 100mg solubilised in 5ml ddH_2O (c=20mg/ml), storage at -20°C	AppliChem GmbH, Darmstadt
SDS	Sodium dodecyl sulphate	AppliChem GmbH, Darmstadt
Sodium chloride	Powder	Sigma-Aldrich Chemie GmbH, Steinheim
D(+)-Succrose	Powder, M=342,30 g/mol	AppliChem GmbH, Darmstadt
Taq DNA polymerase		BioRad Laboratories GmbH, München
TE-Buffer (1x)	pH 8, storage at RT	AppliChem GmbH, Darmstadt
Tris	M=121,14g/mol	Carl Roth GmbH + Co. KG, Karlsruhe
Tris Acetate		AppliChem GmbH, Darmstadt
Tris HCl		AppliChem GmbH, Darmstadt
TritonX-100	t-Octyphenoxypoly-ethoxyethanol	Sigma-Aldrich Chemie GmbH, Steinheim
TSA™ Plus Cyanine 3 System		Perkin Elmer LAS GmbH, Rodgau
Tween 20		Sigma-Aldrich Chemie GmbH, Steinheim

Vectastain® ABC Kit	Peroxidase Standard, PK4000	Vector Laboratories Inc., Burlingame, U.S.A
Vitro-Clud®		R.Langenbrinck, Emmendingen
Xylene	100%	Sigma-Aldrich Chemie GmbH, Steinheim
Xylene cyanol FF		Sigma-Aldrich Chemie GmbH, Steinheim

5.5 Affidavit/ Eidesstattliche Erklärung

I hereby confirm that my thesis entitled “The role of Cadherin-13 in serotonergic neurons during different murine developmental stages” is the result of my own work. I did not receive any help or support from commercial consultants. All sources and / or materials are listed and specified in the thesis.
Furthermore, I confirm that this thesis has not yet been submitted as part of another examination process neither in identical nor in similar form.

Place, Date Signature

Hiermit erkläre ich an Eides statt die Dissertation “ Die Rolle von Cadherin-13 in serotonergen Neuronen während verschiedener Entwicklungsstadien in der Maus” eigenständig, d.h. insbesondere selbstständig und ohne die Hilfe eines kommerziellen Promotionsberaters, angefertigt und keine anderen als die von mir angegebenen Quellen und Hilfsmittel verwendet zu haben.
Ich erkläre außerdem, dass die Dissertation weder in gleicher noch in ähnlicher Form bereits in einem anderen Prüfungsverfahren vorgelegen hat.

Ort, Datum Unterschrift

5.6 Acknowledgement

Zunächst möchte ich meinem Doktorvater Professor Klaus-Peter Lesch für die Möglichkeit danken meine Promotion unter seiner erfahrenen Ägide zu verfassen. In zahlreichen Zwischenstandbesprechungen und Teamdiskussionen gelang es diese anhand neuer Erkenntnisse und Ideen immer weiter zu entwickeln und zu einem hochwertigen Ergebnis zu führen.
Bedanken möchte ich mich an dieser Stelle auch bei meinem Betreuer Dr. Jonas Waider, der mich durch die Höhen und Tiefen des Laboralltags begleitet hat. Vielen Dank für deine Geduld, immerwährende Freundlichkeit und viele Hilfe!

Zu besonderem Dank bin ich auch meiner Zweitbetreuerin Professorin Esther Asan verpflichtet. Mit kritischem Geist und großem Herz hat sie meine Arbeit unbarmherzig auf Präzision übergeprüft, mir Mut gemacht und damit maßgeblich zu deren erfolgreichem Abschluss beigetragen. Vielen herzlichen Dank für all Ihre Zeit und Mühe!

Auch meinem Drittkorrektor Professor Erhard Wischmeyer danke ich für seine Bereitschaft mein Prüfgremium um seine kompetente naturwissenschaftliche Perspektive und Urteilskraft zu ergänzen.

Eine große Rolle bei der Entstehung meiner Arbeit hat auch das Team der Molekularen Psychiatrie gespielt, welches mit seiner Herzlichkeit, Hilfsbereitschaft und Diskussionsfreudigkeit dazu beigetragen hat, dass die vielen Monate Laborarbeit nicht nur produktiv waren, sondern auch Freude bereitet haben. Besonders hervorheben möchte ich Angelika, Sarah, Olga, Christoph, Jann, Dominik, Nicole, Gabi, Marion und Judith, welche mir besonders tatkräftig zur Seite gestanden haben! Vielen Dank euch!

Ebenfalls zu großem Dank verpflichtet bin ich meinen Freunden Franziska Grän, Leonid Gorokowsky und Anna-Sophie Behlich. Sie haben nicht nur mit viel Mühe meine Arbeit Korrektur gelesen, sondern sind mir auch seit Jahren die besten Freunde, die man sich wünschen kann. Ich hoffe sehr, dass ich auch in Zukunft immer ein Teil in eurem Leben sein werde. Aus meinem Leben seid ihr auf jeden Fall nicht weg zu denken! Vielen Dank dafür!

Zuguterletzt möchte ich meinen Eltern Margot und George sowie meinen Geschwistern Sandra und Paul für die vielen Jahre der uneingeschränkten Unterstützung auf allen Ebenen danken. Ihr habt in Zeiten der Frustration immer ein offenes Ohr und in Zeiten des Erfolges immer ein offenes Herz für mich gehabt und seid mir mit Rat und Tat zur Seite gestanden! Ohne euch wäre mein langes Studium, geschweige denn dessen Verlängerung durch eine aufwendige Doktorarbeit und meine Auslandsaufenthalte in dieser Form nicht möglich gewesen. Ich kann nicht sagen, wie wertvoll mir das ist.

Meine letzten Worte gelten meinem Freund Benedikt. Ich bin sehr glücklich, dass du in meinem Leben bist und mit deiner unvergleichlichen Mischung aus Humor, Ruhe und klugem Ratschlag an meiner Seite gehst. Danke für deine Zuversicht, deine Liebe und dein Vertrauen in mich und in uns!

Bonn, 15.08.2017

5.7 Curriculum vitae